THE PERMANENT DEFORMATION OF CIRCULAR CYLINDRICAL SHELLS SUBJECTED TO INTERNAL EXPLOSIVE LOADING

by

S.M. UPSHER

A thesis submitted in partial fulfilment
of the requirements for the degree
Master of Science in Engineering.

Department of Civil Engineering
UNIVERSITY OF CAPE TOWN.

April, 1978.

DECLARATION OF CANDIDATE

I, Stanley Upsher, hereby declare that this thesis is my own work and that it has not been submitted for a degree at another university.

signature removed

Signed by candidate

April, 1978

S Y N O P S I S

This work describes what is primarily an investigation into methods for estimating the maximum permanent deformation of a circular cylindrical shell subjected to internal explosive loadings. A complete rigid-plastic analysis of the transient response is performed. Subsequently the effects of material properties are included. Finally the theoretical predictions are compared with the experimental results obtained from a series of tests on aluminium shell specimens.

ACKNOWLEDGEMENTS

This work was made possible by the use of equipment funded by the Council for Scientific and Industrial Research, and explosives supplied by African Explosives and Chemical Industries Limited.

I am indebted to Professor J.B. Martin who supervised this research and provided much of the inspiration.

My thanks are extended to Mr. Phil Duxbury who machined the shell specimens and Mr. Ray Beverton who was the technician in charge of the explosive testing.

Mr. Dave Hanan, who was familiar with the test instrumentation, made himself freely available to help with the testing. In addition he made helpful comments on the presentation of this work.

Mr. Don Daniels came to my aid and drew the diagrams; also the help of Miss Bridget Spalding, who typed the manuscript and Mr. Harold Cable who reproduced it, is acknowledged with gratitude.

NOTATION

c	$= L^2/3RH$.
e	base of the natural logarithms.
h	distance of material fibres from median surface. deforming wall thickness.
m_x	$= M/M_o$
n	material constant in stress-strain rate law.
n_x	$= N/N_o$
p_o	non-dimensional pressure.
r	current radial position of the median surface.
$\bar{r}$	$= r/R$.
t	time
t_F, t_f	duration of the shell response.
t_f^*	a lower bound for t_f.
u_x, u_ϕ, u_r	axial, circumferential and radial displacements.
$\dot{u}_i^c$	a postulated time-independent, kinematically admissible velocity field.
$u^{(2)}, u^{(1)}$	upper and lower bounds on permanent deformations.
v	radial velocities of the median surface.
v_o	initial uniform radial velocities of the median surface.
v_i	initial prescribed velocity field .
v_1, v_2, v_3	velocity functions of time at $x = 0$ for the first, second and third phases of the motion.
$\bar{v}$	v/v_o.
w	radial displacements of median surface.
w_c	radial displacements of median surface at $x = 0$.
$\bar{w}$	$= \dfrac{N_o}{\rho R v_o^2} \cdot w$
$w(s_i)$	a selected mode shape function.
x	axial co-ordinate of circumferential ring on the median surface. The origin, $x = 0$, is midway between the shell ends.

y		axial location of second plastic hinge.
$\bar{y}$	=	y/L.
z		axial location of first plastic hinge.
$\bar{z}$	=	z/L.
A_o, A		initial and current cross-sectional area of ring.
C		strain hardening rate.
D		material constant in the stress-strain rate law.
$D(\dot{u}_i^c)$		power of dissipation associated with the velocity field $\dot{u}_i^c$.
E		modulus of elasticity or rate of work.
F_i		body forces at a point.
H		initial wall thickness of shell.
I		impulse per unit area.
K		chemical energy of the blast.
L		half the length of the shell.
M_x, M_ϕ		axial and circumferential bending moments per unit length.
M_o	=	$\sigma_o H^2/4$, the fully plastic moment per unit length.
M	=	M_x
N_x, N_ϕ		axial and circumferential membrane forces per unit length.
N_o	=	$\sigma_o H$, the fully plastic membrane force per unit length.
N	=	N_o
P		pressure load.
P_o		static limit pressure load.
P_R		static limit ring load.
R		initial radius of the median surface.
R^L		static limit load.
S		surface area.
S_x		shear force per unit length.
V		volume.
$\bar{V}$	=	$(v/v_o)^2$
W_i		work dissipated in i^{th} shell element.

α	=	$\dfrac{2\sigma_o}{\bar{\rho}\, v_o^2}$
γ	=	$\alpha\,(v_o/RD)^{1/n}$
δ_f		upper bound on plastic displacement
ϵ		strain
$\epsilon_x, \epsilon_\phi$		axial and circumferential strains.
θ		angle turned by plastic hinge at support.
κ_x		curvature in longitudinal direction.
λ	=	$y - z$.
λ_o	=	$\sqrt{3RH} = L/\sqrt{c}$.
$\bar{\lambda}$	=	λ/λ_o.
ρ		surface density.
ρ^*		volume density.
σ		dynamic yield stress.
σ_o		yield stress (rigid plastic approximation).
σ_T		ultimate strength.
σ_y		yield stress (initial).
τ	=	$\dfrac{N_o t}{\rho R v_o}$, the non-dimensional time.
$\tau_I, \tau_{II}, \tau_{III}$		non-dimensional times at the end of the first, second and third phases of the motion.
τ_F		non-dimensional response time.
Δ		uniform radial displacement of impulsively loaded ring.
$(\dot{\ })$	=	$\dfrac{\partial(\ )}{\partial t}$.

INTRODUCTION

The results of a theoretical and experimental investigation into the response of circular cylindrical shells subjected to internal blast loading is presented.

The aspect of the response receiving particular attention is the maximum permanent deformation.

The problem of dynamic structural response is one of increasing importance. Specific examples are the design of containment vessels for nuclear reactors to withstand explosive impulses; the manifold design problems of explosive metal-forming technology; the response of vehicles to impact; and the general dynamic response of structures to blast loadings is an all-inclusive example.

The phenomena which actually occur under such loadings will be complex. Any analysis which attempted to include all the factors would be prohibitively difficult and simplifying assumptions must be introduced. These assumptions would not invalidate the resultant theory provided that the limits of consequent applicability are defined. This work deals with high explosive loadings which may be considered impulsive in nature. Hence, the derived formulae will be applicable to cases where the peak pressures of the disturbance are sufficiently large in comparison with the static collapse pressure of the shell and where the duration of the disturbance does not exceed the response time of the shell. Further, the formulae are derived for uniform initial radial velocities. Simplifying assumptions regarding the yield domain follow previous investigations [3,10] and are fully dealt with later.

The material properties of rate sensitivity and strain hardening will in general play an important role in determining the response. The inclusion of these effects is an added complexity and an exact analysis incorporating them is not always justifiable or easy, compared with rigid-plastic methods. The strong non-linearities in the material rate sensitivity laws invariably necessitate the use of numerical techniques in order to obtain solutions. The rigid-plastic idealization of material behaviour has merit in that it allows the solution of many otherwise insoluble problems in dynamic plasticity. In spite of the simplification, the rigid-plastic solutions will reveal much useful information, and methods to take account of rate sensitivity effects can be applied to these solutions.

The assumptions of elementary rigid-plastic theory are:

(1) The material is represented by a perfectly plastic constitutive equation.
(2) Geometry changes are assumed small.
(3) The yield stress is assumed to be independent of the rate of strain.

As Martin and Symonds [1] pointed out; the rigid-plastic approach is as valid as any other method provided that the limits of applicability are clearly stated. The limits in the case of a rigid-plastic analysis are: displacements must be small in order that geometry changes do not become significant and the initial energy of the motion must exceed, by a significant amount, the energy which can be stored elastically in the structure. The latter condition ensures that plastic strains exceed elastic strains so that the elastic portion of the response is of minor importance. Duffey and Krieg [7] showed that a ratio of at least three between initial kinetic energies and elastic potential of a shell would fulfil this condition.

In the case of some structures, the range of applicability of the rigid-plastic requirements may be very small or may be zero. In spite of this drawback, the usefulness and importance of rigid-plastic theory lies in its ability to provide quick and relatively easy estimates of deformation caused by large dynamic loads.

In this work the complete rigid-plastic solution of the cylindrical shell response is derived in Section 2. In Section 4 these results are compared to the approximate methods developed by Martin and Symonds [1,12]. In the following section, the analysis is based on a rigid linear strain hardening material model and the effects of material rate sensitivity are introduced. Finally the results of a series of experimental tests are compared to both the rigid-plastic theory and the strain hardening, rate sensitive solution. The influence of finite deformations on longitudinal membrane forces was not a consideration as the experimental set-up was designed to eliminate these effects.

Hodge [4,5,6] has studied the response of perfectly plastic shells subjected to various axisymmetric loads. He completed the solution for short shells subjected to pulse loadings and presented equations for long shells. In this work the investigation of the response of long shells to impulse loadings is extended. A complete rigid-plastic solution is presented and an attempt is made to include the influence of material properties. Duffey and Krieg [7] included the influence of material strain hardening and a linear form of strain rate sensitivity in an analysis of elastic-plastic cylindrical shells. They noted that permanent deformations for a rigid-plastic material differed by about 20 % from the corresponding values for an elastic-plastic material when the ratio of plastic to elastic energy was greater than about three. Perrone [8,9] avoided the limitations of the linear strain-rate relation by recognising that the strain rate effect is highly non-linear and that the bulk of the kinetic energy is dissipated early in the deformation. Initial dynamic stresses could therefore be assumed constant throughout the deformation with little resultant error. Jones [10] included the effect of finite deformations in an investigation of the response of short cylindrical shells to impulsive loadings. He reported significant reductions in radial deformations when these deformations approached about one half of the wall thickness.

Witmer, Balmer, Leech and Pian [11] have developed various numerical procedures for the analysis of a number of plastic structures. These computer methods are expensive to develop and use, but are perhaps more accurate in their predictions of dynamical response. Their main advantage is that factors which are normally difficult to take account of analytically, can usually be easily included in an incremental solution.

Martin [12] has derived theorems of general importance. An upper bound on permanent deformations is found for structures subjected to impulsive loadings. Martin and Symonds [1] developed a mode approximation method which produces upper and lower bounds on permanent deformations. These two methods were developed using a rigid-plastic material idealization, but attempts have been made to apply similar methods to problems involving time dependent loading and to other viscous material idealizations.

1. INTRODUCTORY THEORY

1.1 Equilibrium Equation for an Element of a Circular Cylindrical Shell Subjected to Axisymmetric Loading

The dynamic equilibrium equation is the basic requirement for the analysis of the response of a circular cylindrical shell subjected to internal impulsive loadings. The static equilibrium equation is found from consideration of Fig. 1.1 below. The dynamic form of the equilibrium equation is obtained by adding the appropriate inertial term. Fig. 1.1 depicts an element of the shell shown in Fig. 1.2.

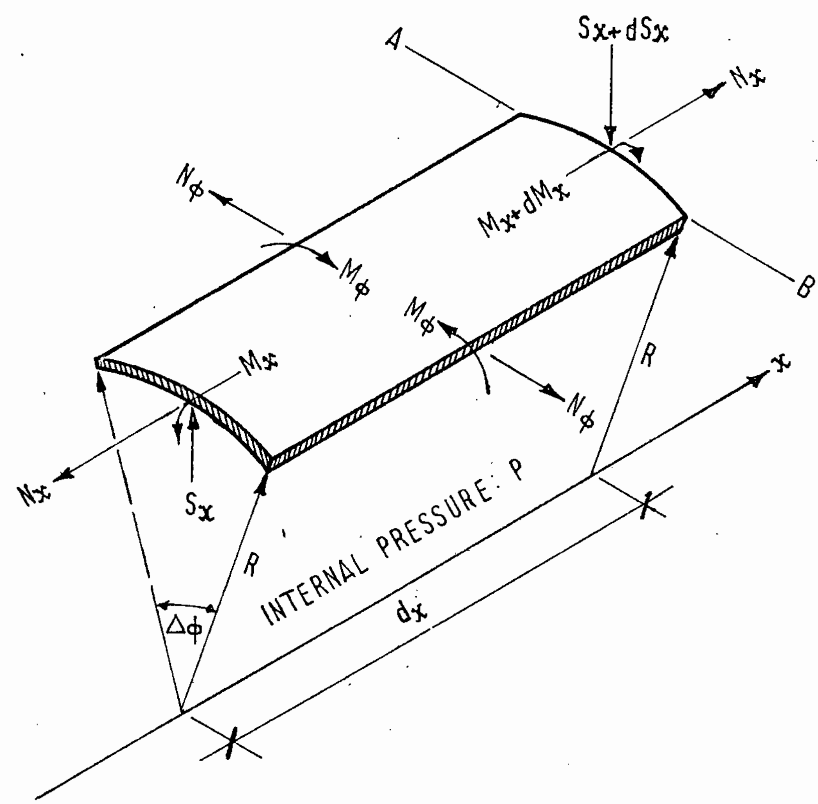

Fig. 1.1 - Shell Element in Static Equilibrium

Note that the moments, shear forces and direct forces are expressed as the appropriate force per unit length.

In the case under consideration the externally applied end loads are zero, consequently $N_x = 0$. It must also be noted that in the case of axi-symmetric loading the circumferential moments, M_ϕ, do not appear in the equilibrium equation which is found by:

(1) Consideration of the radial equilibrium of the element

$$- P(R\Delta\phi)dx + dS_x(R\Delta\phi) + 2N_\phi \sin\frac{\Delta\phi}{2}\,dx = 0,$$

recognising that $\Delta\phi/2$ is a small angle we obtain

$$\frac{RdS_x}{dx} + N_\phi - RP = 0. \qquad (1.1)$$

(2) Consideration of the rotational equilibrium about axis AB

$$- dM_x - S_x d_x - P(R\Delta\phi)dx \cdot \frac{dx}{2} = 0,$$

or $$-\frac{dM_x}{dx} - S_x = 0,$$

hence $$\frac{dS_x}{dx} = -\frac{d^2M_x}{dx^2}. \qquad (1.2)$$

Substituting equation (1.2) in equation (1.1) we obtain the static equilibrium equation

$$-\frac{d^2M_x}{dx^2} + \frac{N_\phi}{R} - P = 0. \qquad (1.3)$$

Modifications to equation (1.3) due to Impulsive Loading and Dynamic Effects

Strictly speaking no blast loadings are truly impulsive in nature. In order to simplify the mathematics the analysis of the shell response will be performed for impulsive type loadings. An impulsive loading is characterised by an infinitely high pressure occurring for an infinitely short duration. The area under such a pressure - time curve constitutes the impulse. However, the important aspect here is that pressure values are zero at any time before or after that at which the impulse occurs. This allows the pressure term, P, to be dropped from equation (1.3). The impulse will impart an outward velocity to the shell wall which will tend to accelerate, or rather de-accelerate for a period following the impulse, until motion ceases. If we call the acceleration $- dv/dt$ then, following Newton's Second Law, the inertial force per unit area is $- \rho(dv/dt)$, where ρ is the surface density.

The dynamic equilibrium equation can now be written,

$$\frac{d^2M}{dx^2} - \frac{N_\phi}{R} - \rho \frac{dv}{dt} = 0 \qquad (1.4)$$

1.2 Limit Analysis of Circular Cylindrical Shells Under Axisymmetric Loading

It is of interest to determine the limit static pressure that a circular cylindrical shell can withstand. The value is of importance in that shells will undergo permanent deformations only if they experience pulse loadings whose peak pressures exceed the static collapse load. It must be understood that in view of the necessary assumptions, the following derivation gives at best a rough estimate of the limit pressure. The accuracy of the calculated limit pressure varies moderately with various shell parameters. Augusti and d'Agostino [20] have conducted tests in an attempt to assess the validity of the theory.

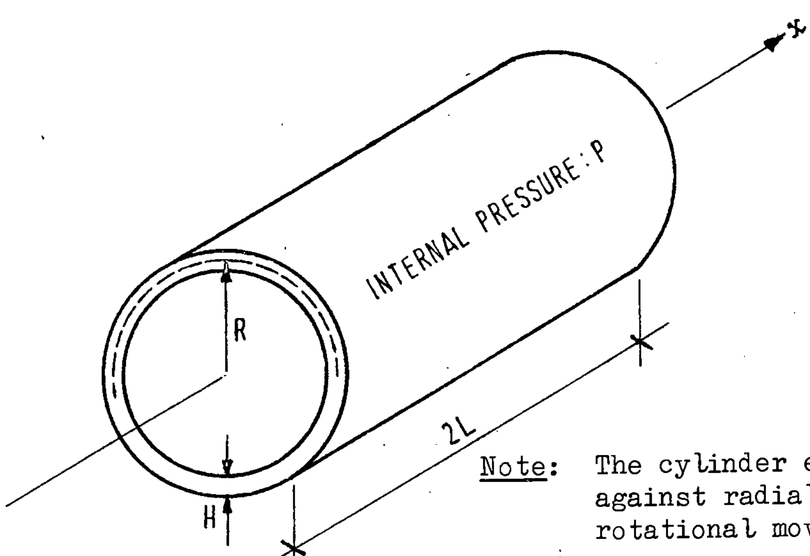

Note: The cylinder ends are fixed against radial and rotational movement.

Fig. 1.2 - Circular Cylindrical Shell

As shown in Fig. 2, the axis of the cylinder has been selected as the x axis. The origin has been chosen to lie midway between the two ends of the shell. The radius, R, is measured to the median surface of the shell wall which has a thickness, H. The length of the shell is 2L.

The only possible displacements of the median surface are u in the axial direction and w in the outward radial direction (for the specified loading). The displacements u and w are functions of x only. We shall make u_x, u_ϕ, u_r the generalised displacements in the axial, circumferential and radial directions respectively. If we make h the distance through the shell wall thickness measured positive outwards from the median surface then,

$$u_x = u - h\frac{dw}{dx},$$

$$u_\phi = 0,$$

$$u_r = w.$$

Consideration of symmetry shows that the shear strains $\gamma_{x\phi}$, $\gamma_{r\phi}$ are zero. The shear strain γ_{rx} may be neglected by assumption [13] and the radial strain ϵ_r does not occur in the analysis.

The strains that are of interest are therefore:

$$\epsilon_x = \frac{du}{dx} - h\frac{d^2w}{dx^2},$$

$$\epsilon_\phi = \frac{w}{R}.$$

The elemental work, W_i, is

$$\int_V \sigma_i \dot{\epsilon}_i \, dV = dx.Rd\phi \int_{-h/2}^{+h/2} (\sigma_x \epsilon_x + \sigma_\phi \epsilon_\phi)\, dh,$$

$$= dx.Rd\phi \left[\frac{du}{dx}\int_{-H/2}^{+H/2} \sigma_x \, dx + \frac{d^2w}{dx^2}\int_{-H/2}^{+H/2} (-h\sigma_x)dh + \frac{w}{R}\int_{-H/2}^{+H/2} \sigma_\phi \, dh\right],$$

$$= dx\, Rd\phi \left[\frac{du}{dx} N_x + \frac{d^2w}{dx^2} M_x + \frac{w}{R} N_\phi\right]$$

or

$$W_i = du\, N_x\, Rd\phi + \frac{d^2w}{dx^2} dx\, M_x\, Rd\phi + \frac{w}{R} Rd\phi\, N_\phi\, dx. \qquad (1.5)$$

In order to utilise equation (1.5) it is necessary to assume some kinematically admissible collapse mechanism for the shell. A simple mechanism is shown in Fig. 1.3. For small deformations the work dissipated in the longitudinal direction is negligible and will be ignored here.

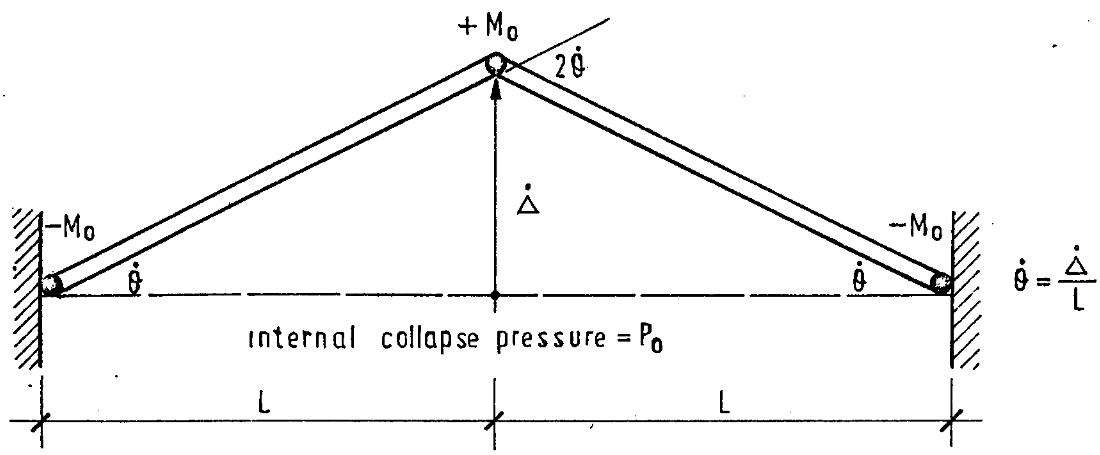

Fig. 1.3 - Assumed Static Collapse Mechanism

The shell is assumed to collapse symmetrically with central deformation rate of $\dot{w}(x = 0) = \dot{\Delta}$. Circumferential plastic hinges are assumed to form at the supports and centre. In the circumferential direction the shell material deforms plastically along the whole length. The collapse pressure shall be termed P_o.

We shall utilise the rate form of equation (1.5) and equate the rate of energy dissipation due to plastic deformations to the rate of work of the internal pressure.

The rate of energy dissipation, D, is

$$D = 4\,\dot{\theta}\,M_o(2\pi R) + 2\,\dot{\Delta}\,\pi\,N_o\,L$$

or

$$D = 4\,\frac{\dot{\Delta}}{L}\,M_o(2\pi R) + 2\,\dot{\Delta}\,\pi\,N_o\,L\,. \tag{1.6}$$

The rate of work, E, by the internal pressure, P_o, is

$$E = 2\,(\frac{\dot{\Delta}}{2}\,P_o\;2\pi RL)\,. \tag{1.7}$$

Equating equation (1.6) and equation (1.7) and using the fully plastic moment, $M_o = \sigma_o H^2/4$, and the fully plastic yield force, $N_o = \sigma_o H$, we obtain

$$P_o = \sigma_o H(\frac{H}{2L^2} + \frac{1}{R})$$

or

$$P_o = \frac{\sigma_o H}{R} \quad \text{if } H \ll L. \quad \text{(i.e. if circumferential considerations predominate)}$$

In terms of the dimensionless parameters $c = \frac{L^2}{3HR}$ and $p_o = \frac{2L^2 P_o}{\sigma_o H^2}$, the static collapse load can be represented as

$$p_o = 1 + 6/c . \tag{1.8}$$

1.3 Yield Domain for the Circular Cylindrical Shell

For a perfectly plastic material, the stress resultants must satisfy certain inequalities which depend upon the yield condition and the cross-section of the shell. This can be expressed in geometrical terms by stating that the stress point with co-ordinates (m_x, n_ϕ) must lie within or on the boundary of a certain bounded domain called the yield domain. The material will be deforming plastically at all points where the corresponding stress point lies on the boundary of the yield domain. The direction of the corresponding strain rate vector will be represented by the normal to the boundary for the particular stress point, although nothing can be said of the magnitude of the rate of deformation from these considerations alone. Elastic stress states are represented by all points that lie within the domain.

Determination of the Yield Domain:

It is assumed that the material of which the shell is composed obeys Tresca's yield condition. In the case under consideration, longitudinal bending stresses and circumferential stresses are accounted for while longitudinal membrane stresses are discounted. This assumption is valid in a small displacement analysis. Thus, Tresca's yield condition has the form,

$$\max\left(|\sigma_x| , |\sigma_\phi| , |\sigma_x - \sigma_\phi| \right) \leq \sigma_o .$$

Any point, at which any of the above equalities hold, will be plastic. It will be evident from consideration of Fig. 1.4 that at any point where $M_x = M_o$ then $0 \leq N_\phi \leq N_o/2$. For N_ϕ to have a greater value we are constrained to accept lesser values for M_x.

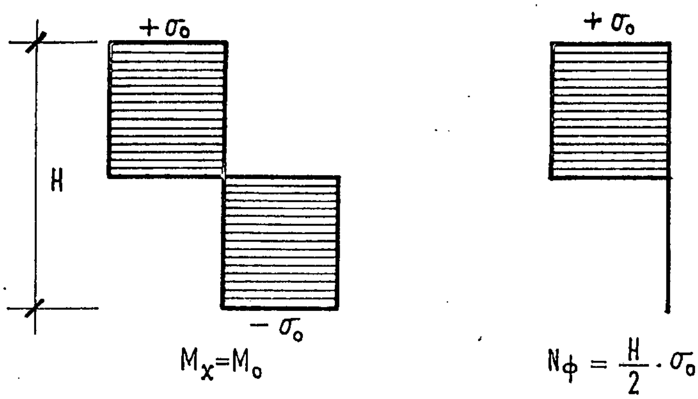

Fig. 1.4

If the value of N_ϕ is allowed to increase to $N_\phi = \sigma_o(\frac{H}{2} + h)$ the compatible moment causing a plastic stress state is $M_x = \sigma_o(\frac{H^2}{4} - h^2)$.

These two stress conditions are shown in Fig. 1.5 below.

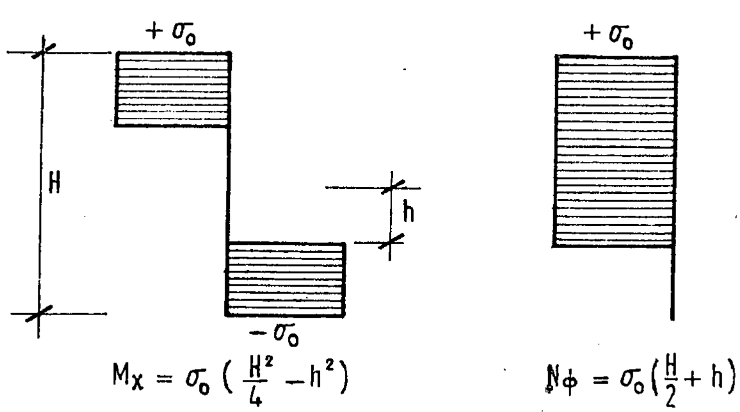

Fig. 1.5

If we put $m_x = M_x/M_o$ and $n_\phi = N_\phi/N_o$ and eliminate h we obtain

$$m_x = 4n_\phi - 4n_\phi^2 \tag{1.9}$$

Equation (1.9) holds for $\frac{1}{2} \leq n_\phi \leq 1$ and is valid for the first quadrant. As the yield domain is symmetrical the entire curve can be obtained by reflection of the first quadrant in the appropriate axes.

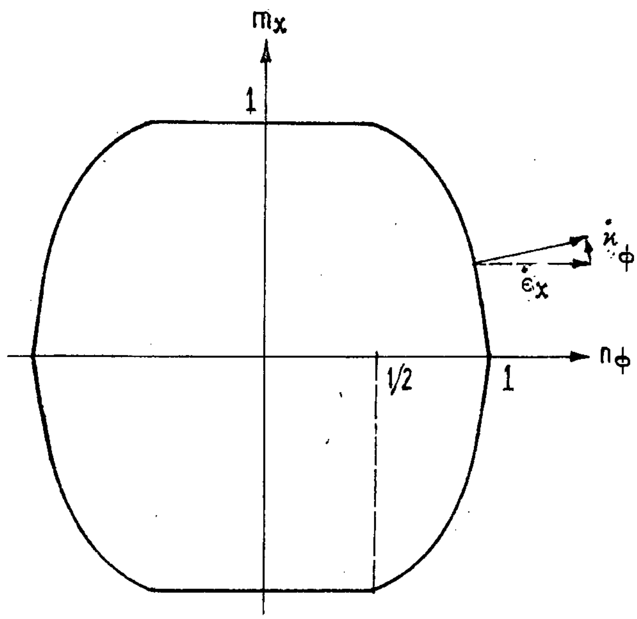

Fig. 1.6 - The Yield Domain

Since the domain has been derived from consideration of statically admissible stress states it is a lower bound. In this case no other alternatives exist, consequently it is the best lower bound.

2. ANALYSIS OF THE RESPONSE OF IMPULSIVELY LOADED CIRCULAR CYLINDRICAL SHELLS

In the analysis to follow, a simplified yield domain as shown in Fig. 2.1 (c) will be considered.

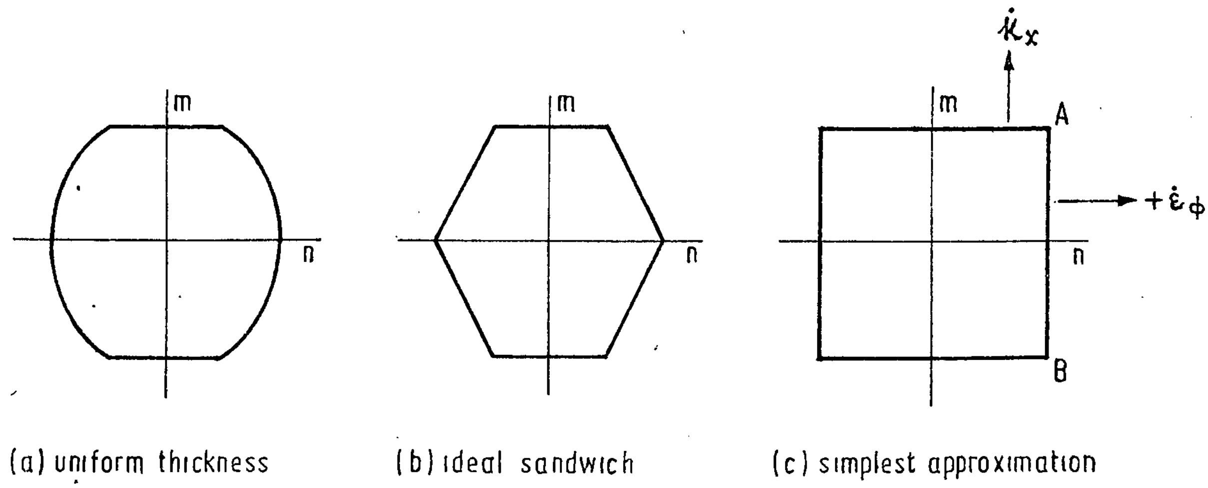

Fig. 2.1 - Yield Domains

It is necessary to choose the simplest form for the yield domain in order to obtain closed form solutions to the problem. Prager [16] has found the three-dimensional yield domain for a cylindrical shell in terms of N_x, N_ϕ, M_x, however, in order to utilise such complicated domains recourse must be taken to numerical techniques. Witmer, Balmer, Leech and Pian [11] have devised computer programs that are capable of the solution of many varied problems of this nature.

2.1 Analysis of the Short Shell

Consider equation (1.4). For simplicity we shall replace M_x with M and N_ϕ with N. The dynamic equilibrium equation thus becomes,

$$\frac{\partial^2 M}{\partial x^2} - \frac{N}{R} - \rho \frac{dv}{dt} = 0 \qquad (2.1)$$

The velocity $v(x,t)$ will be considered as positive outwards and a positive moment will cause tension in the outer fibres of the shell wall. Tensile circumferential stresses are positive. As the shell and loading is symmetrical, only the left hand half of the shell shown in Fig. 1.2 will be considered in the analysis. It is assumed that the initial impulse is absorbed uniformly by the shell. This leads to the assumption that the initial velocity, $v(x,0)$ is constant for x and we shall say $v(x,0) = v_o$.

The kinematics of the deformation must be such that it does not conflict with the chosen yield domain. In order not to violate the conditions of the yield domain of Fig. 2.1 (c) it is necessary to allow a plastic hinge to form at the support and travel towards the centre of the shell. The situation is shown in Fig. 2.2

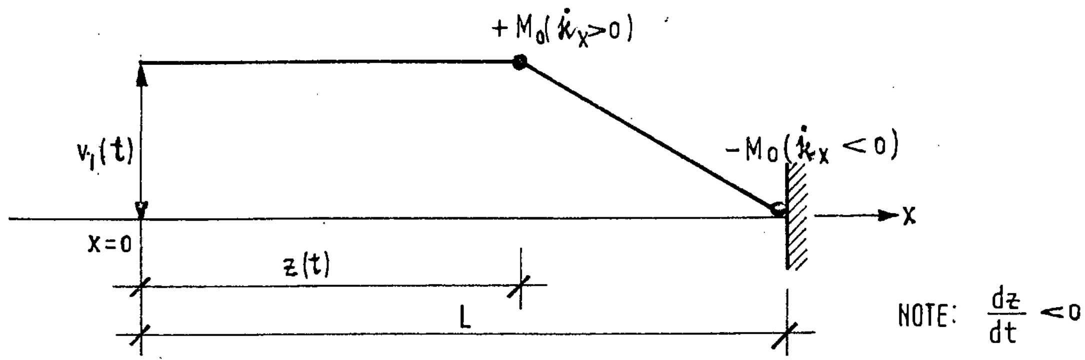

Fig. 2.2 - Velocity Profile (First Phase)

Kinematical Considerations:

$$\text{generally}\quad \dot{K}_x = -\frac{d^2v}{dx^2}, \qquad \dot{\epsilon}_\phi = v/R \tag{2.2a}$$

For internal pressure and outward positive velocity,

$\dot{\epsilon}_\phi > 0$ for $0 \leq x < L$, which corresponds to line AB in Fig. 2.1(c),
$\dot{\kappa}_x > 0$ at $x = z$, " " " point A " " ",
$\dot{\kappa}_x < 0$ at $x = L$, " " " " B " " ".

(2.2b)

Thus the stress condition at all points in the deforming material may be described by a suitable point on line AB of the yield domain and no conflict arises.

The motion of deformation may be separated into two distinct phases namely:

1. The First Phase (Fig. 2.2) which exists for $0 \leq z \leq L$. By definition this phase ceases when $z = 0$ and $t = t_I$.

2. The Second Phase (Fig. 2.3) which exists for $t_I \leq t \leq t_F$.

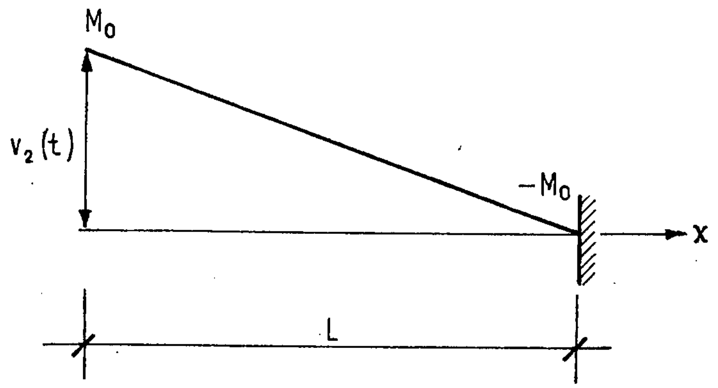

Fig. 2.3 - Velocity Profile (Second Phase)

Analysis of the First Phase:

Consideration of Fig. 2.2 indicates that,

$$v = v_1(t) \qquad \text{for } 0 \leq x \leq z ,$$

$$v = \frac{L - x}{L - z} \cdot v_1(t) \quad \text{for } z \leq x \leq L .$$

Differentiation with respect to time leads to the radial accelerations

$$\frac{dv}{dt} = \frac{dv_1}{dt} \qquad \text{for } 0 \leq x \leq z$$

and

$$\frac{dv}{dt} = \frac{L - x}{L - z} \cdot \frac{dv_1}{dt} + \frac{L - x}{(L - z)^2} \cdot \frac{dz}{dt} \quad \text{for } z \leq x \leq L. \tag{2.3}$$

From equations (2.2b) it is evident that,

$$M = +M_o \qquad \text{for} \quad x = z ,$$
$$M = -M_o \qquad \text{for} \quad x = L . \tag{2.4}$$
$$N = +N_o \qquad \text{for} \quad 0 \leq x \leq L .$$

and clearly $M = M_o$ for $0 \leq x \leq z$.

The analysis now proceeds with the substitution of equations (2.3) into the equilibrium equation (2.1) taking due cognisance of the regions for which they are valid.

Region $0 < x < z$, $M = M_o$

hence $$\frac{dv_1}{dt} = -\frac{N_o}{\rho R} . \tag{2.5}$$

At this point the dimensionless variables $\tau = \dfrac{N_o t}{\rho R v_o}$ and $\bar{v}_1 = \dfrac{v_1}{v_o}$ are introduced. Hence equation (2.5) becomes

$$\frac{d\bar{v}_1}{d\tau} = -1 .$$

Integrating and solving for the resulting constant by using the initial condition $v(x,0) = 1$, we obtain,

$$\bar{v}_1 = 1 - \tau. \tag{2.6}$$

We now investigate the adjacent region. An expression relating the position of the plastic hinge with respect to time will be derived. This expression will then be used to determine the duration of the first phase.

Region $z < x < L$

Combining equations (2.1) and (2.3) we obtain

$$\frac{\partial^2 M}{\partial x^2} - \frac{N_o}{R} - \rho\left(\frac{L - x}{L - z}\frac{dv_1}{dt} + \frac{L - x}{(L - x)^2} v_1 \frac{dz}{dt}\right) = 0 . \tag{2.7}$$

This expression must be integrated twice with respect to x. For convenience we introduce Z which is independent of x, and

$$Z = \frac{N_o}{(L - z)R} - \frac{\dot{z}}{(L - z)^2}\left(\rho v_o - \frac{N_o t}{R}\right), \quad \dot{z} = \frac{dz}{dt}. \tag{2.8}$$

After rearrangement and integration we obtain,

$$\begin{aligned} \frac{\partial M}{\partial x} &= \frac{Z(L - x)^3}{2} - \frac{N_o}{R}(L - x) + A, \\ M &= -\frac{Z(L - x)^3}{6} + \frac{N_o}{2R}(L - x)^2 + A(L - x) + B . \end{aligned} \tag{2.9}$$

Where A and B are the constants of integration and may be found using the boundary conditions

$$\begin{aligned} M(z) &= + M_o, \\ M(L) &= - M_o \text{ (if the shell ends are free to rotate, } M(L) = 0). \end{aligned}$$

Hence,

$$\begin{aligned} A &= \frac{2M_o}{L - z} - \frac{N_o}{2R}(L - z) + \frac{Z(L - z)^2}{6}, \\ B &= - M_o . \end{aligned} \tag{2.10}$$

The actual moment distribution for the region is not of great interest but utilising the condition that the shear force across the travelling plastic hinge is zero leads to a useful result. This condition is evident from considerations of symmetry and may be thus stated,

$$\frac{\partial M}{\partial x}(z) = 0 \tag{2.11}$$

Substituting equations (2.8), (2.10) and (2.11) into equation (2.9) we obtain

$$\frac{dz}{dt} = \frac{-\frac{6M_o}{L - z} - \frac{N_o}{2R}(L - z)}{\rho v_o - \frac{N_o t}{R}} . \tag{2.12}$$

Using the dimensionless variables $\tau = \frac{N_o t}{\rho R v_o}$, $c = \frac{N_o L^2}{12 M_o R}$ and $\bar{z} = \frac{z}{L}$ and integrating this separable differential equation between general limits the relation between the position of the plastic hinge and time is obtained;

$$\tau = 1 - \frac{1}{1 + c(1 - \bar{z})^2} . \qquad (2.13)$$

At this point it is possible to investigate the range of validity of the foregoing analysis. As the value of the moment must at all times lie between $+M_o$ and $-M_o$ it is evident that $\frac{dM}{dx}(L) \leq 0$ always.

Substituting equation (2.12) into equation (2.9) and simplifying and applying the above condition we obtain

$$\frac{(L - z)^2}{L^2} \leq \frac{12\, M_o R}{N_o L^2} .$$

As $\frac{(L - z)^2}{L^2}$ may attain the maximum value of unity the condition

$$\frac{12\, M_o R}{N_o L^2} \geq 1$$

must be satisfied for the foregoing analysis to hold. Using $M_o = \frac{\sigma_o H^2}{4}$ and $N_o = \sigma_o H$ and inverting we may restate the condition as

$$c = \frac{N_o L^2}{12\, M_o R} = \frac{L^2}{3\, HR} \leq 1.$$

Hence, we may define a 'short shell' as one having the parameter $c \leq 1$. For shells with $c > 1$, further analysis is required.

We now return to the main stream of the analysis. In order to determine the duration of the first phase we set $\bar{z} = 0$ in equation (2.13). (The symbol I , used as a subscript, denotes the condition prevailing at the end of the first phase of the motion), hence,

$$\tau_I = 1 - \frac{1}{1 + c} = \frac{c}{1 + c} \qquad (2.14)$$

and the outward velocity at this instant is obtained by substitution in equation (2.6)

$$\bar{v}_I = \frac{1}{1 + c} . \qquad (2.15)$$

We have now provided ourselves with the initial conditions of the second phase; the analysis of which, follows.

Analysis of the Second Phase:

Referring to Fig. 2.3 we may write the equation of the velocity distribution in terms of the central velocity, $v_2(t)$:

$$v(x,t) = \frac{(L - x)}{L} v_2(t). \tag{2.16}$$

This holds for the region $0 \leq x \leq L$. The expression is differentiated with respect to time and the result substituted in equation (2.1). As in the analysis of the first phase, this expression is integrated with respect to the variable x.

Before commencing with the analysis, we will establish the boundary conditions by way of consideration of the kinematics. It is evident from equations (2.2a) and Fig. 2.3 that,

$$\begin{aligned}
\dot{\kappa}_x &> 0 && \text{at } x = 0, \\
\dot{\kappa}_x &< 0 && \text{at } x = L, \\
\dot{\kappa}_x &= 0 && \text{for } 0 < x < L, \\
\dot{\epsilon}_\phi &= \frac{L - x}{L}\frac{v_2}{R} > 0 && \text{for } 0 \leq x < L.
\end{aligned}$$

These stress conditions are represented by line AB of the yield domain of Fig. 2.1(c). The boundary conditions are therefore

$$\begin{aligned}
N_\phi &= N_o && \text{for } 0 \leq x \leq L, \\
M &= M_o && \text{at } x = 0, \\
M &= -M_o && \text{at } x = L.
\end{aligned} \tag{2.17}$$

Differentiating equation (2.16) substituting in equation (2.1) we obtain

$$\frac{\partial^2 M}{\partial x^2} - \frac{N_o}{R} - \frac{\rho}{L}(L - x)\frac{dv_2}{dt} = 0.$$

Rearranging and integrating with respect to x,

$$\frac{\partial M}{\partial x} = -\frac{N_o}{R}(L - x) - \frac{\rho}{2L}\frac{dv_2}{dt}(L - x)^2 + A$$

$$\text{and} \qquad M = \frac{N_o}{2R}(L - x)^2 + \frac{\rho}{6L}(L - x)^3\frac{dv_2}{dt} - A(L - x) + B. \tag{2.18}$$

The constants of integration are determined using the boundary conditions (2.17). They are

$$A = -\frac{2M_o}{L} + \frac{N_oL}{2R} + \frac{\rho L}{6}\frac{dv_2}{dt} ,$$

$$B = -M_o .$$

We now have the complete expression for $M(x,t)$ and may use the condition $\partial M/\partial x(0) = 0$ to isolate an expression for dv_2/dt:

$$\frac{dv_2}{dt} = -\frac{3}{\rho L}\left(\frac{2M_o}{L} + \frac{N_oL}{2R}\right) .$$

This is integrated and the constant of integration determined using the initial condition

$$v(t_I) = v_I = \frac{\rho R v_o}{N_o} \cdot \frac{c}{1 + c} .$$

The results are presented in terms of the non-dimensional parameters c, τ and $\bar{v}_2$ where $\bar{v}_2 = v_2/v_o$:

$$\bar{v}_2 = \frac{3}{2} - \left(\frac{1 + 3c}{2c}\right)\tau . \tag{2.19}$$

Motion ceases when $\bar{v}_2 = 0$. This condition is used in equation (2.19) to determine the time at which the motion ceases. (The symbol F used as a subscript denotes the end of the motion).

$$\tau_F = \frac{3c}{1 + 3c}$$

$$\text{or the actual duration,} \quad t_F = \frac{\rho R v_o}{N_o}\left(\frac{3c}{1 + 3c}\right) . \tag{2.20}$$

The Final Deformation Profile:

It is now possible to obtain expressions giving the final deformation at any point on the median surface. It is necessary to consider the velocity history of a deformed ring at a generic position, x, and integrate the velocity functions with respect to time for the duration for which each was present. The final deformation is obtained by summing the integrated expressions. During the first phase of the deformation the ring will lie in the region $0 < x < z$ and subsequently in the region $z < x < L$. Thereafter deformations will occur in the third phase. We define the three displacements respectively as $w_1(x)$, $w_2(x)$ and $w_3(x)$.

From equation (2.13) we see that the travelling plastic hinge will reach the position x at the time

$$\tau = 1 - \frac{L^2}{L^2 + c(L - x)^2} , \qquad (2.21)$$

hence,

$$w_1(x) = \frac{\rho R v_o^2}{N_o} \int_0^{1 - \frac{L^2}{L^2 + c(L - x)^2}} (1 - \tau)\, d\tau$$

or

$$w_1 = \frac{\rho R v_o^2}{N_o} \left[\frac{c(2 + c)}{2(1 + c)} \right] .$$

The displacement $w_2(x)$ occurs from $\tau = 1 - \dfrac{L^2}{L^2 + c(L - x)^2}$ until the end of the first phase. Reference to equation (2.14) reminds us that $\tau_I = c/(1 + c)$,
hence,

$$w_2(x) = \frac{\rho R v_o^2}{N_o} \int_{1 - \frac{L^2}{L^2 = c(L - x)^2}}^{\frac{c}{1 + c}} \frac{L - x}{L - z} (1 - t)\, dt .$$

This must be expressed in terms of τ using equation (2.21). The integration is lengthy and the result is quoted in the unexpanded form:

$$w_2(x) = \frac{\rho R v_o^2}{N_o}\sqrt{c}\,(L - x)\left[2\sqrt{\tau}\,(1 - \tau)^{3/2} - \frac{3}{4}(1 - 2\tau)\sqrt{\tau - \tau^2} - \frac{3}{8}\sin^{-1}(1 - 2\tau)\right]_{1-\frac{L^2}{L^2 - c(L-x)^2}}^{\frac{c}{1+c}}$$

The displacement $w_3(x)$ occurs between $\tau_I = \frac{c}{1 + c}$ and $\tau_F = \frac{3c}{1 + 3c}$ and is

$$w_3(x) = \frac{\rho R v_o^2}{N_o}\int_{\frac{c}{1+c}}^{\frac{3c}{1+3c}} \frac{L - x}{L}\left\{\frac{3}{2} - \left(\frac{1 + 3c}{2c}\right)\tau\right\} dt \,.$$

The integration yields

$$w_3(x) = \frac{\rho R v_o^2}{N_o}\left(\frac{L - x}{L}\right)\left(\frac{c}{(1 + 3c)(1 + c)^2}\right).$$

The final displacement profile, $w(x)$, is

$$w(x) = w_1(x) + w_2(x) + w_3(x)\,. \tag{2.22}$$

The maximum displacement is of greatest interest and can easily be determined from equation (2.22) using the substitution $x = 0$. The quantity $w_2(x = 0)$ vanishes and the result is

$$w(0) = \frac{\rho R v_o^2}{N_o}\,\frac{c(4 + 3c)}{2(1 + c)(1 + 3c)}\,. \tag{2.23}$$

This is the maximum displacement for a short circular cylindrical shell with rigid supports. An analysis along similar lines for a short shell with ends free to rotate will yield the result

$$w(0) = \frac{\rho R v_o^2}{\sigma_o H}\,\frac{2c(2 + 3c)}{(1 + 2c)(1 + 6c)}\,. \tag{2.24}$$

Both equation (2.23) and equation (2.24) apply for the range $0 \le c \le 1$. The response of each type of shell is compared graphically in Fig. 2.6.

If we define $\bar{w} = \frac{\rho R v_o^2}{N_o}$ and use $\bar{x} = \frac{x}{L}$ and evaluate equation (2.22)

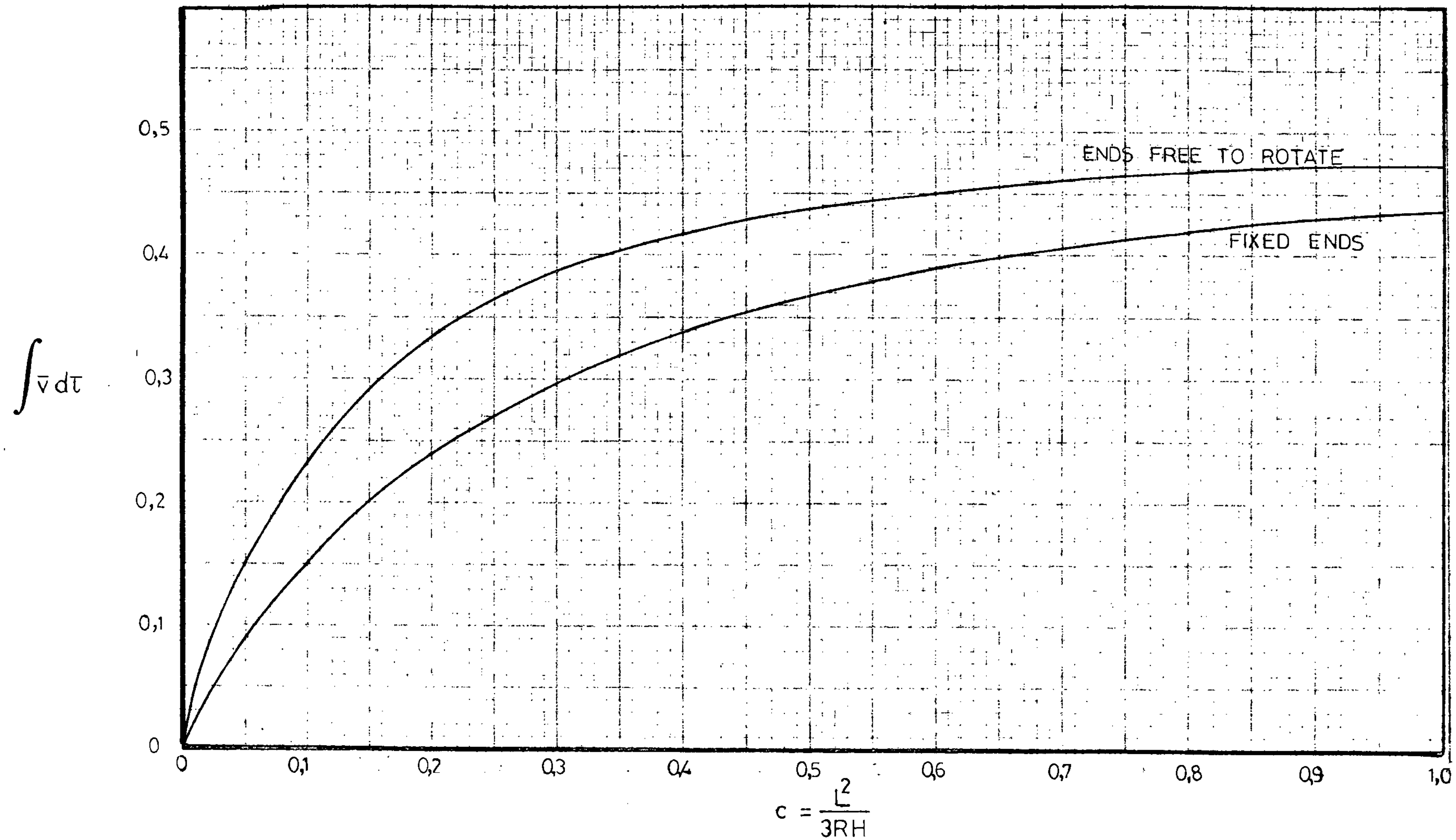

<u>FIG. 2.6</u> - <u>COMPARISON OF MAXIMUM DEFORMATION FOR SHORT SHELLS WITH FIXED ENDS AND ENDS FREE TO ROTATE</u>

for $c = 1$ and $0 \leq \bar{x} \leq 1$ a final deformation profile is obtained. Such a profile is shown in Fig. 2.5.

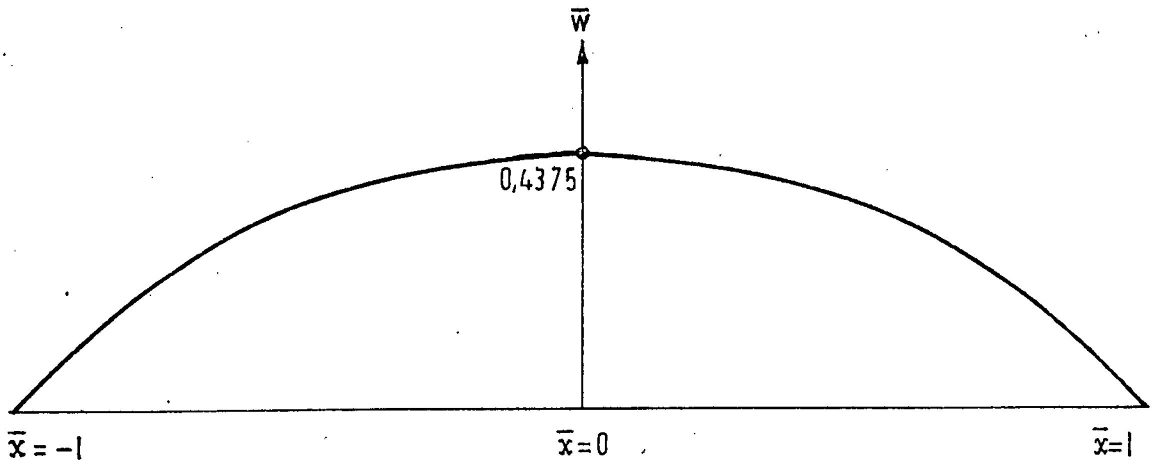

Fig. 2.5 - Short Shell Deformation Profile (c = 1) and Table of Values

$\bar{x}$	$\bar{w}$
0	0,4375 (exact)
0,1	0,4296
0,3	0,4031
0,5	0,3519
0,7	0,2592
0,75	0,2273
0,8	0,1911
0,9	0,1052
0,45	0,0533
1	0

TABLE 1: Non-dimensional short shell deformations, $c = 1$.

This concludes the analysis of the response of the short shell.

2.2 Analysis of the Long Shell

A long shell is defined as one for which the parameter $c = \frac{L^2}{3RH}$

is greater than or equal to unity. In this case it is necessary to allow a second set of plastic hinges to form at the supports and follow the first set towards the centre. It is evident that the second set will form at the instant the first set has travelled the distance $(L - z) = \sqrt{3HR}$. Thus we define the parameter $\lambda_o = \sqrt{3HR}$. Hodge [3] wrote that the motion occurred in four distinct phases. However, it will be shown that the fourth phase occurs only instantaneously at the end of the motion.

The analysis for the first phase is identical to that of the short shell. It occurs during the time interval $0 \leq \tau \leq \tau_I$ and it will be shown that for long shells, $\tau_I = \frac{1}{2}$.

The second phase occurs during the time interval $\tau_I \leq \tau \leq \tau_{II}$ and ends when the first set of plastic hinges reach the position $x = 0$.

The third and last phase occurs during the time interval $\tau_{II} \leq \tau \leq \tau_F$ and is characterised by the second set of hinges moving toward the position $x = \lambda_o$ while the central radial velocity simultaneously drops off to zero.

Analysis of the First Phase:

As previously noted, the analysis of the first phase is essentially identical to that of the short shell with the sole exception that it ends when $(L - z)^2 = L^2/c$ and not when $z = 0$.

Using equation (2.13) and the above condition:

$$\tau_I = \frac{1}{2} .$$

Hence, the central velocity, v_I, at the end of the first phase can be obtained from equation (2.6):

$$\bar{v}_I = 1 - \tau_I = \frac{1}{2}$$

or

$$v_I = \frac{v_o}{2} .$$

Analysis of the Second Phase:

A velocity profile representative of the second phase is shown in Fig. 2.6. The second plastic hinge is a distance y from the centre and is travelling towards the centre at the rate $\dot{y}$.

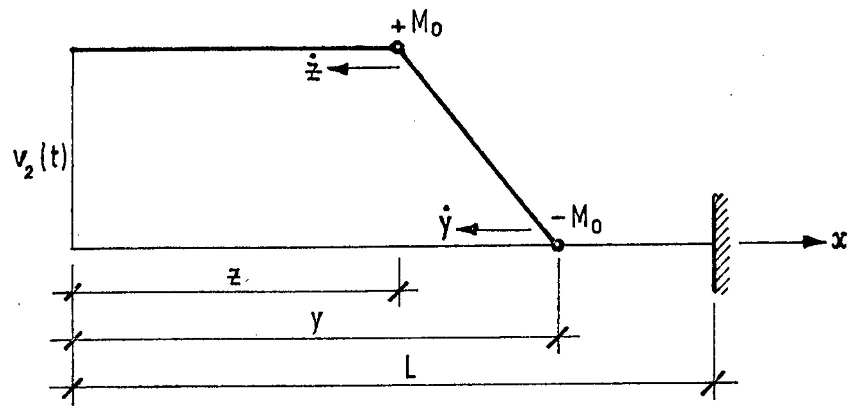

Fig. 2.6 - Velocity Profile during Second Phase

where

$$v = v_2(t) \qquad \text{for} \quad 0 \le x \le z,$$

$$v = \frac{y - x}{y - z} v_2(t) \qquad \text{for} \quad z \le x \le y, \tag{2.25}$$

$$v = 0 \qquad \text{for} \quad y \le x \le L,$$

are the velocity functions for the three regions.

It is evident from equations (2.2a) and (2.25) that

$$\dot{\kappa}_x > 0 \qquad \text{at} \quad x = z,$$

$$\dot{\kappa}_x < 0 \qquad \text{at} \quad x = y,$$

$$\dot{\kappa}_x \doteq 0 \qquad \text{elsewhere},$$

$$\dot{\epsilon}_\phi = \frac{v_2}{R} \qquad \text{for} \quad 0 \le x \le z,$$

$$\dot{\epsilon}_\phi = \frac{y - x}{y - z}\frac{v_2}{R} \qquad \text{for} \quad z \le x \le y,$$

$$\dot{\epsilon}_\phi = 0 \qquad \text{for} \quad y \le x \le L,$$

and it follows that

$$\begin{aligned} M &= +M_o && \text{at} && x = z, \\ M &= -M_o && \text{at} && x = y, \\ N &= N_o && \text{for} && 0 \leq x \leq y, \\ N &= 0 && \text{for} && y \leq x \leq L. \end{aligned} \tag{2.26}$$

The derivatives of the functions (2.25) with respect to time are

$$\begin{aligned} \frac{dv}{dt} &= \frac{dv_2}{dt} && \text{for } 0 \leq x \leq z, \\ \frac{dv}{dt} &= \frac{y - x}{y - z}\frac{dv_2}{dt} + \left\{\frac{(y - z)\dot{y} - (y - x)(\dot{y} - \dot{z})}{(y - z)^2}\right\}v_2 && \text{for } z \leq x \leq y, \\ \frac{dv}{dt} &= 0 && \text{for } y \leq x \leq L \end{aligned} \tag{2.27}$$

and are the radial accelerations for the three regions.

Now that this general information, pertaining to the second phase is available, it is possible to proceed with the analysis of the separate regions.

Analysis of Region $0 \leq x \leq z$

The solution for this region is identical to that of the first phase. From equations (2.1), (2.26) and (2.27) we obtain

$$\frac{dv_2}{dt} = -\frac{N_o}{\rho R}.$$

Integrating with respect to time and solving for the constant of integration using the boundary condition, $v_2 = v_o/2$ when $t = \frac{1}{2}(\rho R v_o/N_o)$, which prevails at the end of the first phase, we obtain the velocity function in terms of the time elapsed:

$$v_2 = v_o - \frac{N_o t}{\rho R}. \tag{2.28}$$

This may be stated in non-dimensional terms as

$$\bar{v}_2 = 1 - \tau .$$

Analysis of the Region $z \leq x \leq y$

In order to simplify the subsequent analysis we introduce the time dependent variable $\lambda = y - z$ and rewrite equation (2.27) in a partially expanded form,

$$\frac{dv}{dt} = (y - x)\frac{d}{dt}\left(\frac{v_2}{\lambda}\right) + \dot{y}\left(\frac{v_2}{\lambda}\right),$$

which is substituted in the equilibrium equation (2.1) to yield

$$\frac{\partial^2 M}{\partial x^2} = \frac{N_o}{R} + \lambda(y - x)\frac{d}{dt}\left(\frac{v_2}{\lambda}\right) + \dot{y}\left(\frac{v_2}{\lambda}\right).$$

This is twice integrated with respect to **x** and the terms grouped by degree of **x**:

$$\begin{aligned}\frac{\partial M}{\partial x} &= \left\{\frac{N_o}{R} + \rho\dot{y}\left(\frac{v_2}{\lambda}\right)\right\} x - \frac{\rho}{2}(y - x)^2\frac{d}{dt}\left(\frac{v_2}{\lambda}\right) + A,\\ M &= \left\{\frac{N_o}{R} + \rho\dot{y}\left(\frac{v_2}{\lambda}\right)\right\}\frac{x^2}{2} - \frac{\rho}{6}(y - x)^3\frac{d}{dt}\left(\frac{v_2}{\lambda}\right) + A + B.\end{aligned} \tag{2.29}$$

The constants of integration, A and B, are solved using the boundary conditions (2.26):

$$\begin{aligned}A &= -\frac{2M_o}{\lambda} - \frac{1}{2}\left\{\frac{N_o}{R} + \rho\dot{y}\left(\frac{v_2}{\lambda}\right)\right\}\frac{(y^2 - z^2)}{\lambda} + \frac{\rho}{6}\lambda^2\frac{d}{dt}\left(\frac{v_2}{\lambda}\right),\\ B &= -M_o\left(1 - \frac{2y}{\lambda}\right) - \frac{1}{2}\left\{\frac{N_o}{R} + \rho\dot{y}\left(\frac{v_2}{\lambda}\right)\right\}\left\{y^2 - \frac{(y^2 - z^2)}{\lambda}\right\} - \frac{\rho}{6}\lambda^2 y\frac{d}{dt}\left(\frac{v_2}{\lambda}\right).\end{aligned}$$

Although the moment equation is not in itself particularly useful we are able to isolate $\dot{y}$ and $\dot{z}$ from equation (2.29) using the conditions

$$\frac{dM}{dx}(z) = 0, \quad \frac{dM}{dx}(y) = 0,$$

and the substitution, $y - z = \lambda$. Equation (2.29) reduces to

$$\frac{N_o}{R}(y - z) + \rho\left(v_o - \frac{N_o}{\rho R}t\right)(\dot{y} + \dot{z}) = 0 \tag{2.30a}$$

which may be written using non-dimensional variables as

$$(\bar{y} - \bar{z}) + (1 - \tau)\left(\frac{d\bar{y}}{d\tau} + \frac{d\bar{z}}{d\tau}\right) = 0 \tag{2.30b}$$

where $\bar{y} = \frac{y}{L}$, $\bar{z} = \frac{z}{L}$ and $\tau = \frac{N_o t}{\rho R v_o}$.

It is impossible to extract separate solutions for $\dot{z}$ and $\dot{y}$ from equation (2.30a). The apparently reasonable solution, $\dot{y} = \dot{z}$, was shown to be incorrect by solving for $\dot{z}$ and checking on the value of dM/dx (y). As the derived value of dM/dx (y) was non-zero the assumption is invalid.

Fortunately the moment equation can be bypassed and expressions for $\dot{y}$ and $\dot{z}$ derived from considerations of the linear momentum and angular moment relations for the deformation.

<u>Linear Momentum Relation</u>:

This can be obtained by integrating the equilibrium equation (2.1) along the length of the shell. This requires the solution of

$$\int_0^L \left(\frac{\partial^2 M}{\partial x^2} - \frac{N}{R} - \rho \frac{dv}{dt} \right) dx = 0.$$

The conditions dM/dx (0) = dM/dx (L) = 0 are used to eliminate the moment terms. The resulting equation is

$$\frac{d}{dt} \int_0^L v \, dx = - \int_0^L \frac{N}{\rho R} \, dx \tag{2.31}$$

which can be evaluated from the known velocities.

<u>Angular Momentum Relation</u>:

This can be derived by integrating the product of the equilibrium equation (2.1) and x along the length of the shell:

$$\int_0^L \left(\frac{\partial^2 M}{\partial x^2} - \frac{N}{R} - \rho \frac{dv}{dt} \right) x \, dx = 0$$

or

$$\int_0^L \frac{\partial^2 M}{\partial x^2} x \, dx - \int_0^L \frac{N}{R} x \, dx - \rho \frac{d}{dt} \int_0^L v \, x \, dx = 0 .$$

The first term is evaluated using integration by parts and employing the conditions,

$$\frac{dM}{dx}(L) = \frac{dM}{dx}(0) = 0,$$
$$M(L) = + M_0,$$
$$M(0) = - M_0.$$

$$\text{Hence,}\quad \int_0^L \frac{\partial^2 M}{\partial x^2}\, x\, dx = -2M_o .$$

After rearrangement of terms the angular momentum relation reduces to

$$\frac{d}{dt}\int_0^L v\, x\, dx = \frac{2M_o}{\rho} - \int_0^L \frac{N}{\rho R}\, x\, dx . \qquad (2.32)$$

Evaluation of the Relations (2.31) and (2.32)

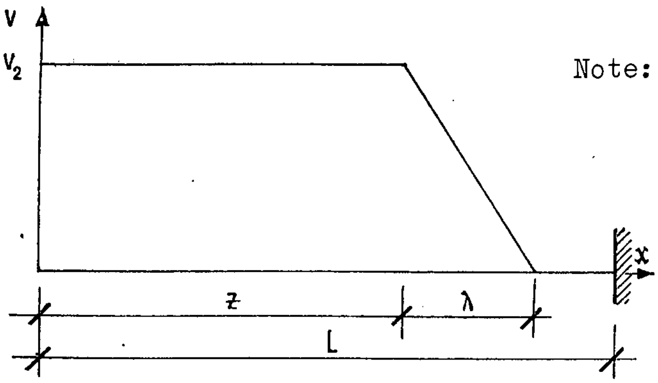

Note: $N = N_o$ for $0 \leq x \leq (z + \lambda)$,
$N = 0$ elsewhere.

Fig. 2.7 - Velocity Profile typical of the Second Phase

The various integrals are easily evaluated using the information in Fig. 2.7:

$$\int_0^L \frac{N}{\rho R}\, dx = \frac{N_o}{\rho R}(z + \lambda),$$

$$\int_0^L \frac{N}{\rho R}\, x\, dx = \frac{N_o}{\rho R}\,\frac{(z+\lambda)^2}{2},$$

$$\frac{d}{dt}\int_0^L v\, dx = \frac{d}{dt}\left(z\, v_2 + \frac{\lambda}{2} v_2\right), \qquad (2.33)$$

and

$$\frac{d}{dt}\int_0^L v\, x\, dx = \frac{d}{dt}\left\{\frac{v_2\, z^2}{2} + v_2 \frac{\lambda}{2}\left(z + \frac{\lambda}{3}\right)\right\} .$$

Substituting the applicable equations (2.33) into the linear momentum relation (2.31) and using equation (2.28) we obtain

$$(\dot{z} + \frac{\dot{\lambda}}{2}) = -\frac{N_o \lambda}{2\rho R v_2} \qquad (2.34)$$

which can be shown to be identical to the previously calculated equation (2.30a).

Similarly, substituting the applicable equations (2.33) into the angular momentum relation (2.32) and using equation (2.28):

$$v_2 z\,(\dot{z} + \frac{\dot{\lambda}}{2}) + v_2\lambda\,(\frac{\dot{z}}{2} + \frac{\dot{\lambda}}{3}) = \frac{2M_o}{\rho} - \frac{N_o}{\lambda R}\,\lambda\,(\frac{z}{2} + \frac{\lambda}{3}) \,. \tag{2.35}$$

Equations (2.34) and (2.35) are solved simultaneously to obtain relations for $\dot{z}$ and $\dot{\lambda}$ and consequently $\dot{y}$. The solutions follow:

$$\dot{\lambda} = \frac{24M_o}{\rho\lambda v_2} - \frac{\lambda N_o}{\rho R v_2}$$

or in non-dimensional form

$$\frac{d\bar{\lambda}}{d\tau} = \frac{2}{\bar{\lambda}\,\bar{v}_2} - \frac{\bar{\lambda}}{v_2}\,, \tag{2.36}$$

where $\bar{\lambda} = \dfrac{\lambda}{\lambda_o}$.

$$\dot{z} = -\frac{12M_o}{\rho\lambda v_2}$$

or
$$\frac{d\bar{z}}{d\tau} = -\frac{1}{\sqrt{c}} \cdot \frac{1}{\bar{\lambda}\,\bar{v}_2}\,. \tag{2.37}$$

Using $\dot{y} = \dot{z} + \dot{\lambda}$,

$$\dot{y} = \frac{12M_o}{\rho\lambda v_2} - \frac{\lambda N_o}{\lambda R v_2}$$

or
$$\frac{d\bar{y}}{d\tau} = \frac{1}{\sqrt{c}}\,(\frac{1}{\bar{\lambda}\,\bar{v}_2} - \frac{\bar{\lambda}}{\bar{v}_2})\,, \tag{2.38}$$

noting that $\bar{y} = \bar{z} + \dfrac{\bar{\lambda}}{\sqrt{c}}$.

A solution, equation (2.39), for λ as a function of time is readily obtainable by solving the separable differential equation (2.36). A graphical representation of the solution is shown in Fig. 2.8.

$$(\frac{\lambda}{\lambda_o})^2 = -2(1 - 4\tau + 2\tau^2)\,. \tag{2.39}$$

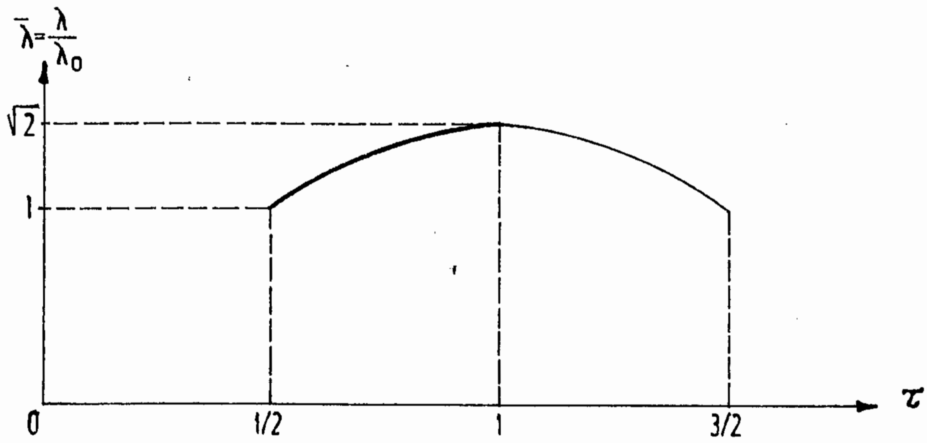

Fig. 2.8 - Variation of $\bar{\lambda}$ with time

It will be shown that the solution for $\bar{\lambda}$ is only physically meaningful for the period $\frac{1}{2} \leq \tau \leq 1$ as the second phase will always end at some time $\tau \leq 1$ dependent on the value of the shell parameter c. It can be seen from Fig. 2.8 that $\dot{z} > \dot{y}$, since $\bar{\lambda}$ increases over the time period of interest. The second phase ceases once $z = 0$ and the third phase continues over the period that $\bar{\lambda}$ approaches unity.

Now that the solution for λ is available it is relatively easy to obtain an expression for z as a function of time.

Using $d\tau = \frac{N_o}{\rho R v_o} . dt$ equation (2.37) can be rewritten as

$$\frac{dz}{d\tau} = - \frac{\lambda_o}{(\frac{\lambda}{\lambda_o})\ \bar{v}_2} . \tag{2.40}$$

Substituting equations (2.39) and (2.28) into equation (2.40) results in the separable differential equation,

$$\frac{dz}{d\tau} = \frac{-\lambda_o}{(1-\tau)\sqrt{-2+8\tau-4\tau^2}} .$$

which, in order to solve, is rewritten

$$\int_{L-\lambda_o}^{z} dz^* = -\lambda_o \int_{\frac{1}{2}}^{\tau} \frac{d\tau^*}{(1-\tau^*)\sqrt{-2+8\tau^*-4\tau^{*2}}}$$

The right hand side is solved by making use of the substitution $u = \frac{1}{1-\tau^*}$

and integrating between the limits u and 2. The solution for z is thus,

$$z = L - \lambda_o \left[1 + \frac{1}{\sqrt{2}} \ln \left\{ \frac{1 + \sqrt{-1 + 4\tau - 2\tau^2}}{(2 + \sqrt{2})(1 - \tau)} \right\} \right] . \tag{2.41}$$

It is now possible to investigate at what time, τ_{II}, the second phase ends. To do so it is necessary to put $z = 0$ in equation (2.41) and solve for τ_{II}. This requires the solution of

$$\frac{L}{\lambda_o} = 1 - \frac{1}{\sqrt{2}} \ln \left\{ \frac{1 + \sqrt{-1 + 4\tau_{II} - 2\tau_{II}^2}}{(2 + \sqrt{2})(1 - \tau_{II})} \right\} . \tag{2.42}$$

Unfortunately it is impossible to obtain τ_{II} explicitly as a function of L/λ_o. It is clear, however, that the right hand side of equation (2.42) is defined for $\frac{1}{2} \leq \tau_{II} < 1$. A plot of L/λ_o versus τ_{II} is shown in Fig. 2.9.

τ_{II}	$\frac{L}{\lambda_o} = \sqrt{c}$	2nd Phase Duration
0,5	1	0
0,6	1,2	0,1
0,7	1,44	0,
0,8	1,75	0,3
0,9	2,25	0,4
0,95	2,75	0,45
0,975	3,23	0,475
0,99	3,88	0,49
0,99	5,51	0,499

<u>TABLE 2:</u> Duration of Second Phase

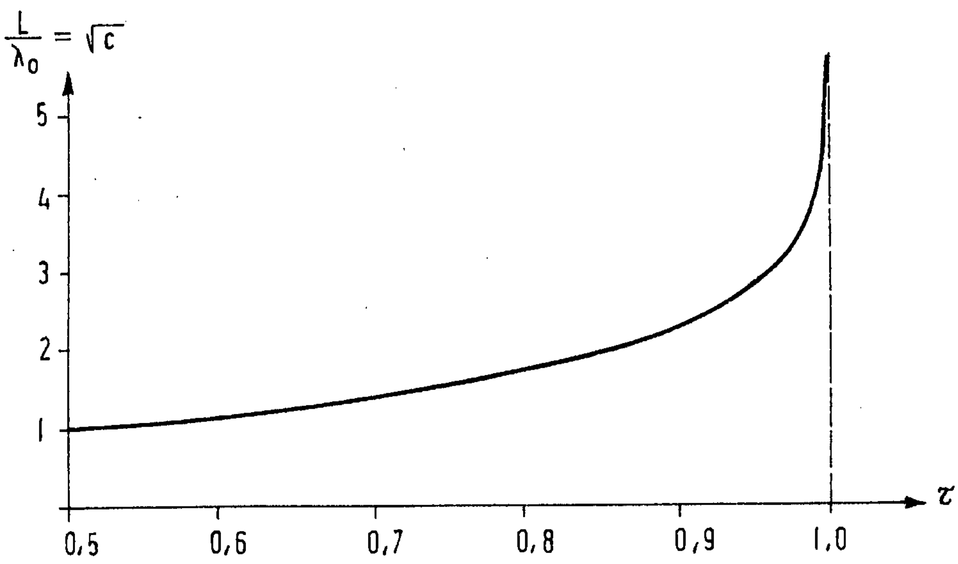

Fig. 2.9 - Time, τ_{II}, at end of Second Phase as a Function of L/λ_o

The solution till the end of the Second Phase is now effectively complete. The moment distribution for the region $z \leq x \leq y$ at a particular instant can be determined from equation (2.29) using equations (2.28), (2.36), (2.38) and (2.41).

No motion occurs for the region $y \leq x \leq L$ and the stress values for this region are $M = - M_o$ and $N = 0$.

Analysis of the Third Phase:

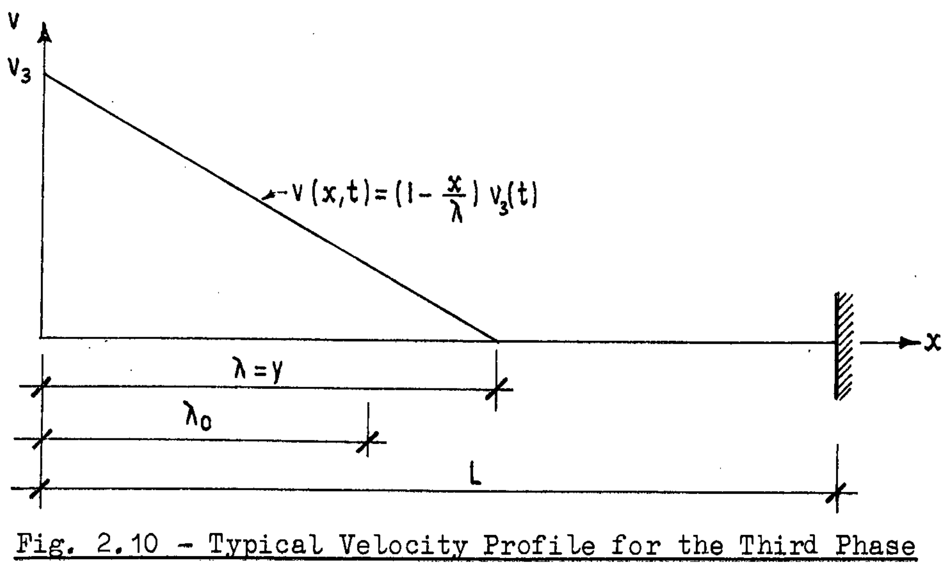

Fig. 2.10 - Typical Velocity Profile for the Third Phase

Again, it is evident from kinematical considerations that,

$$\dot{\kappa}_x > 0 \quad \text{at} \quad x = 0\,,$$

$$\dot{\kappa}_x < 0 \quad \text{at} \quad x = \lambda\,,$$

$$\dot{\kappa}_x = 0 \quad \text{elsewhere}$$

$$\dot{\epsilon}_\phi = (1 - \frac{x}{\lambda})\frac{v_3}{R} \quad \text{for} \quad 0 \leq x \leq \lambda\,,$$

$$\dot{\epsilon}_\phi = 0 \quad \text{for} \quad \lambda \leq x \leq L\,.$$

It clearly follows that

$$\begin{aligned} M &= M_o \quad \text{at} \quad x = 0, \\ M &= -M_o \quad \text{at} \quad x = \lambda, \\ N &= N_o \quad \text{for} \quad 0 \leq x \leq \lambda, \\ N &= 0 \quad \text{for} \quad \lambda \leq x \leq L. \end{aligned} \tag{2.43}$$

For completeness the velocity functions are repeated:

$$v(x,t) = (1 - \frac{x}{\lambda})\, v_3(t) \quad \text{for} \quad 0 \leq x \leq \lambda,$$

and

$$v(x,t) = 0 \quad \text{for} \quad \lambda < x \leq L.$$

The acceleration functions are obtained by differentiating the velocity functions with respect to time:

$$\frac{dv}{dt} = (1 - \frac{x}{\lambda})\frac{dv_3}{dt} - \frac{x\dot{\lambda}}{\lambda^2} v_3 \quad \text{for} \quad 0 \leq x \leq \lambda,$$

and

$$\frac{dv}{dt} = 0 \quad \text{for} \quad \lambda \leq x \leq L. \tag{2.44}$$

<u>Analysis of Region $0 \leq x \leq \lambda$:</u>

Substituting equation (2.44) into the equilibrium equation (2.1) and rearranging:

$$\frac{\partial^2 M}{\partial x^2} = (\frac{N_o}{R} + \rho\,\frac{dv_3}{dt}) + \rho(\frac{\dot{\lambda}}{\lambda^2}\, v_3 - \frac{1}{\lambda}\frac{dv_3}{dt})\; x\,.$$

Integrating twice partially with respect to x leads to the moment equation.

$$M \;=\; \left(\frac{N_o}{R} + \rho\,\frac{dv_3}{dt}\right)\frac{x^2}{2} + \frac{\rho}{6}\left(\frac{\lambda}{\lambda^2}\,v^3 - \frac{1}{\lambda}\,\frac{dv_3}{dt}\right)x^3 + A_x + B. \qquad (2.45)$$

The constants of integration, A and B, are solved using the conditions (2.43).

$$A \;=\; -\frac{2M_o}{\lambda} - \left(\frac{N_o}{R} + \rho\,\frac{dv_3}{dt}\right)\frac{\lambda}{2} - \rho\left(\frac{\dot{\lambda}v_3}{\lambda^2} - \frac{1}{\lambda}\,\frac{dv_3}{dt}\right)\frac{\lambda^2}{6}$$

and

$$B \;=\; -\,M_o.$$

Hence,

$$M \;=\; M_o\left(1 - \frac{2x}{\lambda}\right) + \tfrac{1}{2}\left(\frac{N_o}{R} + \rho\,\frac{dv_3}{dt}\right)(x^2 - \lambda x) + \frac{\rho}{6}\left(\frac{\dot{\lambda}v_3}{\lambda^2} - \frac{1}{\lambda}\,\frac{dv_3}{dt}\right)(x^3 - \lambda^2 x). \qquad (2.46)$$

Once again it is possible to isolate an expression for $\dot{\lambda}$ and dv_3/dt using the conditions $dM/dx\,(0) = dM/dx\,(\lambda) = 0$.

Differentiating equation (2.46) partially with respect to x provides us with

$$\frac{\partial M}{\partial x} \;=\; -\frac{2M_o}{\lambda} + \tfrac{1}{2}\left(\frac{N_o}{R} + \rho\,\frac{dv_3}{dt}\right)(2x - \lambda) + \frac{\rho}{6}\left(\frac{\dot{\lambda}v_3}{\lambda^2} - \frac{1}{\lambda}\,\frac{dv_3}{dt}\right)(x^3 - \lambda^2 x)\;.$$

Application of the shear conditions lead to two related expressions:

$$\begin{aligned} -\frac{2M_o}{\lambda} - \tfrac{1}{2}\left(\frac{N_o}{R} + \rho\,\frac{dv_3}{dt}\right)\lambda - \frac{\rho}{6}\left(\frac{\dot{\lambda}v_3}{\lambda^2} - \frac{1}{\lambda}\,\frac{dv_3}{dt}\right)\lambda^2 &= 0 \\ -\frac{2M_o}{\lambda} + \tfrac{1}{2}\left(\frac{N_o}{R} + \rho\,\frac{dv_3}{dt}\right)\lambda + \frac{2\rho}{6}\left(\frac{\dot{\lambda}v_3}{\lambda^2} - \frac{1}{\lambda}\,\frac{dv_3}{dt}\right)\lambda^2 &= 0. \end{aligned} \qquad (2.47)$$

It is easily shown that $\dot{\lambda} = 0$ when $\lambda^2 = 12M_oR/N_o (= \lambda_o^2)$ by substituting zero for $\dot{\lambda}$ in equations (2.47) and solving for λ. This condition defines the end of the third phase. Nothing can yet be said of the radial velocities. The implication is that some non-zero velocities would be present after time τ_{III}, at which the end of the third phase occurs. This motion would constitute the fourth and final phase of the total deformation. Fig. 2.11 depicts the expected velocity profile for the fourth phase.

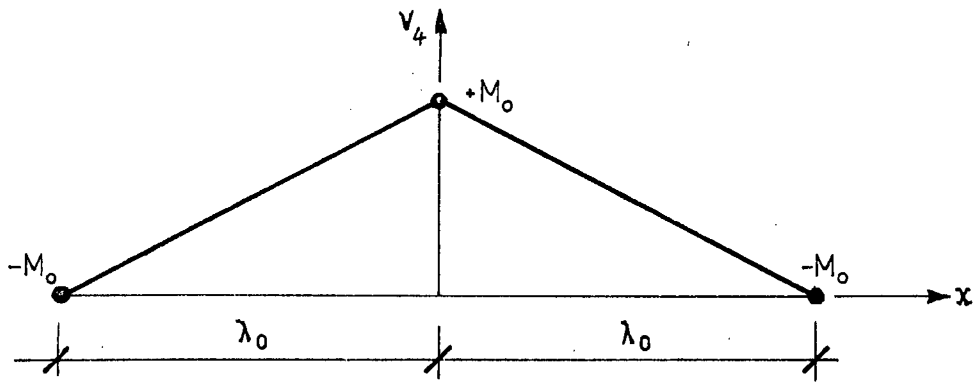

Fig. 2.11 - Expected Velocity Profile for the Fourth Phase
(For the full shell)

The velocity profile of Fig. 2.11 fulfils the conditions for the mode shape of Martin and Symonds [1], however, it appears that the fourth phase never occurs, except instantaneously at the end of the third phase. In other words λ approaches λ_o simultaneously as v_3 approaches zero. This is more fully discussed later.

Equations (2.47) can be manipulated to extract simplified expressions containing $\dot{\lambda}$ and dv_3/dt.

They are

$$\frac{dv_3}{dt} = -\frac{N_o}{\lambda R}\left\{\left(\frac{\lambda_o}{\lambda}\right)^2 + 1\right\}$$

and

$$\lambda = \frac{N_o}{\rho R}\left\{\frac{\lambda_o^2}{\lambda v} - \frac{\lambda}{v}\right\} . \qquad (2.48)$$

Using the already described substitutions

$$\bar{\lambda} = \frac{\lambda}{\lambda_o}, \quad \bar{v}_3 = \frac{v_3}{v_o} \quad \text{and} \quad \tau = \frac{N_o t}{\rho R v_o}$$

equations (2.48) may be rewritten non-dimensionally as

$$\frac{d\bar{v}_3}{dt} = -\left(\frac{1}{\bar{\lambda}^2} + 1\right) ,$$

$$\frac{d\bar{\lambda}}{d\tau} = \frac{1}{\bar{v}_3}\left(\frac{1}{\bar{\lambda}} - \bar{\lambda}\right) . \qquad (2.49)$$

The non-dimensional forms are preferred as they lend themselves more easily to a computerised numerical solution. It is impossible to obtain closed-form solutions to equations (2.49). In any event explicit expressions for the initial conditions, v_{II} and λ_{II} are unavailable.

In passing, it should be noted that, at the end of the third phase, $dv_3/dt = -2N_o/\lambda R$, and would remain so for the duration of the expected fourth phase. This information is obtained from equation (2.43) on setting $\lambda = \lambda_o$. This corresponds to the result obtained from the analysis of the second phase of the short shell deformation, which see equation (2.19). On differentiating equation (2.19) and setting $c = 1$, $dv_2/dt = -2N_o/\lambda R$ is obtained.

Equations (2.49) are rewritten using the first order finite difference substitutions:

$$\frac{d\bar{v}}{d\tau} = \frac{\bar{v}_{i+1} - \bar{v}_i}{\Delta\tau},$$

$$\frac{d\bar{\lambda}}{d\tau} = \frac{\bar{\lambda}_{i+1} - \bar{\lambda}_i}{\Delta\tau},$$

which after rearrangement of terms become

$$\begin{aligned} \bar{v}_{i+1} &= -\Delta\tau\left(\frac{1}{(\bar{\lambda}_i)^2} + 1\right) + \bar{v}_i , \\ \bar{\lambda}_{i+1} &= \frac{\Delta\tau}{\bar{v}_i}\left(\frac{1}{\bar{\lambda}_i} - \bar{\lambda}_i\right) + \bar{\lambda}_i . \end{aligned} \qquad (2.50)$$

The subscript 3 in $\bar{v}_3$ has been omitted.

For any particular shell with length, radius, wall thickness and material properties known, it is thus possible to effect a complete solution based on the results of a numerical treatment of the equations (2.50). Naturally the values of $\bar{v}_3 = \bar{v}_3(\tau_{II})$ and $\bar{\lambda} = \bar{\lambda}(\tau_{II})$ must be obtained as a first step to the numerical solution. The value of τ_{II} is obtained from equation (2.42), that of $\bar{v}_I$ from equation (2.28) and that of λ_{II} from equation (2.39).

Small time increments, $\Delta\tau$, are chosen. The smaller $\Delta\tau$ is, the more accurate is the solution. The solution was performed by a UNIVAC 1108 computer using $\Delta\tau = 0{,}0001$. The calculation was allowed to run until $\bar{\lambda}$ became equal to or just less than unity. In all cases v_3 approached zero simultaneously as $\bar{\lambda}$ approached unity. It is on this evidence that the conclusion of the non-existence of a fourth phase of motion is based. This is certainly not a rigorous proof and it is indeed possible that a discrete fourth phase follows the third. However, from the practical viewpoint of calculating deformations the effect of this final phase is certainly negligible.

Maximum Radial Deformation:

The maximum radial deformation can be readily determined by integrating the central velocities with respect to time. A non-dimensional plot of velocity versus time is shown in Figure 2.12.

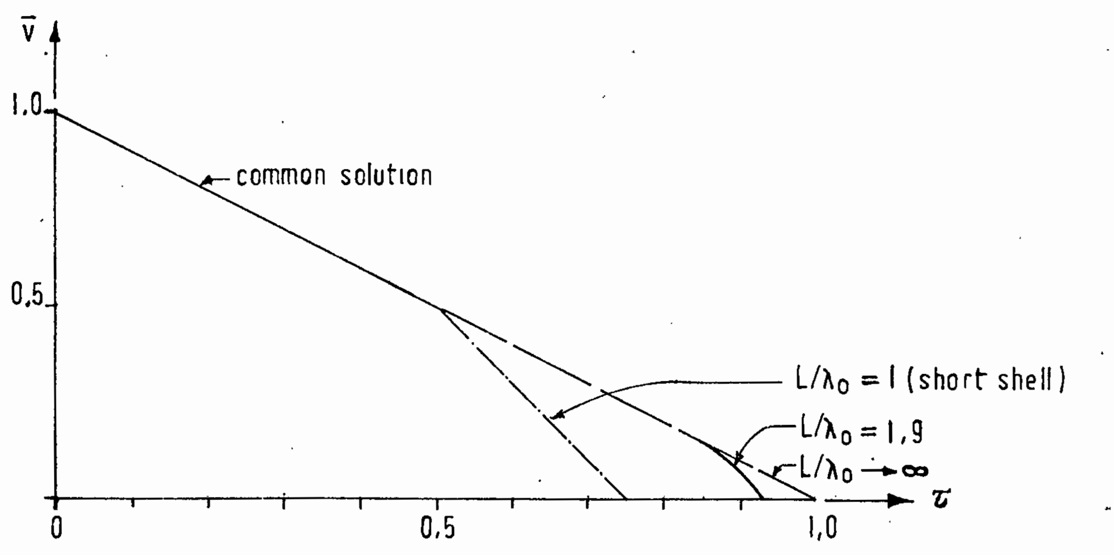

Fig. 2.12 - Non-dimensional Plot of Central Velocity versus time

A cursory inspection of Fig. 2.12 and Fig. 2.13 (a plot of $\int \bar{v}d\tau$ vs L/λ_0) readily reveals that

$$\int_0^{\tau_F} \bar{v}\,d\tau \doteqdot \tfrac{1}{2} \qquad \text{for } \frac{L}{\lambda_0} \geq 1{,}5 \tag{2.51}$$

For virtually all practical purposes of estimating the central deformation of long shells, this generalization is valid.

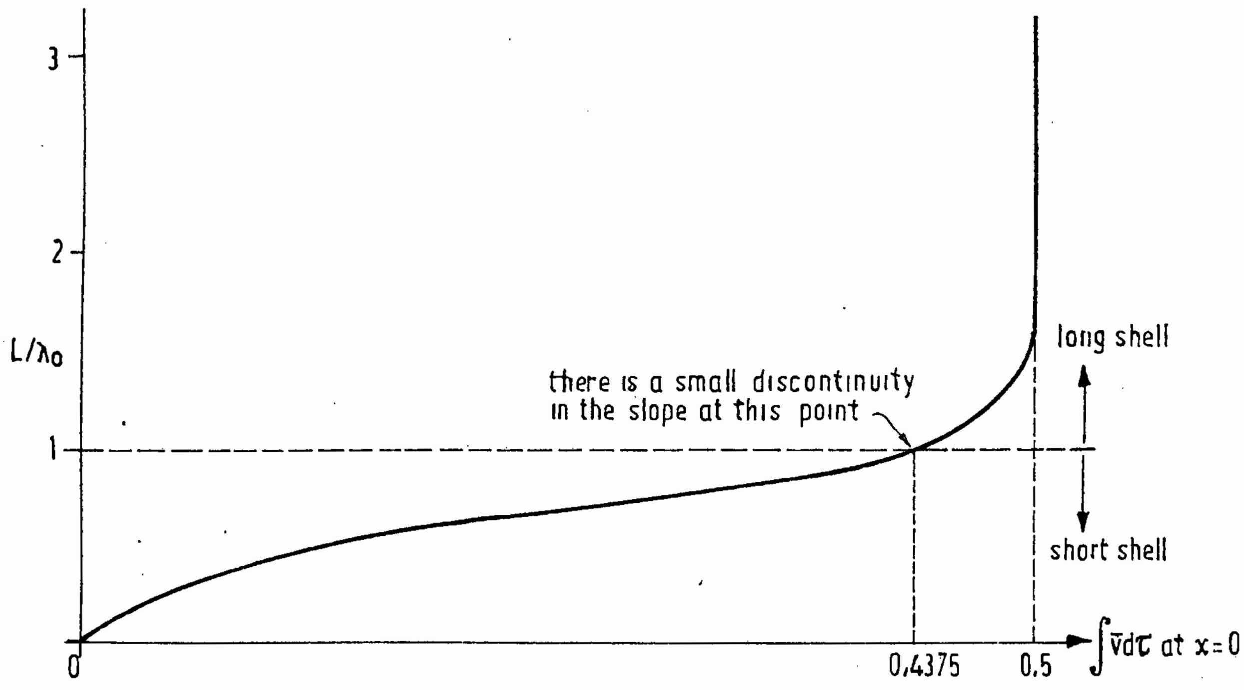

Fig. 2.13 - Non-dimensional Maximum Displacement versus L/λ_o

The actual central displacement, w_c, is given by

$$w_c = \int_0^{t_f} v \, dt = \frac{\rho R v_o^2}{N_o} \int_0^{\tau_F} \bar{v} \, d\tau \qquad (2.52)$$

The final deformation profile was calculated numerically and the result for the specific case of $L/\lambda_o = 1,9$ is shown in Figure 2.14. A time incremental procedure was used and the integration was effected taking due cognisance of the appropriate operating velocity function.

$\bar{x}$	$\bar{w}$
0	0,495
0,1	0,494
0,2	0,492
0,3	0,487
0,4	0,478
0,5	0,462
0,6	0,434
0,7	0,383
0,8	0,305
0,9	0,182
1,0	0

TABLE 3: Non-dimensional Long Shell Deformation Profile $L/\lambda_o = 1,9$

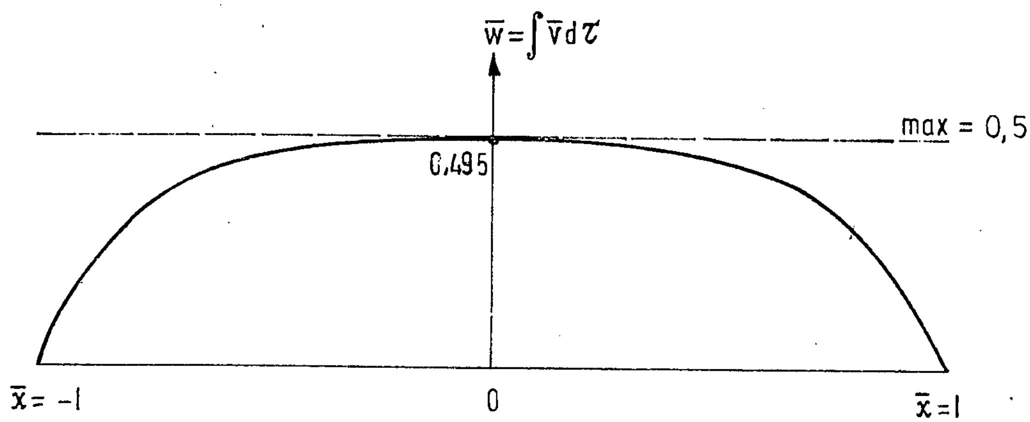

Fig. 2.14 - Non-dimensional Deformation Profile for Long Shell $L/\lambda_o = 1,9$

This concludes the exact rigid plastic analysis.

3. DISCUSSION OF THE RESULTS OF SECTION 2

Expressions for the maximum deformation experienced by a circular cylindrical shell under uniform impulsive loading have been developed. In so far as a 'square' yield domain was used as the basis for the analysis we have assumed the structure to be somewhat stiffer than it actually is. Hodge [5] reported that collapse loads may be predicted with approximately 12,5 % accuracy by this simple domain, but that similar accuracies may not apply to displacements.

In order that the reader may get a feeling for the relative values of the shell variables L, R and H for short and long shells, we shall briefly look at a typical case.

Consider a shell with $L = R = 50$ mm; for the shell to be on the boundary of the two types, $c = 1$ or

$$\frac{L^2}{3RH} = 1.$$

Hence, $$H = \frac{50}{3} \text{ mm.}$$

This is clearly a rather solid shell and there would be real practical difficulties in deforming such a shell significantly under laboratory test conditions. As a first step it would be sensible to investigate the response of shells with variables in the order of $(L, R, H) = (50, 50, 2)$ mm.

For such shells, c, would be approximately 8. Hence using equations (2.51), (2.52) and $N_o = \sigma_o H$ the expression for the maximum deformation, w_c, simplifies to

$$w_c = \frac{\rho R v_o^2}{2\sigma_o H}.$$

If we define I as the impulse per unit area of the curved surface, the expression for w_c can be rewritten as

$$w_c = \frac{RI^2}{2\rho\sigma_o H}. \tag{3.1}$$

For very long shells ($c > 1,5$) the response duration is given by $\tau = 1$ or

$$t = \frac{\rho R v_o}{\sigma_o H} = \frac{RI}{\sigma_o H} . \tag{3.2}$$

Equation (3.1) loses validity once the pressure pulse duration exceeds the response time given by equation (3.2).

It is of interest to compare this expression to that of the deformation of a uniformly impulsively loaded rigid plastic ring of length $2L$, radius R and wall thickness H. The ring deforms uniformly by the amount Δ. The circumferential strain is Δ/R and the energy dissipated as plastic work is $2\pi\Delta(2LH\sigma_o)$. The initial kinetic energy of the shell wall is $\frac{1}{2}\rho v_o^2 (2\pi R.2L)$ which in terms of the impulse $I(=\rho v_o)$ is $I^2/\rho(2\pi LR)$.

On equating the initial kinetic energy to the non-recoverable energy dissipated as plastic work, an expression involving the uniform deformation, Δ, is obtained. This simple treatment ignores the recoverable energy that would be temporarily stored as elastic strain energy, however, if the initial energy of the disturbance is a factor of three or higher than the elastic potential of the ring, the approximation for Δ is good.

It should be noted that the effect of finite deflections can easily be included in this simple treatment but this is ignored for the present.

The expression for Δ is

$$\Delta = \frac{RI^2}{2\rho\sigma_o H} ,$$

which is identical to equation (3.1). This result indicates that for shells where L/λ_o is approximately equal to or greater than 1,5, the end support conditions have a negligible effect on the final central deformations. It is evident that for such shells the circumferential forces play the major part in limiting the deformation whereas the longitudinal moments play a very small role.

In passing, another observation can be noted.

The factor,

$$\frac{c(4 + 3c)}{(1 + c)(1 + 3c)} ,$$

in equation (2.23) rapidly approaches unity as c increases. Thus the expression for maximum deformations in the case of short shells is nearly similar to that for maximum long shell deformations for $c \geq 1$.

4. APPROXIMATE METHODS

4.1 Bounds on Displacements and Response Time

The approximate method here discussed, first described by Martin [12], requires that initially, at time $t = 0$, the velocity be prescribed at all points, i, on the structure. At times $t > 0$ either the displacement rates, $\dot{u}_i$, or the surface fractions, T_i, are zero. Changes in geometry are ignored. As plastic deformation is a dissipative process, no energy can be stored in a rigid-plastic continuum. The velocities must therefore vanish after some time, t_f.

The deformation time, t_f, can be bounded from below and it has been shown that

$$t_f \geq \frac{\int_V \rho^* \, v_i \, u_i^c \, dV}{D(u_i^c) - \int_V F_i \, u_i^c \, dV}, \tag{4.1}$$

where,

ρ^* is the volume density,

v_i are the initial prescribed velocities,

$\dot{u}_i^c$ is any postulated time independent, kinematically admissible velocity field,

$D(\dot{u}_i^c)$ is the corresponding power of dissipation,

F_i are the body forces,

V = volume of the continuum.

Martin demonstrated that there is an upper bound, δ_f, on the displacements and

$$\delta_f \leq \frac{\int_V \frac{\rho^*}{2} v_i \, v_i \, dV}{R^L} = \frac{K_o}{R^L}, \tag{4.2}$$

where,

K_o is the total kinetic energy imparted by the initial disturbance to the structure and

R^L is the static limit load. (Normally a point load at the point under consideration).

4.1.1 Bounds for a Short Shell

The rigid plastic expressions (2.20) and (2.23) for the deformation time and maximum displacement of a short shell are quoted for convenience:

$$t_F = \frac{\rho R v_o}{N_o} \left(\frac{3c}{1 + 3c}\right), \tag{4.3}$$

$$w_c = \frac{\rho R v_o^2}{N_o} \frac{c}{2} \frac{(4 + 3c)}{(1 + c)(1 + 3c)} . \tag{4.4}$$

Provided that $c = \frac{L^2}{3RH} \leq 1.$

In this case it is known that the initial velocities $v_i = v_o$ everywhere.

Knowing the results of the analysis of Section 2 it is easy to select a final deformation rate field, $\dot{u}_i^c$. Such a field corresponds exactly to that of the second phase of the deformation of the short shell and is shown in Fig. 4.1.

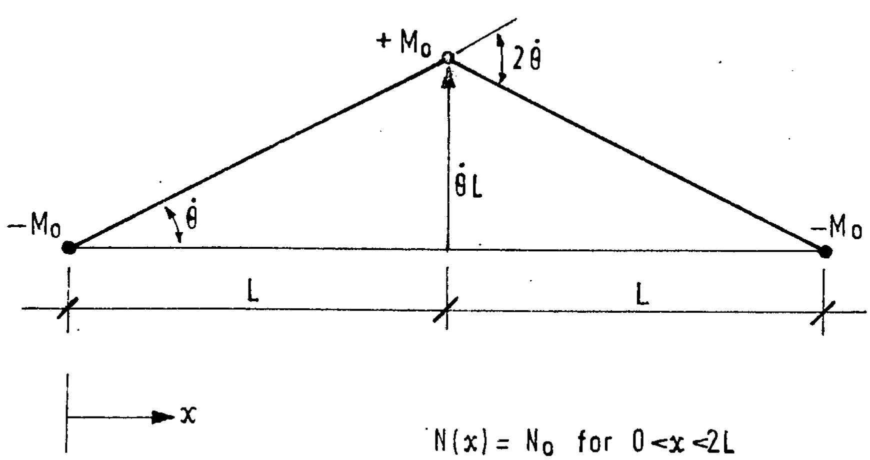

Fig. 4.1 - Circumferentially Non-varying Final Deformation Rate Field for a Short Shell

The quantities M_o and N_o retain the same meaning and the body forces are neglected. The terms in equation (4.1) become,

$$\int_S \rho\, v_i\, \dot{u}_i^c\, dS = 2\int_0^L 2\pi R\, \rho\, v_o\, x\, \dot{\theta}\, dx,$$

$$= 2\pi R\, \rho\, v_o\, L^2\, \dot{\theta}$$

and

$$D(\dot{u}_i^c) = 4M_o\, \dot{\theta}\, (2\pi R) + 2\left[\frac{L\dot{\theta}}{2}.\frac{1}{R}.2\pi R.2LN_o\right],$$

$$= 2\pi\, \sigma_o\, H\, \dot{\theta}\, [RH + 2L^2].$$

Hence,

$$t_f \geq \frac{\rho R v_o}{\sigma_o H}\left[\frac{L^2}{RH + 2L^2}\right].$$

It can be easily shown that the above equality is identical to equation (4.3).

In order that the bound on the maximum final displacement may be computed, it is necessary that central static limit ring load be known. This problem has been investigated by various researchers including Prager [16] who found the static limit ring load, P_R, based on the exact yield domain. This is;

$$P_R = 1{,}82\, \sigma_o H \sqrt{\frac{H}{R}} \text{ per unit length of the circumference.}$$

Hence, an upper bound on the maximum displacement is

$$\delta_f \leq \frac{\int_S \rho v_o^2\, dS}{2\pi R\, .\, P_R}$$

or

$$\delta_f \leq \frac{\rho L v_o^2}{1{,}82\, \sigma_o H \sqrt{\frac{H}{R}}}.$$

This can be written in terms of c as

$$\delta_f \leq \frac{\rho R v_o^2}{1{,}82 \sigma_o H}\sqrt{3c}\,. \qquad (4.5)$$

This upper bound exceeds the value obtained from the exact analysis by approximately a factor of two for values of c close to unity. (Note that the analysis as set out in Section 2 is referred to as the exact analysis)

4.1.2 Bounds for Long Shells

Little can be said about the bounds as applied to long shells. A possible displacement rate field, $\dot{u}_i^c$, is one similar to that of Fig. 4.1 but with $L = \sqrt{3HR}$. As previously stated this field only exists instantaneously at the end of the motion but if used, the analysis follows that for the short shell. The results for t_f and δ_f will be similar to those for short shells but with $c = 1$. Hence, for long shells,

$$t_f \geq \frac{\rho R v_o}{\sigma_o H}(0{,}75),$$

$$\delta_f \leq \frac{\rho R v_o^2}{1{,}82\ \sigma_o H}(\sqrt{3}).$$

The exact analysis provided us with the expressions

$$t_f = \frac{\rho R v_o}{\sigma_o H}$$

and

$$\delta_f = \frac{\rho R v_o^2}{2\sigma_o H}$$

for $c > 1{,}5$ approximately.

The results of the exact analysis therefore fall within the bounds of the theorem. Not much, however, can be said of the relative accuracies of the two methods except to note that the exact analysis was based on an approximated and stiffer yield domain while the bound was calculated using the correct yield domain.

4.2 Mode Approximations

This method, devised by Martin and Symonds [1], is an extension of the method of Section 4.1. It also requires that a time independent deformation shape, known as the mode shape, be available. The mode approximation equations follow:

$$u^{(1)} = \tfrac{1}{2}\, v_i\, t_f^*\ ,$$

$$u^{(2)} = \tfrac{1}{2}\, w(s_i)\, \frac{\int_S \rho\ v_i\ w\ dS}{\int_S \rho\ w\ w\ dS}\, t_f^*\ ,$$

$$\int_S \rho\ v_i\ w\ dS = 2\int_0^L 2\pi R\ \rho\ v_o \frac{x}{L}\,dx$$

$$= 2\pi R\ \rho\ v_o\ L\ ,$$

$$\int_S m\ w\ w\ dS = 2\int_0^L 2\pi R \quad (\frac{x}{L})^2\,dx$$

$$= \frac{4}{3}\,\pi R\ \rho\ L\ ,$$

$$\int_S D(\dot{q}^w)\ dS = 4(\frac{1}{L})\ 2\pi R\ M_o + 2[\pi\ N_o\ L]$$

$$= 2\pi(\frac{4RM_o}{L} + N_o\ L)\ .$$

Hence, from equations (4.6) and using $c = L^2/3HR$,

$$t_f^* = \frac{\rho R v_o}{\sigma_o H}\,(\frac{3c}{1 + 3c}) \qquad \text{as before,}$$

$$u^{(1)} = \frac{\rho R v_o^2}{2\sigma_o H}\,(\frac{3c}{1 + 3c})\ ,$$

$$u^{(2)} = \frac{3}{2}\,u^{(1)}\ .$$

The rigid plastic result, equation (2.23), lies between the two bounds, $u^{(1)}$ and $u^{(2)}$, for all values of c.

4.2.2 Mode Approximations for Long Shells.

Although no mode shape appears to exist in this case, the central radial acceleration is similar to that of the short shell at the cessation of motion. Thus, if a mode shape similar to that shown in Fig. 4.2, with L replaced with $\sqrt{3RH}$, is utilised, the expressions for t_f^*, $u^{(1)}$ and $u^{(2)}$ are found to be;

$$t_f^* = \frac{3}{4}\,\frac{\rho R v_o}{\sigma_o H}\ ,$$

$$u^{(1)} = \frac{3}{4}\,\frac{\rho R v_o^2}{2\sigma_o H}\ . \tag{4.7}$$

$$u^{(2)} = \frac{9}{8}\,\frac{\rho R v_o^2}{2\sigma_o H}\ .$$

Whereas the central displacement obtained from long shell theory is

$w_c = \rho R v_o^2 / 2\sigma_o H$ for $c > 1{,}5$ approximately, it is apparent that the two bounds $u^{(1)}$ and $u^{(2)}$ are close in value and that the value obtained from the exact analysis lies between them. Thus, the results of the two methods are in good accord for both short and long shells. Fig. 4.3 depicts non-dimensional $\bar{u}^{(1)}$, $\bar{u}^{(2)}$ and $\bar{w}_c$ plotted against c, where

$$u^{(1)} = \bar{u}^{(1)} \frac{\rho R v_o^2}{2\sigma_o H}, \quad u^{(2)} = \bar{u}^{(2)} \frac{\rho R v_o^2}{2\sigma_o H}, \quad w_c = \bar{w}_c \frac{\rho R v_o^2}{2\sigma_o H}.$$

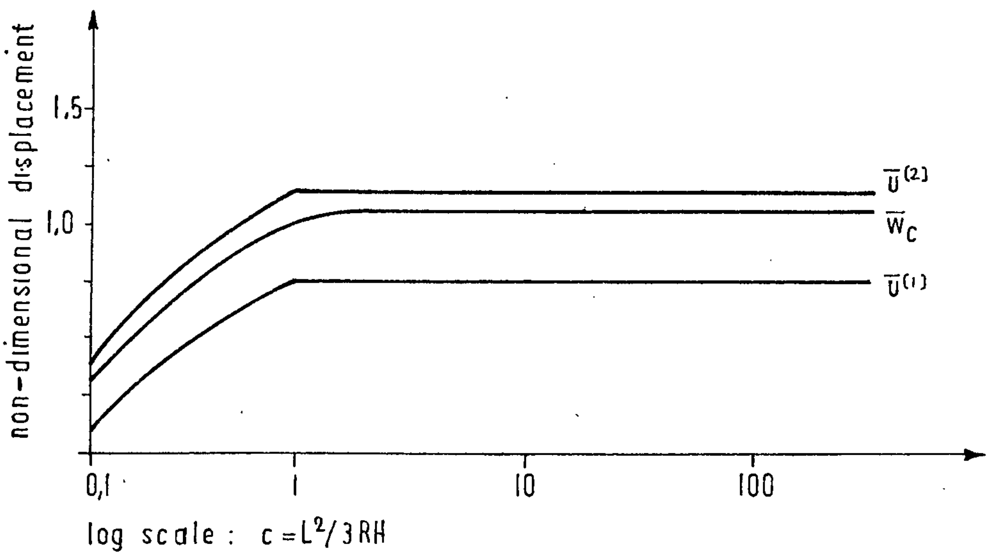

Fig. 4.3 - Comparison of the Mode Method and Exact Solution

5. RATE SENSITIVITY AND STRAIN HARDENING EFFECTS

5.1 Rate Sensitivity Effects

Hodge [2] reported that the degree of end fixity has a negligible effect on the response of long circular cylindrical shells subjected to pressure loadings. In addition, it is evident from Fig. 2.5 that the degree of end fixity has a small effect on the response of short shells. Moreover, in the case of long shells, the fact has emerged that the end conditions have a negligible effect on the final displacements of the central region. The central region, thus, behaves as a ring with zero end fixity. This result was discussed in Section 3. In view of the above, the problem of the long cylindrical shell, in respect of maximum deformation, has degenerated to that of a ring. In the case of a ring expanding uniformly, the only operative stresses are circumferential and the inclusion of rate effects is relatively simple.

Following previous investigations [3], the yield stress-strain law for perfectly plastic rate sensitive materials is assumed to be of the following form:-

$$\frac{\sigma}{\sigma_y} = 1 + \left(\frac{\dot{\varepsilon}}{D}\right)^{1/n}, \qquad (5.1)$$

where $\dot{\varepsilon}$ = strain rate,

σ_y = static yield stress,

σ = dynamic yield stress,

D,n = material constants.

The material constants, D and n, must be determined experimentally. Perrone [9] quoted the values,

$n = 5$, $D = 40,4$ per second for mild steel

and $n = 4$, $D = 6500$ per second for 6061 T6 aluminium alloy.

(6061T6 Al. corresponds to D65S South African Al.)

Analysis of the Expanding Ring:

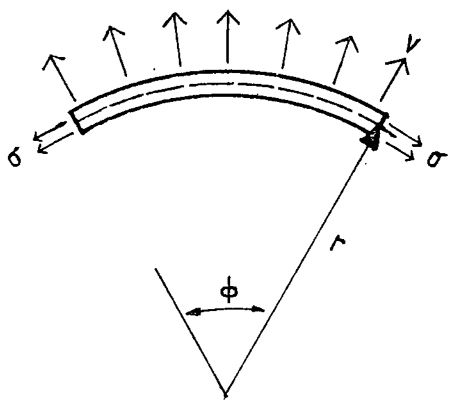

Fig. 5.1 - Element of Expanding Ring

The following variables are defined (some of which are already familiar):

v_o = initial, uniform radial velocity.
v = current radial velocity.
R = initial radius of the median surface.
r = current location of the median surface.
ρ^* = mass density.
t = time.
A_o, A = initial and deformed cross-sectional area.
ϵ = v/r, the true strain rate.

The equilibrium equation for the ring is easily obtained from consideration of Fig. 5.1. It is

$$2A\sigma \sin\frac{\phi}{2} + \rho^* r\phi A \frac{dv}{dt} = 0 .$$

Using $\sin\frac{\phi}{2} = \frac{\phi}{2}$ and simplifying, we obtain

$$\rho^* r \frac{dV}{dt} = -\sigma . \qquad (5.2)$$

The dynamic yield stress, σ, in equation (5.2) is replaced using equation (5.1),

$$\frac{dV}{dr} = \frac{d^2r}{dt^2} \quad \text{and} \quad \dot{\epsilon} = \frac{v}{r}.$$

Hence,

$$\rho^* r \frac{d^2r}{dt^2} = - \sigma_y \left[1 + \left(\frac{v}{rD}\right)^{1/n}\right]. \tag{5.3}$$

Using $\frac{d^2r}{dt^2} = \frac{1}{2}\frac{d(v^2)}{dr}$ equation (5.3) may be rewritten as

$$\frac{d(v^2)}{dr} = - \frac{2\sigma_y}{\rho^* r} - \frac{2\sigma_y}{\rho^*} \cdot \frac{1}{r^{1+1/n}} \left(\frac{v}{D}\right)^{1/n}. \tag{5.4}$$

Equation (5.4) is expressed in the non-dimensional form as

$$\frac{d\bar{V}}{d\bar{r}} = - \frac{\gamma \bar{V}^{\frac{1}{2}n}}{\bar{r}^{1+1/n}} - \frac{\alpha}{\bar{r}}, \tag{5.5}$$

where, $\bar{V} = \left(\frac{v}{v_o}\right)^2,$

$$\bar{r} = \frac{r}{R},$$

$$\alpha = \frac{2\sigma_y}{\rho^* v_o^2},$$

$$\gamma = \alpha \left(\frac{v_o}{RD}\right)^{1/n}.$$

Equation (5.5) is non-linear and a closed form solution is unobtainable. However, a numerical solution is easily obtainable by employing the first order finite difference approximation,

$$\frac{d\bar{r}}{d\bar{V}} = \frac{\bar{r}_{i+1} - \bar{r}_i}{\Delta \bar{V}},$$

and programming a computer to perform the solution.

The equation requiring treatment is

$$\bar{r}_{i+1} = - \Delta\bar{V} \left[\frac{1}{\frac{\gamma \bar{V}^{\frac{1}{2}n}}{\bar{r}^{1+1/n}} + \frac{\alpha}{\bar{r}_i}} \right] + \bar{r}_i, \tag{5.6}$$

where the initial condition is $\bar{V}(0) = 1$
and the final condition is $\bar{V}(t_F) = 0.$

Perrone [2] has shown that for simple structures, differences of up to only 6% exist between exact rate sensitivity solutions and rigid plastic solutions where the dynamic yield stress is assumed constant but has the value dependent upon the strain rate as defined by equation (5.1). The reason being that the bulk of the initial kinetic energy is dissipated before the stresses in the deforming material drop appreciably from the initial value.

Hence, for rate sensitive materials, insertion of the modified yield stress into equation (3.1) or (5.7) can be expected to produce reasonable results.
Equation (3.1) can be marginally improved to take account of finite deflections by allowing the initial wall thickness, H, to vary as h. The result is derived in the following.

Equate the initial kinetic energy, K, to the plastic energy dissipated in deforming the ring by an amount Δ. (The ring has length 2L)

Hence,

$$K = \int_R^{R+\Delta} 2Lh\sigma_o \,.\, 2\pi \, dr \,.$$

Using,

$$h = \frac{RH}{r} \,, \quad K = \tfrac{1}{2}(2L.2\pi R.H\rho^*)\, v_o^2$$ and integrating and rearranging:

$$\Delta = R\left(e^{\frac{\rho^* v_o^2}{2\sigma_o}} - 1\right) .$$

In terms of an impulse per unit area, I, the expression for the final deformation can be rewritten as

$$\Delta = R\left(e^{\left\{\frac{I^2}{2\rho^*\sigma_o}\right\}} - 1\right) .$$

5.2 Inclusion of Strain Hardening Effects

The mathematical model demonstrating a rigid linear strain hardening material is shown in Fig. 5.2. The yield stress, σ_o, and the strain hardening rate, C, are the two pertinent material parameters. For a perfectly plastic material, the strain hardening rate would be zero.

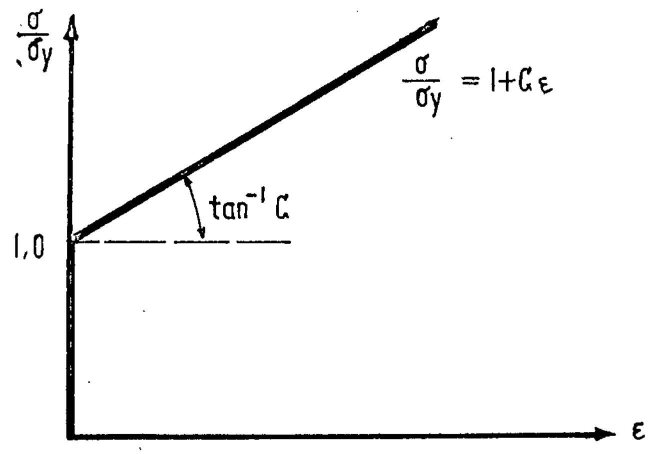

Fig. 5.2 - Rigid Linear Strain Hardening Material

Malvern [19] recommended the model of strain hardening rate sensitive behaviour shown in equation (5.8).

$$\dot{\epsilon} = f\,[\,\sigma(\epsilon) - \sigma_y\,]\;. \qquad (5.8)$$

Both the laws of equations (5.1) and (5.8) suffer in analytical applications from very strong non-linearities. A product type strain hardening rate sensitivity law has been introduced [19] which delineates the strain hardening and rate sensitivity aspects. An example of such a law is shown in equation (5.9):

$$\frac{\sigma}{\sigma_y} = \left[1 + \left(\frac{\dot{\epsilon}}{D}\right)^{1/n}\right](1 + C\epsilon)\;. \qquad (5.9)$$

In the case of a ring

$$\epsilon = \bar{r} - 1\;.$$

If similar lines to those of Section 5.1 are followed, the equation of motion may be readily derived. It is

$$\frac{dv}{dr} = -\frac{2v_o}{\rho^* v_o^2}\left[1 + \left(\frac{\dot{\epsilon}}{D}\right)^{1/n}\right]\left[\frac{1 + C(\bar{r} - 1)}{\bar{r}}\right]. \qquad (5.10)$$

Equation (5.10) may be expressed in the more convenient non-dimensional form as

$$d\bar{r} = \frac{-\,d\bar{V}}{\left[\alpha + \dfrac{\bar{V}^{\frac{1}{2}n}}{\bar{r}^{1/n}}\gamma\right]\left[\dfrac{1 + C\,(\bar{r} - 1)}{\bar{r}}\right]} \,. \tag{5.11}$$

The variables retain their previous meanings.

As in Section 5.1, a numerical solution to equation (5.11) is readily obtainable by replacing the differential quantities by finite changes and programming a computer to accomplish the integration. As previously stated the initial values of $\bar{r}$ and $\bar{V}$ are both unity. It is a simple matter to compute the response time by calculating and summing the time for each incremental step. The necessary program was written for a WANG 720 C programmable calculator and an increment of $\Delta\bar{V} = -\,0{,}002$ was chosen. The results are compared to experimental test results in the following section.

6. EXPERIMENTAL RESULTS

6.1 Introduction

Tests were performed on shell specimens machined from 150 mm solid rounds of annealed D65S aluminium alloy. The South African D65S is the equivalent of the American 6061 T6 alloy. The material was purchased in two consignments. Tensile tests were done in order to determine points of first yield, the strain hardening characteristics and the ultimate strength of the material. Tensile test specimens were cut in three mutually orthogonal directions from the waste for each shell specimen. The material from the first consignment did not vary in behaviour by more than about 2 % with respect to all parameters. Material from the second consignment varied considerably in behaviour with regard to first yield and ultimate strength. The material was, however, found to be essentially isotropic in all cases for particular shell specimens. Fig. 6.1 shows a typical stress-strain curve for the material from the first consignment.

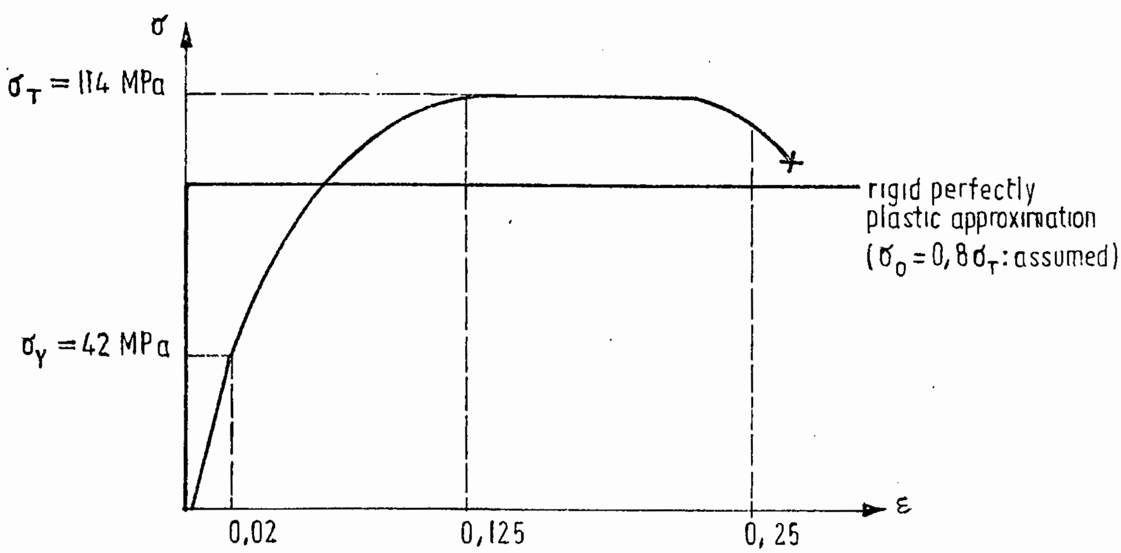

Fig. 6.1 - Stress-Strain Relation for Annealed D65S Al. Alloy

The material from the second consignment was generally higher in strength and proved to be less ductile. The supposition was that the second batch was not fully annealed as specified. The properties are given in Table 6.1.

EXPERIMENTAL RESULTS

SHELL SPECIMENS									MATERIAL PROPERTIES				THEORETICAL PREDICTIONS				
Shell No.	H	I	Peak Pressure	L_c	Pulse Duration	v_o	δ_f actual	Comments	Ultimate Yield σ_T	First Yield σ_y	c	Ductility (Strain to fracture)	Rate sensitivity and strain hardening		Rigid Plastic		E_t/E_e
	mm	Pa.s	MPa	cm	μs	m/s	mm		MPa	MPa		%	δ_f mm	t_f μs	δ_f mm	t_f μs	
													Eq. (5.11)		Eq. (3.1)	Eq. (3.2)	
													D = 6500/s	D = 6500/s	$\sigma_o \approx 0{,}8 \times \sigma_T$		
1	4,06	231	9,43	20,0	46	20,5	0,664		114	42	33	29	0,424	39,6	0,320	31	9,7
2	2,01	264	8,98	17,5	60	47,5	1,6		114	42	33	29	1,608	61,4	1,703	72	52
3	1,91	259	8,98	17,5	53	48,9	1,77		114	42	33	29	1,675	62,0	1,819	74	55
4	2,03	229	7,18	17,5	55	40,9	1,6		114	42	33	29	1,288	57,9	1,256	62	39
5	0,86	200	7,63	17,5	49	83,8		Ruptured	221	121	?						43
6	0,88	174	7,18	12,0	56	71,6	1,514	Buckled	198	117	31	16	1,355	34,8	2,247	62	39
7	0,93	201	7,41	12,0	75?	78,0		Ruptured	132	42	33	20	3,005		4,000		104
8	3,11	220	7,40	17,5	55	25,4	0,343		173	70	30	20	0,404	29,7	0,325	26	6,45
9	1,55	190	7,18	17,5	45	44,1	2,5	Some degree of buckling evident.	114	42	33	29	1,444	59,7	1,485	67	45
10	1,63	214	7,63	18,0	42	47,3	2,05		121	42	35	16	1,573	60,2	1,605	68	46
11	1,63	205	7,6	18,0	45	44,6	1,50		176	65	33	20	1,04	42,6	0,98	45	19

L_c = length of Cordtex

E_t/E_e = ratio of initial shell wall kinetic energy to shell elastic potential (E = 69 GPa)

TABLE 6.1: Experimental Results and Theoretical Predictions

The impulsive loadings were obtained by detonating a length of Cordtex (PETN detonating fuse) by means of an electrically triggered detonator. A number of preliminary tests were necessary to determine a reasonable experimental configuration. Pressure values with respect to time were measured by an oscilloscope via a pressure transducer. Difficulty was experienced in designing the experimental set up as the transducer was rated for a maximum of only 10 MPa. This necessitated the use of very thin-walled cylinders in order to obtain permanent deformations where the bulk of the energy was dissipated as plastic work. The very thin walled cylinders were particularly vulnerable to rupture. This was primarily due to the walls being punctured by shrapnel from the detonator casing. Efforts were made to shield vulnerable areas from shrapnel.

6.2 The Experimental Configuration

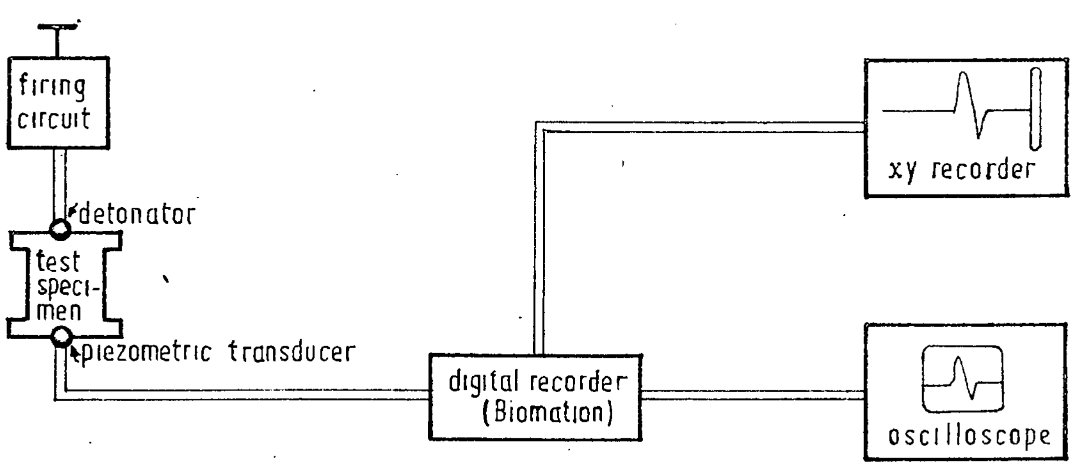

Fig. 6.2 - Schematic Diagram Showing the Main Components of the Experimental Layout

On detonation, the pulse, as recorded by the transducer, triggered the digital recorder which stored the information. The pulse was simultaneously displayed by the oscilloscope from which the peak pressure could be read. A hard copy of the pulse was produced on the xy recorder from the data held by the digital recorder.

A detailed longitudinal section of the test specimen is shown in Fig. 6.3.

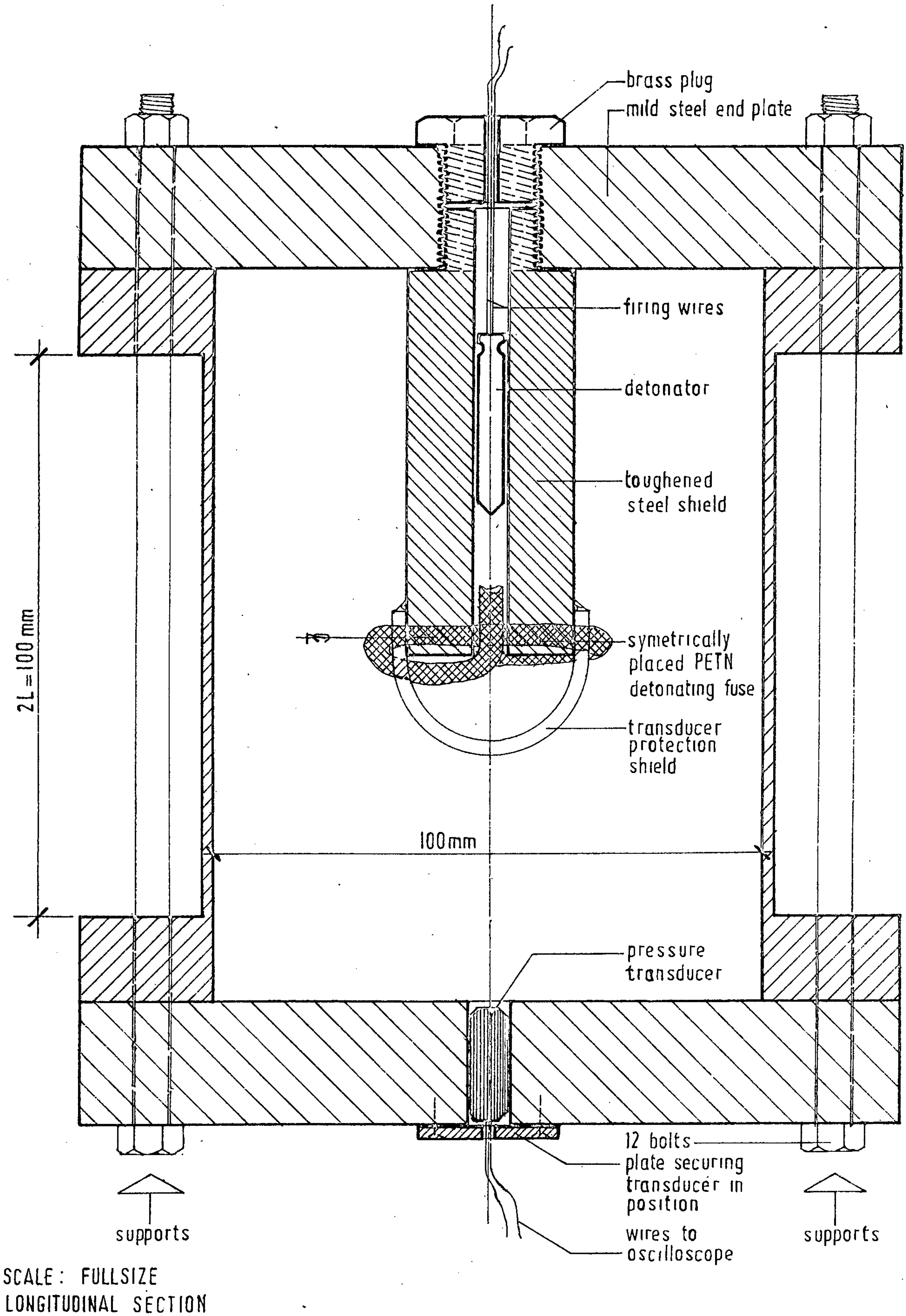

FIG. 6.3 - CIRCULAR CYLINDRICAL SHELL TEST SPECIMEN

(Showing 2 mm shell wall thickness)

The length and the internal diameter of the shell wall was kept constant at 0,10 m for all specimens. The wall thickness was made to vary from approximately 1,5 mm to 4 mm. Hence, the radius of the median surface varied slightly. One disadvantage of the thin walls has already been mentioned. Another manifested itself in that the pressure transducer could not be located in the side wall. The pulse experienced by the central region of the shell wall was of primary interest, however, this was directly unobtainable. The best alternative was to place the transducer in the position shown in Fig. 6.3 and make the assumption that the measured pulse was essentially identical to that occurring at the central curved region. The aluminium specimens were machined from solid rounds to provide end fixity for the shell walls. The open ends of the shell were covered by heavy mild steel plates, and 12 high tensile bolts (as shown in Fig. 6.3) were used to secure the plates to the specimens. The bolts were lightly tensioned. In this manner, longitudinal membrane forces were eliminated from the shell wall. The shell ends were in fact free to collapse inwards and this tendency was clearly evident in the tested specimens. In fact, the thinner walled specimens reduced in length by approximately 5 %.

6.3 The Measured Pressure Pulse and Energy Losses

Fig. 6.4 depicts the pulse measured for test specimen 3. The second peak can be explained as a reflection from either the opposite end plate or the shield. It is difficult to say much more about this as the acoustic properties of the air within the cylinder must have undergone indeterminable modifications. Based on an air sound speed of 330 m/s a wave would take 273 µs to return from the shield and a considerably greater length of time to return from the end plate. The second peak may therefore result from a reflection from the shield. A remarkable fact concerning the pulse is the sharp decay of the initial peak. It was expected that in a confined area, such as the cylinders tested, superposition of reflected waves would cause the pulse to be less impulsive in nature. In calculating the impulsive loadings on the cylinder, only the initial portion of the pulse was considered. Other peaks were ignored as they occurred well after the theoretical response time and as their origin was obscure. Quite aside from reflections, the subsequent peaks may be the result of elastic waves within the end plate.

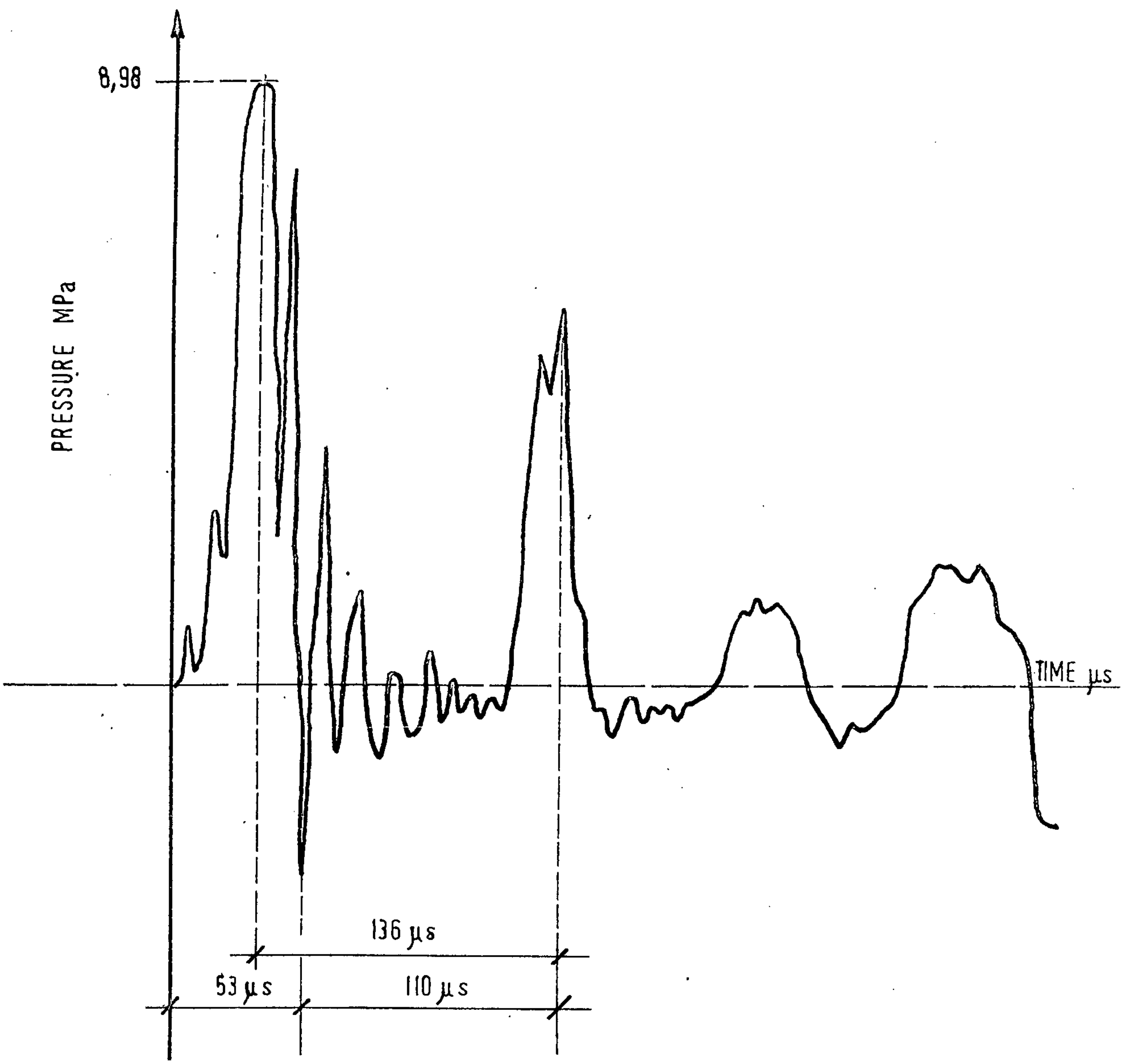

FIG. 6.4 - PRESSURE PULSE OBTAINED FROM TEST 3
(Typical of all tests)

According to the manufacturers, 1 g of PETN contains 10,705 kJ of chemical energy and 100 mm of the grade of Cordtex used contains 1 g of PETN. One detonator of the type used is equivalent to 0,34 g of PETN. As the detonators were almost totally shielded it was assumed that their contribution to the total chemical energy was negligible.

In the case of Test Specimen 3, 175 mm of Cordtex having a chemical energy of 18,73 kJ was detonated. The expected deformation, based purely on an energy balance formulation and ignoring the effects of elastic strain energy storage and energy losses, is given by

$$\Delta = \frac{K}{4\pi\sigma_o LH},$$

where K = chemical energy,

σ_o = 0,8 of the ultimate strength (assumed average rigid plastic yield).

Substituting the appropriate values $L = 0{,}05$, $H = 1{,}908$ mm, $\sigma_o = 0{,}8 * 114$ MPa and $K = 18{,}73$ kJ, we obtain

$$\Delta = 171{,}3 \text{ mm}.$$

As the actual deformation was 1,77 mm it is evident that $\pm$ 99 % of the chemical energy of the blast was lost in the conversion to kinetic energy of the shell wall. This small calculation indicates the difficulty in correctly applying energy balances of this type.

Table 6.1 lists the length of Cordtex, the corresponding peak pressures and the measured impulse per unit area. Although the correlation between peak pressure and length of Cordtex was reasonably good there was poor correlation between the length of Cordtex and the measured impulse per unit area. The phenomenon is difficult to explain. It is possible that the amount of PETN varied greatly with length of Cordtex, but it seems unlikely. Another possibility is that inconsistent tensioning of the clamping bolts allowed varying degrees of pressure reduction within the cylinder. The results are too inconsistent to categorically state that the wall thickness influenced the size or peak pressure, although it appears that the correspondingly higher pulses occurred within the stiffer shells.

The theory, as set out in Section 2, neglected the effect of finite deflections on energy dissipation due to plastic flow in the longitudinal direction. If stress interactions are neglected, an estimate can easily be made of the proportion of energy dissipated longitudinally using Table 3. This is not done here as the experimental set-up was designed to eliminate longitudinal stresses.

6.4 Comparison of Rigid Plastic Predictions and Experimental Results

The full set of experimental results is set out in Table 6.1 and a graphical presentation of the results as compared to the theory in Fig. 6.5. The primary problem in calculating the expected deformations lies in the selection of a representative value for the yield stress. With mild steel there is no such problem as there is a marked point of first yield and considerable perfect plastic flow thereafter, until strain hardening occurs. With aluminium it is necessary to estimate an average constant yield stress. This estimation must be based on the total strain that the material experiences.

Generally, the shells experienced deformations of up to 2,5 mm. In other words the maximum strain achieved was 0,5. It is clear from Fig. 6.1 that the full strength of the material is never utilised. A value of four fifths of the ultimate strength was chosen for σ_o. The exact value chosen is not critical as the true average would probably not differ from that chosen by more than 10 %. Such accuracies are acceptable for rigid plastic estimations.

Deformation Profiles:

The deformation profiles of certain tested specimens were investigated. It was apparent that the thinner walled the specimen the more closely did its deformed profile match that of the theory. However, the response of the thinnest walled specimens (e.g. Specimen 6) also exhibited some degree of non-uniform radial deformation. The thicker walled specimens deformed uniformly but their deformation profiles were more triangular in shape.

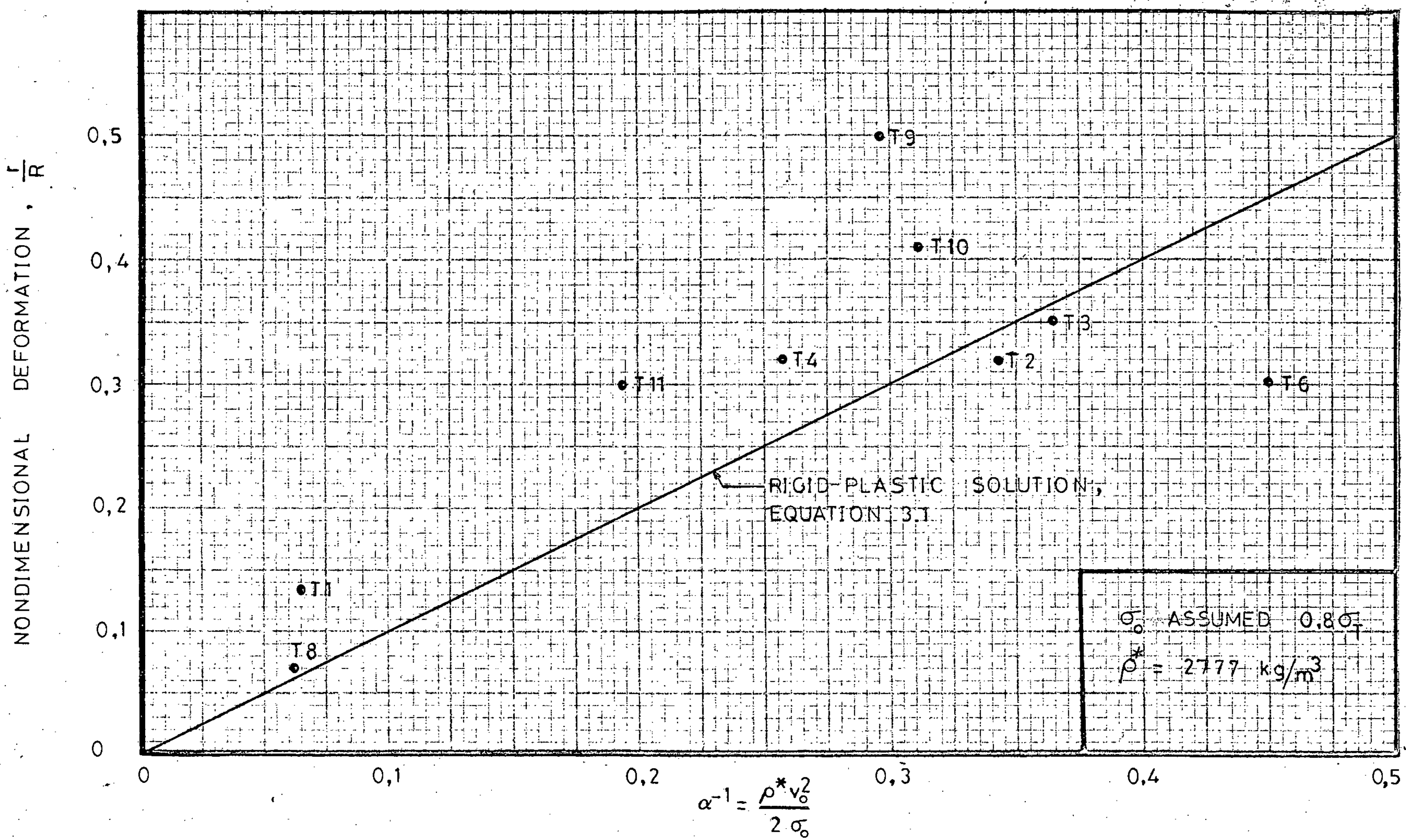

FIG 6.5 - COMPARISON OF RIGID PLASTIC SOLUTION AND EXPERIMENTAL RESULTS

Energy Ratios:

A check on the ratios of initial shell wall kinetic energy to the elastic potential should be made. Consider a narrow band about the shell centre having a certain volume.

The elastic potential is $\frac{1}{2}$(volume) σ_o^2/E and the kinetic energy can be found using the calculated initial radial velocity v_o.

The initial kinetic energy is $\frac{1}{2}$(volume) $\rho^* v_o^2$.

The ratio of energy input to the system , to the energy that can be stored elastically by the system is

$$\frac{\rho^* v_o^2 E}{\sigma_o^2} .$$

(E for D65S Aluminium is approximately 69 GPa)

This ratio ranged from 6 to 100 for the shells tested. These values are above the value of 3 which is recommended [7] as the lower limit for which a rigid plastic analysis retains validity.

As can be seen from Fig. 6.5, the experimental results are somewhat scattered as a result of the difficulty in choosing a good representative value for σ_o. The results are nevertheless good; especially in the range of the higher deformations.

6.5 Comparison of Predictions of the Rate Sensitive - Strain Hardening Model and the Experimental Results.

The analysis for a material displaying rate sensitivity and strain hardening properties was developed in Section 5.2. It was necessary to utilize certain material constants quoted by Perrone [9] for the American 6061 T6 Aluminium Alloy (equivalent of D65S S.A.), see Section 5, page 48.

The yield stress and the strain hardening coefficient were individually determined for each shell specimen from the tensile test stress-strain curve. The results are listed in Table 6.1. An advantage of this method is that it can easily be extended by approximating the stress-strain relation with any number of linear segments. The problem remains simple from the viewpoint of a numerical computer solution. In the present analysis, however, the stress-strain relation was simply approximated as a rigid linear strain hardening material as shown in Fig. 6.6.

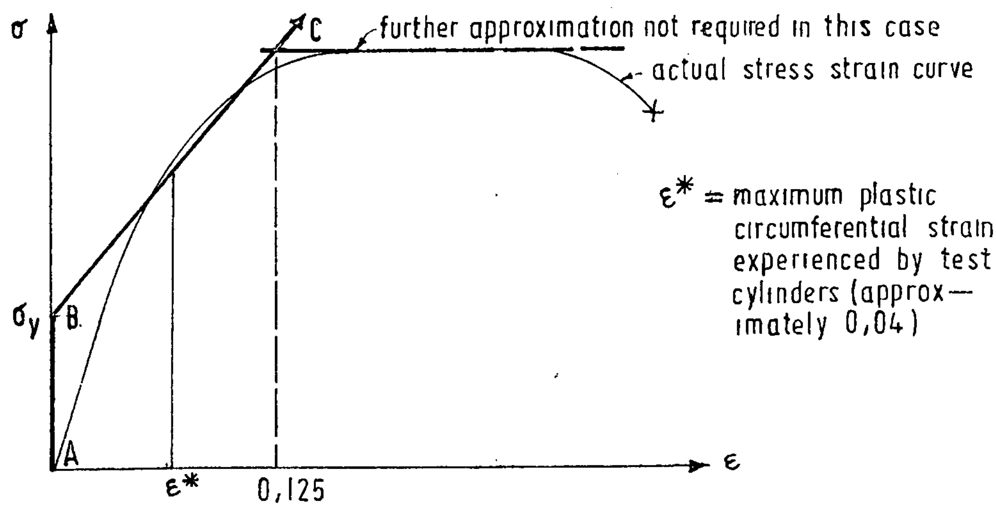

Fig. 6.6 - Rigid Linear Strain Hardening Approximation (line ABC)

A graphical presentation of the experimental deformations as compared to those expected from the theory is shown in Fig. 6.7. The correlation is better than that obtained from the rigid plastic approach.

It should be noted that the theoretical curve shown in Fig. 6.7 was derived for R = 0,051 m. Different values for R produce slightly different curves (equation 5.11) but the difference is negligible in practice and not noticeable at the scale used.

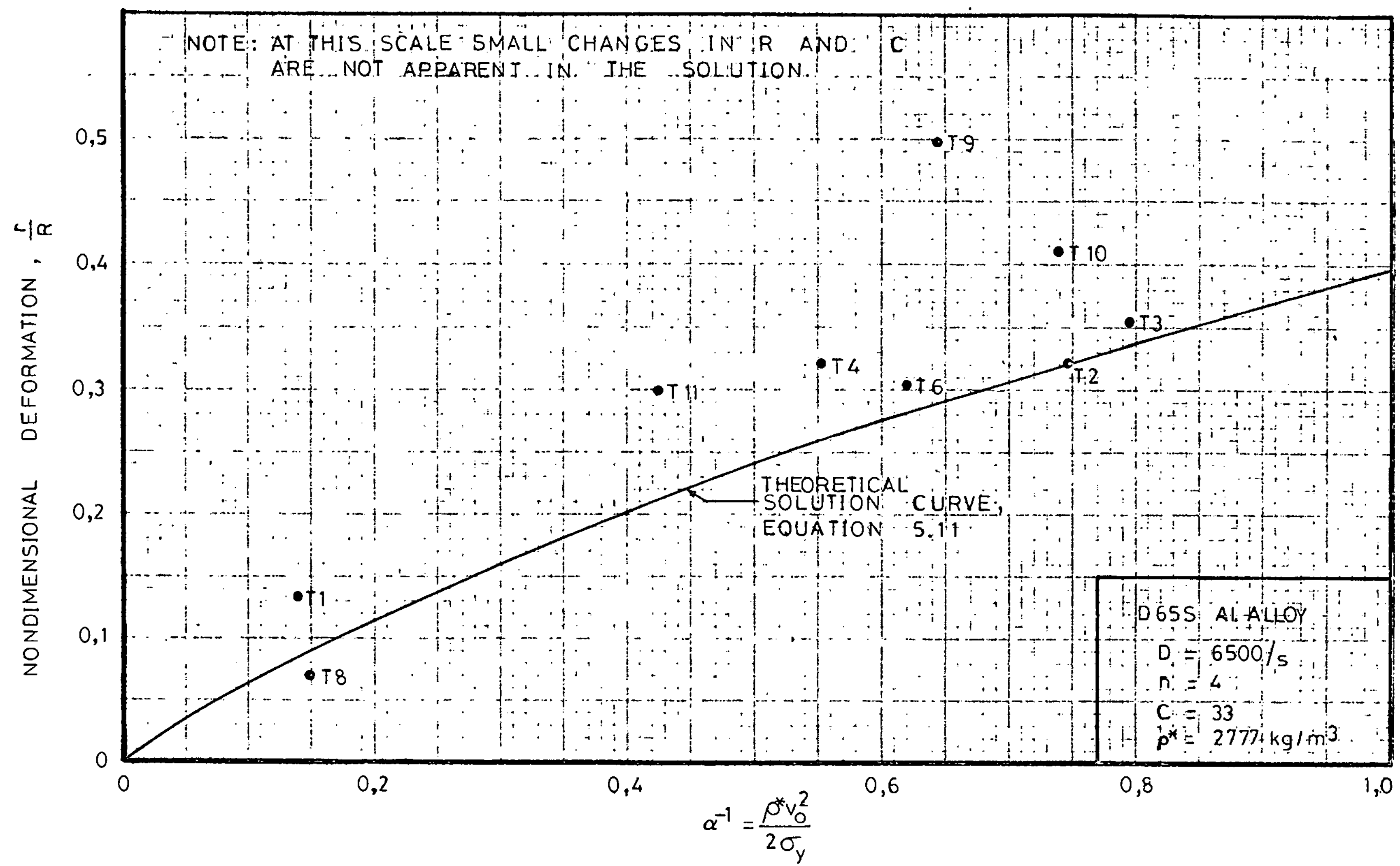

FIG. 6.7 - COMPARISON OF RATE SENSITIVE LINEAR STRAIN HARDENING MODEL AND EXPERIMENTAL RESULTS

C O N C L U S I O N S

Formulae for the transient response to impulsive loading of uniformly expanding cylinders governed by rigid-plastic material laws, and rings governed by rate-sensitive, strain hardening laws, were developed. The results of the exact rigid-plastic analysis were compared with the deformation bounds calculated, using established rigid-plastic approximate methods. The two methods were in accord. The results of this work therefore constitute additional supporting evidence for these methods.

The approximate methods, require for their application, the existence of a time independent kinematically admissible velocity field. Such a field was shown to exist in the case of short shells. However, in the case of long shells all velocity fields from commencement to cessation of motion, possessed time dependent shapes. Thus, for these structures it appears that no mode shape exists, but it is to be noted that this statement is based on the results of a numerical analysis which cannot constitute conclusive proof. Application of the mode approximation method using the velocity field shown to exist instantaneously at the end of the motion, yielded acceptable deformation values, even though the approximation of the response time differed from that of the exact analysis by 25 %.

It was evident from the results of the rigid-plastic analysis that the cylinder end support conditions have essentially no influence on the maximum deformation of shells with $c > 1,5$. The influence is small, even for shorter shells. Reference to Fig. 2.6 shows that the maximum deformation for a shell with $c = 0,65$ and fully fixed ends, is approximately 20 % less than the radial deformation of an equivalent ring with no end fixity. (For a ring: $\int \bar{v} d\tau = \frac{1}{2}$). For engineering purposes, and in view of the numerous assumptions necessary for the tractability of the analysis, a 20 % difference is not significant. Thus, it would be conservative and economical to treat all but the shortest of impulsively loaded cylinders as expanding rings for purposes of estimating the maximum deformation. This procedure will allow the effects of material properties to be more easily included.

The potential difficulty in accurately applying total energy balances for purposes of estimating initial structure kinetic energies, was clearly demonstrated. In the instance quoted, approximately 1 % of the explosive chemical energy was absorbed by the shell wall as kinetic energy, while the remainder was dissipated by other mechanisms.

The experiments were intended to constitute tests of a preliminary nature and to provide guidelines for improvements in technique. Further experimental research could include the use of rate sensitive material and investigate the response of short shells. The theoretical assumptions would be more closely approached if sheet explosive was uniformly placed on the internal surface of the shell wall and greater control would be achieved if pulse measurements were made at the points under consideration. Measurement of the response accelerations and times would provide valuable additional items of information for comparative checks.

In spite of the low degree of control exercised in the current series of tests, the results compared favourably with the theoretical estimates. The rigid-plastic model did not produce as consistent a set of results as did the rigid linear strain hardening model, but the degree of correspondence obtained between the test results and the theory was in both cases encouraging.

REFERENCES

[1] MARTIN, J.B. and SYMONDS, P.S., "Mode Approximations for Impulsively-Loaded Rigid-Plastic Structures", Journal of the Engineering Mechanics Division, ASCE, Vol. 5, Oct., p 43, 1966,

[2] PERRONE, N., "On a Simplified Method for solving Impulsively Loaded Structures of Rate Sensitive Materials", Journal of Applied Mechanics, Trans. ASME, Vol. 32, pp 489-492, 1965.

[3] BODNER, S.R. and SYMONDS, P.S., "Experimental and Theoretical Investigation of the Plastic Deformation of Cantilever Beams subjected to Impulsive Loading", Journal of Applied Mechanics, Vo. 29, Trans. ASME, p 719, 1962.

[4] HODGE, P.G., "The Influence of Blast Characteristics on the Final Deformation of Circular Cylindrical Shells", Journal of Applied Mechanics, Vol. 23, p 617, 1956.

[5] HODGE, P.G. "Impact Pressure Loading of Rigid-Plastic Cylindrical Shells", Journal of the Mechanics and Physics of Solids, Vol. 3, p 176, 1955.

[6] .HODGE, P.G., "Effect of End Conditions on the Dynamic Loading of Plastic Shells", Journal of the Mechanics and Physics of Solids, Vol. 4, p 53, 1956.

[7] DUFFEY, T. and KRIEG, R., "The Effects of Strain-Hardening and Strain-Rate Sensitivity on the Transient Response of Elastic-Plastic Rings and Cylinders", International Journal of Mechanics and Science, Vol. 11, p 825, 1969.

[8] PERRONE, N., "Impulsively Loaded Strain-Hardened Rate Sensitive Rings and Tubes", International Journal of Solids and Structures, Vol. 6, p 1119, 1970.

[9] PERRONE, N., "On a Simplified Method for Solving Impulsively Loaded Structures of Rate-Sensitive Materials", Journal of Applied Mechanics, Vol. 32, p 489, 1965.

[10] JONES, N., "The Influence of Large Deflections on the Behaviour of Rigid-Plastic Cylindrical Shells Loaded Impulsively", Journal of Applied Mechanics, Vol. 37, p 416, 1970.

[11] WITMER, E.A., BALMER, H.A., LEECH, J.W. and PIAN, T.H.H., "Large Dynamic Deformations of Beams, Circular Rings, Circular Plates and Shells", A.I.A.A. Journal, Vol. 6, p 2352, 1968.

[12] MARTIN, J.B., "Impulsive Loading Theorems for Rigid-Plastic Continua", Proc. A.S.C.E., Vol. 90, p 27, 1964.

[13] HODGE, P.G., "Plastic Response of Structures", McGraw-Hill, 1959.

[14] PRAGER, W. and HODGE, P.G., "Theory of Perfectly Plastic Solids", John Wiley and Sons Inc., 1951.

[15] GOODIER, J.N. and HODGE, P.G., "Elasticity and Plasticity", John Wiley and Sons Inc., 1958.

[16] PRAGER, W., "An Introduction to Plasticity", Addison Wesley Pub. Co. Inc., 1959.

[17] HERRMAN, G. and PERRONE, N., "Dynamic Response of Structures", Proceedings of a Symposium held at Stanford University, California, Pergamon Press Inc., 1971.

[18] PERRONE, N., "A Mathematically Intractable Model of Strain Hardening Rate-Sensitive Plastic Flow", Journal of Applied Mechanics, Vol. 33, pp 210-211, 1966.

[19] MALVERN, L.E., "The Propagation of Plastic Waves of Deformation in Bar of Material Exhibiting a Strain Rate Effect", Journal of Applied Mechanics, Vol. 18, pp 203-208, 1951.

[20] AUGUSTI, G. and D'AGOSTINO, S., "Tests of Cylindrical Shells in the Plastic Range", Journal of the Engineering Mechanics Division, ASCE, pp 69-81, Feb. 1964.

COURSES COMPLETED IN PARTIAL FULFILMENT OF THE M.Sc. (ENG.) DEGREE AT THE UNIVERSITY OF CAPE TOWN

COURSE	DATE CREDITED	CREDIT VALUE
CE 506 - Properties of Concrete	1974	4
AM 407 - Mathematical Programming	1974	6
CE 523 - Continuum Mechanics	1974	3
CE 504 - Probability and Engineering Statistics	1974	4
CE 508 - Skeletal Structures	1975	5
CE 513 - Waste Water Treatment	1975	10
	Total	32

Total credit requirements for the M.Sc.(Eng.) Degree: 40

Course Credits:	32
Quarter Thesis:	10
Total:	42

UNIVERSITY OF CAPE TOWN

DEPARTMENT OF CIVIL ENGINEERING

UNIVERSITY EXAMINATION: JUNE 1974

COURSE CE 506 - PROPERTIES OF CONCRETE

M.Sc. IN ENGINEERING

Time Allowed: THREE HOURS

Candidates are required to attempt ALL questions in Part A, and not more than FOUR questions from Part B.

PART A

1. What are the four principle oxides in Portland cement? (1)

2. Give two methods of manufacturing a Portland cement with rapid hardening properties. (2)

3. In what way do the setting time and the ultimate strength of ordinary Portland cement differ from those of rapid hardening Portland cement? (1)

4. Briefly explain the phenomena of bleeding in concrete, and give the beneficial affect and the adverse affects of bleeding. (3)

5. Explain what is meant be self-dessication of a cement paste. (1)

6. Under what environmental conditions does concrete made with high alumina cement undergo an irreversible retrogression of strength? (1)

7. Why does concrete considered in No. 6 above become susceptible to sulphate attack? (1)

8. Calculate the maximum horizontal pressure on the formwork for a concrete column of dimensions 0,5 x 1 x 5 m to be cast at a vertical rate of placing of 5 m/hr at an estimated concrete temperature of 15°C. A vibrator is used with approximately 60% continuity to compact the concrete. The slump of the concrete is 100 mm and there is a delay of approximately ten minutes between the mixing and placing of the concrete.

   The placing of the concrete is effected in such a manner that there is no appreciable pressure surcharge due to impact. (The weight density of concrete may be taken as 24 $kN/_{m}{}^{3}$.) (1)

9. What factor has the greatest influence on the durability of concrete? (1)

10. Why is the sulphate attack of concrete by $MgSO_4$ regarded as being more severe than sulphate attack by $CaSO_4$? (1)

11. Explain two possible ways of increasing the resistance of concrete to freezing and thawing. (3)

12. Why is the triaxial compressive strength of concrete higher than the uniaxial compressive strength? (1)

13. How does the rate of loading affect the uniaxial compressive strength of concrete? (1)

PART A (continued)

14. Give three reasons why the transverse bending test overestimates the true tensile strength of concrete. (3)

15. Briefly state the possible mechanisms of creep in concrete. Indicate whether the creep is recoverable or irrecoverable in each instance. (5)

16. In what way does aggregate influence the creep of concrete? (1)

(TOTAL : 30 MARKS)

CE 506 : Examination - June 1974

PART B

1. Explain and illustrate the following:

   (a) the hydration of the mineral compounds constituting Portland cement with particular reference to their respective contributions to strength and heat of hydration,

   (b) the structure of hardened cement paste, with particular reference to the different categories of water contained in the paste. (18)

2. (a) Show why a cement paste having a W/C ratio < 0,36 (by mass) and continuously cured under water will never achieve 100% hydration.

   (b) Three cement pastes made with 314 g cement and having W/C ratios of 0,2; 0,4 and 0,6 respectively are placed in stoppered test tubes:

   (i) What is the maximum hydration that is possible for each of the respective pastes?

   At maximum hydration of the 0,6 W/C ratio paste calculate:

   (ii) the volume of gel formed,

   (iii) the chemically combined water and water in the gel pores,

   At maximum hydration of each of the pastes calculate: (16)

   (iv) the water in the capillary pores.

3. The results from a trial mix of 33 kg of water : 50 kg of cement : 140 kg dry sand : 170 kg dry stone are slump of 130 mm and a real mortar excess of 6%. It is assumed that the densities of water, cement, sand and stone are 1000, 3100, 2600 and 2800 kg/m^3 respectively and that the dry stone contains 50% voids. What mix would you suggest if the slump and real mortar excess required are 75 mm and 1% respectively? (16)

4. Discuss: (a) factors which influence concrete strength, and

   (b) the stress/strain relation of concrete in terms of crack initiation and crack propagation. (18)

5. Discuss drying shrinkage and carbonation shrinkage of concrete. (18)

oooo0oooo

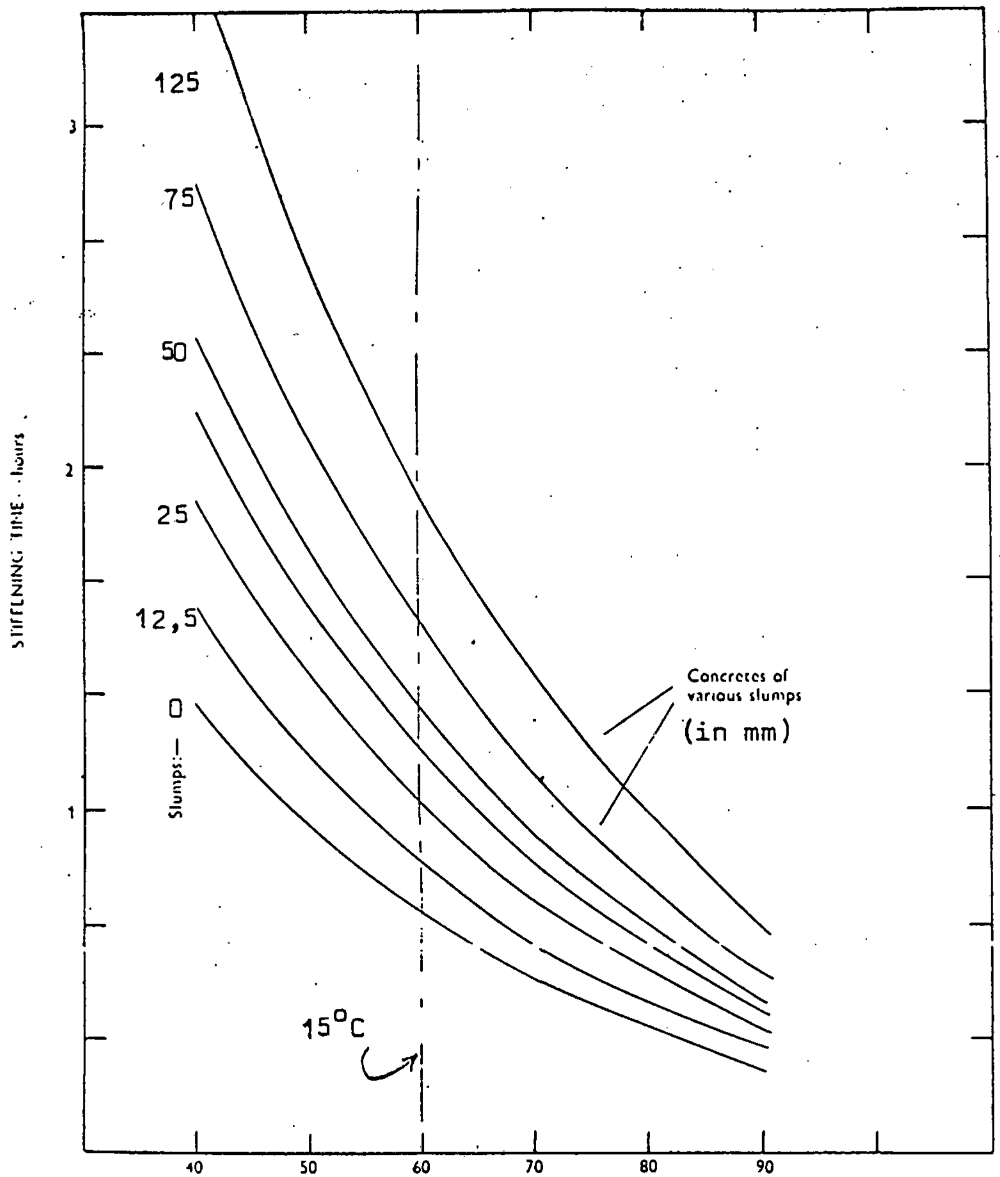
STIFFENING TIME - hours
Slumps:—
0
12,5
25
50
75
125
15°C
Concretes of various slumps
(in mm)
1
2
3
40
50
60
70
80
90

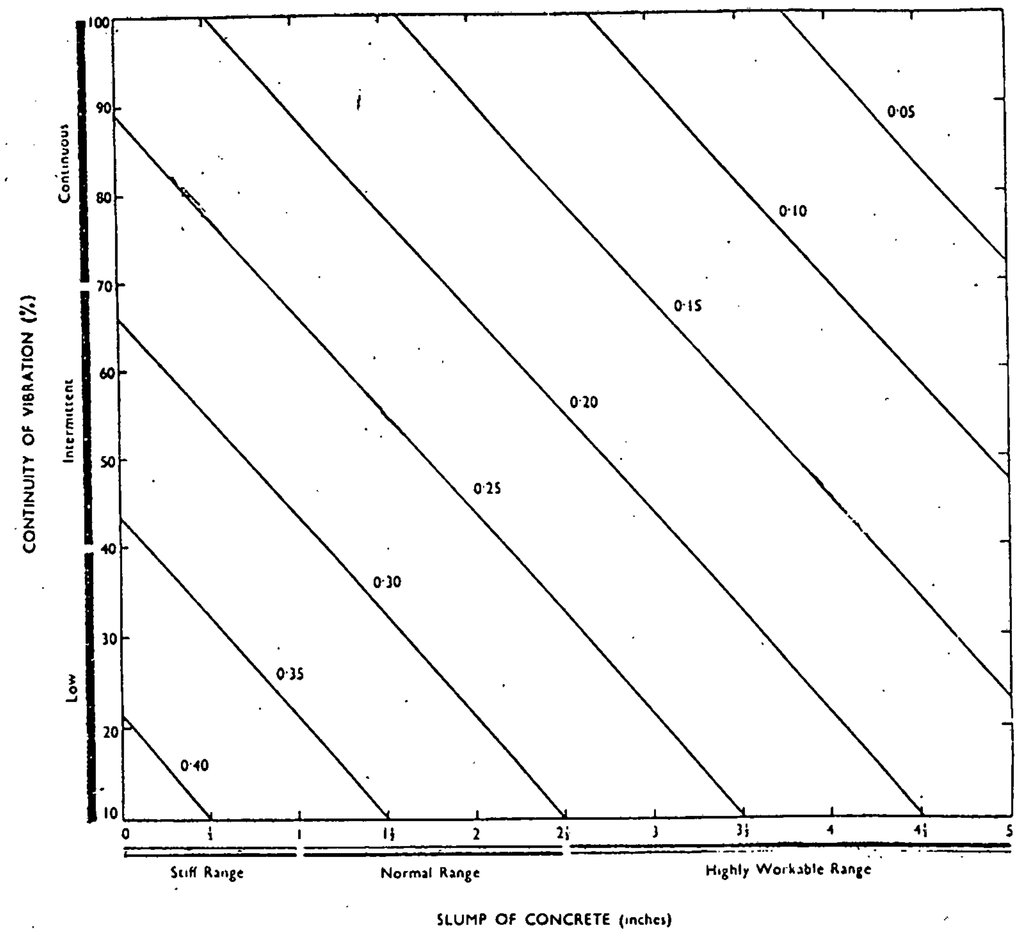
CONTINUITY OF VIBRATION (%)
Low
Intermittent
Continuous
0·40
0·35
0·30
0·25
0·20
0·15
0·10
0·05
Stiff Range
Normal Range
Highly Workable Range
SLUMP OF CONCRETE (inches)

(1" = 25 mm)

4. Define the dual of the primal problem:

$$Ax \leq q \ , \quad x \geq 0 \ , \quad \max z = cx \ .$$

Prove that if the primal has an optimal solution so does the dual, and that the optimal values are equal.

Assuming (if necessary) that the problems of the players of a 2-person zero-sum game form a primal-dual pair of linear programming problems, find the optimal strategies in a game with payoff matrix

$$\begin{pmatrix} 2 & 2 & 1 \\ 3 & 1 & 4 \\ 2 & 3 & 4 \\ 1 & 2 & 3 \end{pmatrix}$$

(22)

5. Show how a Transportation Problem (TP) with m origins and n destinations can be written in LPP form with a large but simple constraint matrix A whose columns fall into m batches each containing n columns.

Let P_{ij} denote the i^{th} column in the j^{th} batch. You may assume that for any suffixes $i_1, i_2, \ldots, i_k ; \ j_1, j_2, \ldots, j_k$

$$P_{i_1 j_1} - P_{i_1 j_2} + P_{i_2 j_2} - \ldots - P_{i_k j_1} = 0$$

and that any linearly dependent set of columns of A contains a subset of the form $P_{i_1 j_1}, P_{i_1 j_2}, P_{i_2 j_2}, \ldots, P_{i_k j_1}$.

Describe the NW corner method for finding an initial solution of a TP and prove that the solution found is a basic solution.

Show how the Simplex Algorithm rules may be translated into a simpler algorithm for the TP .

Find (by any method) an initial basic feasible solution of the TP with costs and requirements given in the array:

					a_i
	9	2	6	3	18
	6	7	8	8	17
	2	9	3	1	10
b_j	15	5	14	11	

Find the optimal solution to this problem.

(22)

6. Describe the excess capacity method for finding the greatest total flow through a capacitated network and prove that at termination a cut may be defined with capacity equal to the total flow.

Show how the labelling process used in the above method can be adapted to find the 'least cost' route from source to sink in a network where the costs for each arc are given.

Find the least cost route from A to G in the network with the symmetric cost matrix:

	A	B	C	D	E	F	G
A	0	1	5	x	2	6	x
B	1	0	4	3	1	2	x
C	5	4	0	6	3	1	6
D	x	3	6	0	2	4	5
E	2	1	3	2	0	3	8
F	6	2	1	4	3	0	7
G	x	x	6	5	8	7	0

('x' indicates that there is no arc joining the two vertices).

(21)

7. Prove that if a transportation problem has integer requirements then the optimal solution has integer components.

Describe the method of Gomory cuts for finding the optimal integer solution of a general LPP.

(21)

UNIVERSITY OF CAPE TOWN

DEPARTMENT OF CIVIL ENGINEERING

UNIVERSITY EXAMINATION: NOVEMBER 1974

COURSE CE 523: CONTINUUM MECHANICS

M.Sc. IN ENGINEERING

Time allowed: 3 hours 9th November, 1974

Read the attached paper and answer the following questions. Notes are permitted.

1. Draw a stress-strain diagram, plotting one component of stress against one component of strain, which demonstrates diagrammatically the basis of inequality (6).

2. (a) In inequality (14) which of the fields σ_{ij}, ϵ_{ij} or σ^*_{ij}, ϵ^*_{ij} is the actual solution of the problem?

   Explain why.

   (b) In inequality (15) which of the fields σ_{ij}, ϵ_{ij} or σ^*_{ij}, ϵ^*_{ij} is the actual solution? Explain why.

3.

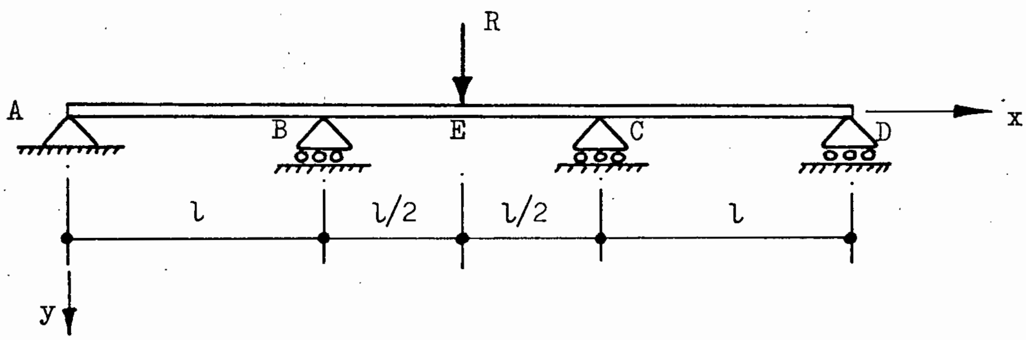

The three-span beam shown is uniform, with flexural rigidity EI and mass m/unit length. Neglect the gravity forces on the beam. Refer to bending moment as M and bending strain as $\varkappa$. Then $\varkappa = M/EI$, shear strain being neglected.

(a) Draw some equilibrium bending moment diagrams for the beam.

(b) What is the form of the complementary energy theorem (inequality 15) for this structure?

(c) How is the complementary energy theorem used to find the exact solution of the problem?

(d) How is the answer to (c) changed if the support D has settled by an amount δ ?

(e) Removing the load R, a mass M is dropped onto the beam at the point E, from a height h. How can an upper bound on the dynamic displacement of E be calculated.

J. Mech. Phys. Solids, 1964, Vol. 12, pp. 165 to 175. Pergamon Press Ltd. Printed in Great Britain.

A DISPLACEMENT BOUND TECHNIQUE FOR ELASTIC CONTINUA SUBJECTED TO A CERTAIN CLASS OF DYNAMIC LOADING*

By J. B. Martin
Division of Engineering, Brown University

(*Received* 20*th January*, 1964)

Summary

The paper presents a general inequality relating statically admissible stress fields and kinematically admissible strain and displacement fields in an elastic continuum. The relation between the inequality and the classical energy theorems is discussed, and the inequality is used to compute displacement bounds for elastic continua subjected to certain types of impulsive loading.

1. Introduction

It was shown in an earlier paper (Martin 1963) that a bound on localized surface displacements can be computed for rigid/plastic continua for a certain class of dynamic loading. The disturbance was specified to be of the form where displacement rates throughout the continuum are specified at time $t = t_0$; thereafter it was assumed that over the entire surface of the continuum either the displacement rates or the surface tractions were identically zero. Body forces (not including inertia forces) were assumed to be constant during the response, and displacements resulting from the initial disturbance were assumed to be small.

It will be shown in this paper that a similar bound can be computed for an elastic material for a similar disturbance. The bound may be computed only for a stable elastic material; this restriction will be discussed in the following section.

We shall develop a principle for infinitesimal elasticity involving a consistent inequality, using the restriction of material stability. This principle is a generalized energy theorem, and it will be shown that it may be reduced to the minimum potential energy and minimum complementary energy theorems. The principle is generally valid for boundary value problems in infinitesimal elasticity; the nature of the specific form of dynamic loading chosen allows it to be used to bound localized displacements resulting from the imposed disturbance.

2. Material Stability

We consider stresses σ_{ij} and infinitesimal strains ϵ_{ij} in an elastic solid. We assume a constitutive relation of the form

*The results presented in this paper were obtained in the course of research sponsored by the David Taylor Model Basin, Washington, D.C., under Contract Nonr 4017 (00) (X).

$$\sigma_{ij} = \frac{\partial W}{\partial \epsilon_{ij}} \tag{1}$$

where W is a function of ϵ_{ij}. W is the strain energy or work function, and may be calculated as $\int \sigma_{ij}\, d\epsilon_{ij}$. We require that $\sigma_{ij} = 0$ when $\epsilon_{ij} = 0$. We shall consider also the complementary energy function Ω, calculable as $\int \epsilon_{ij}\, d\sigma_{ij}$. Ω is thus a function of stress σ_{ij}, and

$$\epsilon_{ij} = \frac{\partial \Omega}{\partial \sigma_{ij}}. \tag{2}$$

A further restriction will be placed on the constitutive equations (1) and (2). Consider any pair of strain states ϵ_{ij}, ϵ^*_{ij} and the corresponding stress states σ_{ij}, σ^*_{ij} obtained from equation (1). We require that

$$\int_{\epsilon^*_{ij}}^{\epsilon_{ij}} (\sigma_{ij} - \sigma^*_{ij})\, d\epsilon_{ij} \geqslant 0 \tag{3}$$

where σ^*_{ij} in the integrand remains constant during integration over any path from ϵ^*_{ij} to ϵ_{ij}. A material characterised by equations (1) and (2) and satisfying (3) will be termed a *stable elastic material.* Inequality (3) follows directly from the postulate of material stability introduced by DRUCKER (1951).

Inequality (3) may be written in various alternative forms. Making use of the equation

$$W + \Omega = \int (\sigma_{ij}\, d\epsilon_{ij} + \epsilon_{ij}\, d\sigma_{ij}) = \sigma_{ij}\, \epsilon_{ij}, \tag{4}$$

it may readily be seen that inequality (3) may be written in the following three forms :

$$\Omega\,(\sigma^*_{ij}) + W\,(\epsilon_{ij}) \geqslant \sigma^*_{ij}\, \epsilon_{ij} \tag{5}$$

$$W\,(\epsilon_{ij}) - W\,(\epsilon^*_{ij}) \geqslant \sigma^*_{ij}\,(\epsilon_{ij} - \epsilon^*_{ij}) \tag{6}$$

$$\Omega\,(\sigma^*_{ij}) - \Omega\,(\sigma_{ij}) \geqslant \epsilon_{ij}\,(\sigma^*_{ij} - \sigma_{ij}) \tag{7}$$

The forms given in (6) and (7) have been discussed in detail by HILL (1956), who noted that they expressed the requirement that W and Ω be convex. If a strict inequality holds in (3), (5), (6) and (7) (except for $\epsilon^*_{ij} = \epsilon_{ij}$, $\sigma^*_{ij} = \sigma_{ij}$), W and Ω are strictly convex, and it may also be shown that the solution to any standard boundary-value problem is determined uniquely at all points in the body.

3. GENERALIZED ENERGY PRINCIPLE

We consider now a continuum formed of a stable elastic material. Body forces F_i act on the continuum. We shall assume that all displacements are infinitesimally small, so that the effects of geometry changes can be ignored We suppose that a stress field σ^*_{ij} and a strain field ϵ_{ij} are known for the continuum.

We require that the stress field σ^*_{ij} be in internal equilibrium with the body forces F_i. Thus at any point in the interior of the continuum

$$\partial_j\, \sigma^*_{ij} + F_i = 0, \tag{8}$$

where ∂_j signifies spatial differentiation. Surface tractions T^*_i are defined by the requirements of external equilibrium; at any point on the surface of the continuum

$$\sigma^*_{ij}\,\nu_j = T^*_i \tag{9}$$

where ν_j is the unit outward normal at the point under consideration.

We require that the strains ϵ_{ij} are compatible with continuous displacements u_i. Thus, if u_i is continuously differentiable,

$$\epsilon_{ij} = \tfrac{1}{2}\,(\partial_j\, u_i + \partial_i\, u_j). \tag{10}$$

We note here that the fields σ^*_{ij}, ϵ_{ij} are completely independent of each other, and that no boundary conditions have been prescribed.

Since T^*_i, F_i, σ^*_{ij} are in equilibrium, and u_i, ϵ_{ij} are compatible, we may write by the principle of virtual work

$$\int\limits_A T^*_i\, u_i\, dA + \int\limits_V F_i\, u_i\, dV = \int\limits_V \sigma^*_{ij}\, \epsilon_{ij}\, dV. \tag{11}$$

The integrals are taken over the area A and volume V of the continuum.

Now consider inequality (5). σ^*_{ij}, ϵ_{ij} is an admissible pair of states, in terms of the discussion of the previous section, at all points in the body. Thus we may integrate (5) over the volume of the continuum and retain the inequality; substituting from equation (11), we obtain

$$\int\limits_V \Omega\,(\sigma^*_{ij})\, dV + \int\limits_V W\,(\epsilon_{ij})\, dV \geqslant \int\limits_A T^*_i\, u_i\, dA + \int\limits_V F_i\, u_i\, dV. \tag{12}$$

This inequality is a generalized energy theorem and is of primary interest in this paper. We note that the equality holds only when $\epsilon_{ij} = \epsilon^*_{ij}$ (or when $\epsilon_{ij} = \partial\Omega/\partial\sigma^*_{ij}$) at all points in the continuum. When this occurs σ^*_{ij}, ϵ_{ij} may be regarded as the solution of some (unspecified) boundary value problem.

It is also of interest to note that the alternative forms of the inequality lead to the wellknown energy theorems. The development of the theorems given here follows Hill (1956).

First, consider inequality (6). We may again integrate over the volume and retain the inequality. Suppose, in addition, that ϵ^*_{ij} (given by $\epsilon^*_{ij} = \partial\Omega/\partial\sigma^*_{ij}$) is compatible with displacements u^*_i, and that $u^*_i = u_i$ over part of the area of the surface of the body A_u. Let the remainder of the surface be given by A_T. Then, by the principle of virtual work,

$$\int\limits_V \sigma^*_{ij}\,(\epsilon_{ij} - \epsilon^*_{ij})\, dV = \int\limits_A T^*_i\,(u_i - u^*_i)\, dV = \int\limits_{A_T} T^*_i\,(u_i - u^*_i)\, dV. \tag{13}$$

Substituting equation (13) into inequality (6), after integrating over the volume of the body, and rearranging, we obtain

$$\int\limits_V W\,(\epsilon_{ij})\, dV - \int\limits_{A_T} T^*_i\, u_i\, dA \geqslant \int\limits_V W\,(\epsilon^*_{ij})\, dV - \int\limits_{A_T} T^*_i\, u^*_i\, dA. \tag{14}$$

With the boundary conditions of the starred system interpreted as a boundary value problem with T^*_i given on A_T and u^*_i given on A_u, inequality (14) becomes the minimum potential energy theorem. If W is strictly convex, the equality holds only when $\epsilon^*_{ij} = \epsilon_{ij}$ at all points in the body.

Second, consider inequality (7), and integrate over the volume. Here we suppose that σ_{ij} (obtained from $\sigma_{ij} = \partial W/\partial\epsilon_{ij}$) is in internal equilibrium with the body forces F_i, and in external equilibrium with surface tractions T_i. We suppose also that $T^*_i = T_i$ on A_T, the remainder of the surface being represented by A_u. By a process similar to that in the preceding paragraph, it may be shown that

$$\int_V \Omega(\sigma^*_{ij})\, dV - \int_{A_u} T^*_i\, u_i\, dA \geqslant \int_V \Omega(\sigma_{ij})\, dV - \int_{A_u} T_i\, u_i\, dA. \tag{15}$$

Inequality (15) may be interpreted as the minimum complementary energy theorem.

To sum up, the inequality (3) expressing material stability has been shown to lead to three energy theorems for an elastic continuum. The second and third theorems are classical results, and will not be discussed further. The first result, inequality (12), has been termed a generalized energy theorem : 'generalized' is used here to emphasize the fact that the stress field σ^*_{ij} and strain field ϵ_{ij} are *completely* independent of each other; this is not so in the classical results.

In the following section we shall make use of the complete independence of the stress and strain fields of inequality (12) to find bounds on displacements for certain dynamic loading problems. This approach differs radically from applications of the classical energy theorems, where use is made of the fact that the left and right hand sides of inequalities (14) and (15) can be made arbitrarily close, but can nevertheless lead to useful results.

4. Application to Dynamic Loading

We consider a continuum of density ρ. The boundary value problem we consider is as follows :

(i) At time $t = t_0$ the velocity $\dot{u}_i{}^0$ is given at each point in the continuum.

(ii) For times $t > t_0$, the surface tractions are prescribed zero over part of the surface of the continuum A_T, and the displacement rates are prescribed zero over the remainder of the surface A_u.

(iii) Body forces F_i (not including inertia terms) may act on the continuum, but remain constant.

We shall be concerned with the displacements resulting from both the body forces and the dynamic disturbance. Suppose that at time $t > t_0$ the displacements, displacement rates and strains are given by u_i, $\dot{u}_i$, ϵ_{ij}. It is also necessary to introduce the displacements and strains u'_i, ϵ'_{ij} which are due to the body forces alone, and which are present at time $t \leqslant t_0$. An energy balance equation may be written to relate quantities at any time $t > t_0$ and time t_0 :

$$\int_V W(\epsilon_{ij})dV + \int_V \tfrac{1}{2}\rho\, \dot{u}_i \dot{u}_i dV = \int_V W(\epsilon'_{ij})dV + \int_V \tfrac{1}{2}\rho\, \dot{u}_i{}^0 \dot{u}_i{}^0 dV + \int_V F_i(u_i - u'_i)dV. \tag{16}$$

Rearranging,

$$\int_V W(\epsilon_{ij})\,dV = \int_V \tfrac{1}{2}\rho\,\dot{u}_i^0\,\dot{u}_i^0\,dV + \int_V F_i\,u_i\,dV - \int_V \tfrac{1}{2}\rho\,\dot{u}_i\,\dot{u}_i\,dV - \int_V \{F_i\,u'_i - W(\epsilon'_{ij})\}\,dV. \tag{17}$$

The strain and displacement field ϵ_{ij}, u_i are certainly compatible, hence we may substitute (17) into (12). We require only that the stress field σ^*_{ij} should be in internal equilibrium with the same body forces F_i as those of the dynamic problem. We obtain

$$\int_V \tfrac{1}{2}\rho\,\dot{u}_i^0\,\dot{u}_i^0\,dV - \int_V \tfrac{1}{2}\rho\,\dot{u}_i\,\dot{u}_i\,dV - \int_V \{F_i\,u'_i - W(\epsilon'_{ij})\}\,dV + \int_V \Omega(\sigma^*_{ij})\,dV \geqslant \int_A T^*_i\,u_i\,dA. \tag{18}$$

In addition

$$\int_V \tfrac{1}{2}\rho\,\dot{u}_i\,\dot{u}_i\,dV \geqslant 0 \tag{19}$$

and

$$\int_V \{F_i\,u'_i - W(\epsilon'_{ij})\}\,dV \geqslant 0. \tag{20}$$

Hence it follows that

$$\int_V \tfrac{1}{2}\rho\,\dot{u}_i^0\,\dot{u}_i^0\,dV + \int_V \Omega(\sigma^*_{ij})\,dV \geqslant \int_A T^*_i\,u_i\,dA. \tag{21}$$

By a suitable choice of T^*_i, therefore, bounds on certain properties of the displacement field u_i may be computed in terms of the known initial kinetic energy of the problem and the complementary energy of a stress field in equilibrium with T^*_i, F_i. Should either of the terms given in inequalities (19) and (20) be known, it is of course not necessary to eliminate them from (18).

It must be emphasized that the stresses in the starred (σ^*_{ij}) and unstarred ($\sigma_{ij} = \partial W/\partial\epsilon_{ij}$) systems satisfy different field equations, and hence the left and right hand sides of (21) cannot be made arbitrarily close. In the examples given in the following section, the choice of T^*_i will be dictated entirely by those properties of the displacement field u_i for which a bound is desired. Having made a choice of T^*_i, it is obvious that the best value of $\int \Omega(\sigma^*_{ij})\,dV$ occurs when the complementary energy is a minimum, i.e. when σ^*_{ij} is the correct solution to a boundary value problem specifying F_i in the body and T^*_i over the entire surface.

It should also be noted that the entire preceding argument may be carried out in terms of generalized stresses and strains for one- or two-dimensional continua without loss of generality. For simplicity the examples in the following section are all for one-dimensional continua. It is also possible to compare computed bounds to the solutions of simple vibration problems in these cases.

5. ILLUSTRATIVE EXAMPLES

As examples of the application of the principle to bound computations, we will consider a simply supported beam subjected to two distributed impulsive loadings, and compare the computed bound with the exact answer in each case. Body forces (other than inertia forces) will be taken to be zero.

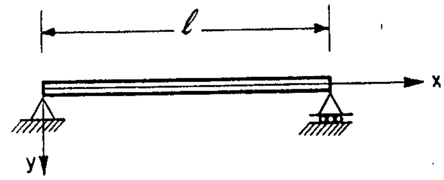

FIG. 1. Mass/unit length in flexural rigidity EI.

The beam, span l, flexural rigidity EI and mass m/unit length, is shown in Fig. 1. Shear deformation will be neglected. The theoretical analysis will follow TIMOSHENKO (1955). The differential equation of motion for free vibration of a beam is

$$\frac{\partial^2 y}{\partial t^2} + a^2 \frac{\partial^4 y}{\partial x^4} = 0, \quad a^2 = \frac{EI}{m}, \tag{22}$$

where x is measured along the beam and y is the transverse displacement. The solution to this equation, including appropriate boundary conditions for the simply supported case, is

$$y = \sum_{i=1}^{i=\infty} \sin \frac{i\pi x}{l} (C_i \cos p_i t + D_i \sin p_i t) \tag{23a}$$

where

$$p_i = a \left(\frac{i\pi}{l}\right)^2, \tag{23b}$$

$$C_i = \frac{2}{l} \int_0^l f(x) \sin \frac{i\pi x}{l} dx, \tag{23c}$$

$$D_i = \frac{2}{l p_i} \int_0^l f'(x) \sin \frac{i\pi x}{l} dx, \tag{23d}$$

$$(y)_{t=0} = f(x), \tag{23e}$$

$$(\dot{y})_{t=0} = f'(x). \tag{23f}$$

In all cases we shall assume that the beam is undeformed at time $t = 0$, i.e. $f(x) = 0$.

Consider first that at time $t = 0$ an impulse acts on the beam such that the velocity at time $t = 0$ is given by

$$(\dot{y})_{t=0} = f'(x) = v_0 \sin \frac{\pi x}{l}. \tag{24}$$

It is readily seen that such an impulse excites only the first mode, and that the solution is given by

$$y = \frac{v_0 l^2}{a\pi^2} \sin \frac{\pi x}{l} \sin \frac{a\pi^2}{l^2} t. \tag{25}$$

Let the maximum central displacement be δ^I. This occurs at a time t' such that

$$\sin \frac{a\pi^2}{l^2} t' = 1$$

and it follows that

$$\delta^I = \frac{v_0\, l^2}{\pi^2} \sqrt{\left(\frac{m}{EI}\right)}. \tag{26}$$

Consider, secondly, that at time $t = 0$ an impulse acts on the beam such that the velocity at time $t = 0$ is given by

$$(\dot{y})_{t=0} = f'(x) = v_0. \tag{27}$$

Then, from (23d),

$$D_i = \frac{2v_0}{lp_i} \int_0^l \sin \frac{i\pi x}{l}\, dx. \tag{28}$$

It is readily seen that the disturbance excites only odd modes. After integration, (28) gives

$$D_1 = \frac{4v_0\, l^2}{a\pi^3}, \quad D_3 = \frac{4}{27} \frac{v_0\, l^2}{a\pi^3}, \quad D_5 = \frac{4}{125} \frac{v_0\, l^2}{a\pi^3} \text{ etc.} \tag{29}$$

The solution for the central displacement is

$$y\left(\frac{l}{2}\right) = \frac{4v_0\, l^2}{a\pi^3} \left\{ \sin \frac{a\pi^2}{l^2} t - \frac{1}{27} \sin \frac{9a\pi^2}{l^2} t + \frac{1}{125} \sin \frac{25a\pi^2}{l^2} t - \frac{1}{343} \sin \frac{49a\pi^2}{l^2} t + \dots \right\}. \tag{30}$$

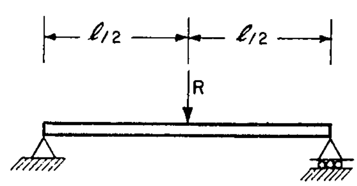

FIG. 2.

In order to compute the bound we consider as an equilibrium system a transverse central point load R (Fig. 2) on the simply supported beam. The complementary energy of the system in Fig. 2 is thus given by

$$C^* = 2 \int_0^{l/2} \tfrac{1}{2} \left(\frac{Rx}{2}\right)^2 \frac{dx}{EI} = \frac{R^2\, l^3}{96EI}. \tag{31}$$

C^* is analogous to $\int_V \Omega\, (\sigma^*_{ij})\, dV$ in (21). Let K^0 be the term analogous to $\int_V \tfrac{1}{2}\rho\, \dot{u}_i{}^0\, \dot{u}_i{}^0\, dV$ in (21), and let δ be the maximum transverse central displacement of the beam. Then (21) becomes

$$\delta \leqslant \frac{K^0 + C^*}{R}. \tag{32}$$

It is clear at this point that the equilibrium system of Fig. 2 is appropriate for a bound on the central displacement relative to the fixed supports. We may choose any specific value for R; the optimum bound can be obtained, however, by minimizing the right hand side of (32). This requires

$$\frac{dC^*}{dR} = \frac{K^0 + C^*}{R}. \tag{33}$$

Substituting from (31), we obtain

$$\frac{Rl^3}{48EI} = \frac{K^0 + \dfrac{R^2\, l^3}{96EI}}{R},$$

$$\text{i.e. } R = \sqrt{\left(\frac{96EI\, K^0}{l^3}\right)}. \tag{34}$$

The optimum bound is thus

$$\delta \leqslant \frac{K^0\, l^3}{24EI}. \tag{35}$$

For the first example we have

$$K^0 = \int_0^l \tfrac{1}{2}m \left(v_0 \sin\frac{\pi x}{l}\right)^2 dx = \frac{mlv_0^{\,2}}{4}. \tag{36}$$

Substituting this value into (35), the bound is

$$\delta^I \leqslant v_0\, l^2 \sqrt{\left(\frac{m}{96EI}\right)} = 0{\cdot}102\, v_0\, l^2 \sqrt{\left(\frac{m}{EI}\right)}. \tag{37a}$$

The computed value is

$$\delta^I = \frac{v_0\, l^2}{\pi^2} \sqrt{\left(\frac{m}{EI}\right)} = 0{\cdot}101\, v_0\, l^2 \sqrt{\left(\frac{m}{EI}\right)}. \tag{37b}$$

In the second example we have

$$K_0 = \int_0^l \tfrac{1}{2}m\, v_0^{\,2}\, dx = \tfrac{1}{2}mlv_0^{\,2}. \tag{38}$$

Substituting this value into (35) we have

$$\delta^{II} \leqslant v_0\, l^2 \sqrt{\left(\frac{m}{48EI}\right)} = 0{\cdot}144\, v_0\, l^2 \sqrt{\left(\frac{m}{EI}\right)}. \tag{39a}$$

Approximately, the computed value of δ^{II}, equation (30), is given by

$$\delta^{II} = 0{\cdot}126\, v_0\, l^2 \sqrt{\left(\frac{m}{EI}\right)}. \tag{39b}$$

The accuracy of the bound in the first example, equations (37), is no doubt due to the fact that the disturbance excites only the first mode. The bound in the second example is approximately 14 per cent greater than the exact value. This is a reasonable answer for many purposes.

It would appear also that the principle can be applied under certain conditions where strains are small but displacements may be large. We shall treat such an example briefly.

Consider a free ring, of radius r, mass m per unit length and flexural rigidity EI. Axial and shear strains will be neglected. We suppose that the ring (Fig. 3a) is subjected to some initial velocity distribution which is distributed symmetrically over some part of the ring. All velocities will be taken to lie in the plane of the ring. Let the initial energy be K^0.

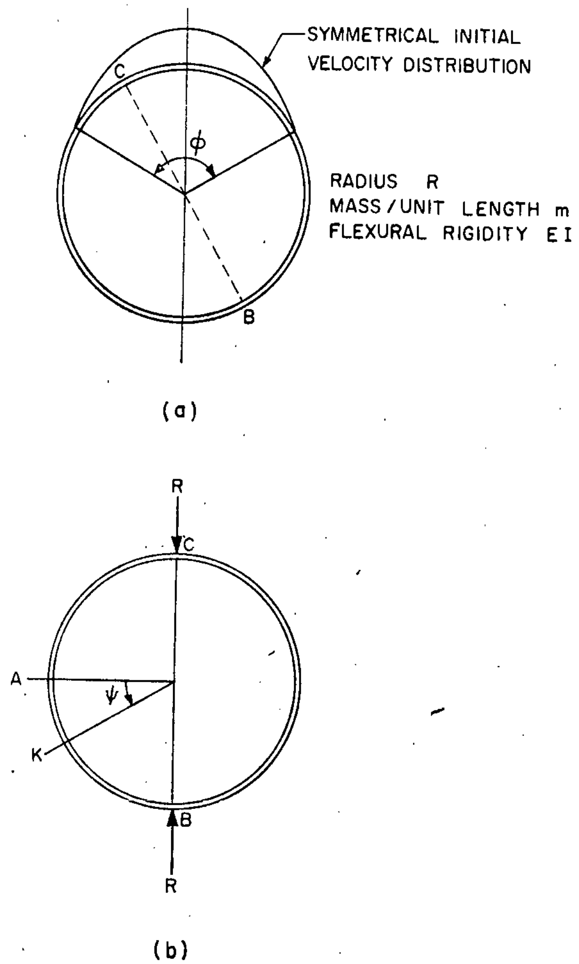

FIG. 3. Free ring with impulsive load.

As an equilibrium system consider the equal and opposite forces R in Fig. 3b. The elastic solution to this loading pattern gives bending moments M_K for the quadrant AB as

$$M_K = (\tfrac{1}{2}\cos\psi - 0{\cdot}182)\,R. \tag{40}$$

It follows that the complementary energy of the system is

$$C^* = \frac{0{\cdot}132\, r^3 R^2}{EI}. \tag{41}$$

We may now apply the principle to the disturbed ring (Fig. 3a) and the static system (3b). Let u_t^B, u_t^C be the displacements of the points B and C; in Fig. 3a

B and C may be *any* diametrically opposite points. It is readily seen that the term analogous to $\int T_i u_i \, dA$ becomes merely the force R multiplied by the diametrical contraction or expansion of the ring, say e. Thus

$$Re \leqslant K^0 + C^* = K^0 + \frac{0{\cdot}132\, r^3 R^2}{EI}. \tag{42}$$

It can readily be shown that optimization gives

$$e \leqslant 0{\cdot}727 \sqrt{\left(\frac{r^3 K_0}{EI}\right)}. \tag{43}$$

Thus an upper bound is established on the maximum diametrical expansion or contraction for any diameter.

The examples given here have neglected shear and axial deformations. The bound is thus a bound on the displacements given by an exact solution which also neglects shear and axial deformation. The bound can be extended merely by including shear and axial complementary energy in the term C^* : the bound is then a bound on an exact solution which includes shear and axial deformations.

6 CONCLUSIONS

The illustrative examples presented in the preceding section are extremely simple, and exact solutions are readily obtainable The significance of the bound computation lies, however, in that it may be applied with little additional difficulty to a wide variety of structures and continua. A consistent bound to localized displacements can be found, for the boundary value problem and material described, for cases where an exact solution would be tedious if not impossible.

The accuracy of the bound is of course a matter of great importance, especially in view of the fact that the bound can never be made arbitarily close to the correct solution. The two examples presented here give no indication of accuracy in more complex cases. It would be extremely useful to compare the bound to exact values for a wide variety of problems. It may nevertheless be expected that the bound will in almost all cases give at least the order of magnitude of the displacement of any point, and such an estimate, coupled with the ease with which the bound may be computed, and the fact that the bound is a safe bound, should be of great practical value.

A further problem of practical interest is whether a given disturbance will lead to strains beyond the elastic range of the material, and the effect of such strains on the displacements. The present principle gives no information about local strains; neither is it likely that any principle of this nature will do so. However, the principle can be extended to bound displacement resulting from disturbances which cause part of the continuum or structure to behave inelastically. In a further paper we shall generalize the results of this and an earlier paper (MARTIN 1963) to show that an analogous principle may be written for a broad class of elastic and inelastic materials.

ACKNOWLEDGMENTS

THE author is indebted to Professors P. S. Symonds, E. T. Onat and D. C. Drucker for their valuable advice and criticism in the preparation of this paper.

References

Drucker, D. C.	1951	*Proc. 1st U.S. Nat. Congr. Appl. Mech.*, 487.
Hill, R.	1956	*J. Mech. Phys. Solids* 5, 66.
Martin, J. B.	1963	Tech. Rept. BU/DTMB/1 from Brown University to David Taylor Model Basin.
Timoshenko, S. P.	1955	*Vibration Problems in Engineering*, p. 331 (Van Nostrand).

UNIVERSITY OF CAPE TOWN

DEPARTMENT OF CIVIL ENGINEERING

UNIVERSITY EXAMINATION, NOVEMBER 1974

CE 504: PROBABILITY AND STATISTICS FOR ENGINEERS

Total marks: 100 Time allowed: 3 hours

External Examiner : Professor D.M. Schultz

Internal Examiners: Professor G.v.R. Marais
Mr. M.S. Green

Attempt ALL questions in Section A and FOUR questions from Section B and C. Use separate answer book for Section C.

Name: ....

SECTION A

Note: Answer these questions in the spaces provided on this question paper. Do not show calculations, enter only the final answer.

1. Give formulae for:

   (a) the coefficient of variation;

   (b) the mean deviation about the mode.

2. Find the standard deviation of the data: 2; 6; 10.

3. In a particular experiment the result of 10 weighings showed 4 values between 20 and 25 g, 4 values between 25 and 30 g and 2 values between 30 and 35 g. What was the median weight?

4. An engineering firm has 100 electrical components in stock, 25 manufactured by process A and 75 manufactured by process B. Unknown to the firm, 13 of those manufactured by A are defective and 18 of those manufactured by B are defective.

   A component is chosen at random from the 100 components. What is the probability that this component is:

   (i) manufactured by B and defective?

   (ii) either manufactured by A or is a defective component?

5. An item of radar equipment has three critical components A, B, C. The frequency of defect for component A was found to be 5 per 100, for B to be 6 per 100, and for C to be 8 per 100. Estimate the probability that a given item of equipment is defective.

6. A biased coin which has twice the probability of falling heads as falling tails is tossed with two unbiased coins. What is the probability:

   (i) of at least two heads occurring?

   (ii) of no heads occurring?

7. At a telephone exchange the average number of calls passed per hour in the morning is 96 and the rate can be regarded as constant. Calculate the probability of:

   (i) exactly 3 calls in a period of 5 minutes;

   (ii) more than 3 calls in a period of 5 minutes.

8. Packets are filled automatically and on the average, 5 per cent are underweight. An inspector takes a batch of twelve collected randomly. What is the probability that he will find 25 per cent or more underweight?

9. The mean diameter of steel rods produced by a process is 2 cm and the standard deviation is 0,05 cm. Assuming the diameters are normally distributed, find the value such that only 5 per cent of the rods will have a diameter exceeding this value.

10. A sample of 11 lengths of plastic were tested and found to have a standard deviation of 35. A second sample of 9 lengths of plastic, treated by a different process, was tested and found to have a standard deviation of 20. Test whether the standard deviations differ significantly.

11. State the assumptions required for the use of the t-test for the difference between the means of two independent samples.

12. If one denotes by y' the values of y which are calculated by means of the equation of the regression line, what is the least squares criterion?

13. Give the formula for the variance of the mean value of y, that is $\bar{y}$, where y is estimated from a regression line.

14. Give the formula for the correlation coefficient for two variables x and y.

15.

	Defective	Good	Total
Process A	25	15	40
Process B	35	25	60
Total	60	40	100

Test whether there is a difference between process A and process B in the above table.

SECTION B

Answer these questions in the answer books provided

1. A laboratory balance is used to weigh the same object 100 times. The values are given in the table below.

Weight in g	Number of observations
4,55 - 4,65	10
4,65 - 4,75	20
4,75 - 4,85	45
4,85 - 4,95	15
4,95 - 5,05	10
	100

(a) Using this data calculate:

(i) the mean,
(ii) the mode,
(iii) the median,
(iv) the variance and standard deviation,
(v) the coefficient of variation.

(b) By fitting a normal distribution to the data, find the expected frequencies in the first two class intervals.

2. (a) Derive the binomial distribution from first principles and hence derive the Poisson distribution from the binomial distribution.

(b) The probability of a light bulb failing during the first twelve hours of service is 0,0049. If 1000 light bulbs are installed, use the Poisson distribution to find the probability of exactly ten bulbs failing within the first twelve hours.

(c) A machine is known to produce piston rings of which 10 per cent are defective. Find the probability that in a random sample of 400 rings:

(i) at most 35 rings will be defective;
(ii) between 35 and 50 will be defective.

3. (a) Define with diagram a type I error, type II error and the power of a test.

(b) The outputs from two production plants A and B were measured on each of 5 days. The data was given as follows:

Output (tons)

Plant A	Plant B
2,0	2,2
1,7	2,0
2,6	2,7
1,7	1,7
2,0	1,9

3. (b) (Continued)

Test whether the output of Plant B is significantly higher than that of Plant A at the 5 per cent level of significance if:

(i) sample A was considered to be independent of sample B:

(ii) it was believed that the day on which the observation was made was a relevant factor, and the observations were considered to be paired.

4. An experiment was carried out to measure the resistance of wire from three sources by taking five samples from each source.

(a) Use analysis of variance to determine whether or not there is a significant difference between the resistance of the wire from the three sources.

Sample \ Source	A	B	C
1	7,2	8,5	8,3
2	7,3	8,6	8,6
3	7,4	9,0	8,6
4	7,9	8,7	8,7
5	7,7	8,7	8,8

(b) It is believed that the 5 samples for each source were taken on consecutive days and that the resistance increased each day due to an external factor. Explain how you would test this hypothesis <u>for Source A only</u>.

SECTION C

(Answer this question in a separate answer book).

1. (a) In a set of 10 compressive tests on concrete cubes, two of the tests exceeded the capacity of the testing machine (12 MPa). The 8 definite test results were (in MPa):

11,9 8,0 8,8 11,3 10,7 10,7 9,9 9,7.

For the set of 10 cubes, determine graphically the mean compressive stress and its standard deviation.

(b) On two succeeding days a set of data was obtained on the concentration of bacteria in the effluent from a sewage works. The two sets of ranked data are:

Set 1:	400	700	850	1200	1900					
Set 2:	750	1200	1700	1900	2400	3100	3600	5000	6000	11000

The data is expected to be log-normally distributed.

1. (b) (Continued)

(i) Determine (using graphical procedures) the log-mean, geometric-mean of each set of data.

(ii) Test if the log-means are significantly different at 96 per cent level of significance.

(iii) Briefly explain why you performed the test for significance (in (ii) above), on the differences of the log-means and not on the differences of the geometric and arithmetic-means.

(c) List the conditions which must prevail for (i) a normal, (ii) a log-normal, distribution to arise.

UNIVERSITY OF CAPE TOWN

DEPARTMENT OF CIVIL ENGINEERING

UNIVERSITY EXAMINATION: JUNE, 1975

COURSE CE 508 - SKELETAL STRUCTURES

Time allowed: 4 hours

Notes are allowed

Part A: For each of the five structures shown below determine the degree of static and of effective kinematic indeterminateness, select the most suitable method of analysis, give the order of all the relevant matrices required for solution by the chosen method. State clearly what assumptions are made.

[40 marks]

Part B: Compile the matrices for any two of these structures; one analysed by the FORCE method and one analysed by the DISPLACEMENT method. Do not attempt to complete all the arithmetic processes, but give sufficient detail to show clearly the principles and operations involved.

[60 marks]

1. Jetty with vertical and horizontal loads applied to the top surface in the xy plane. The pile rows are at 3 m spacing along the jetty.

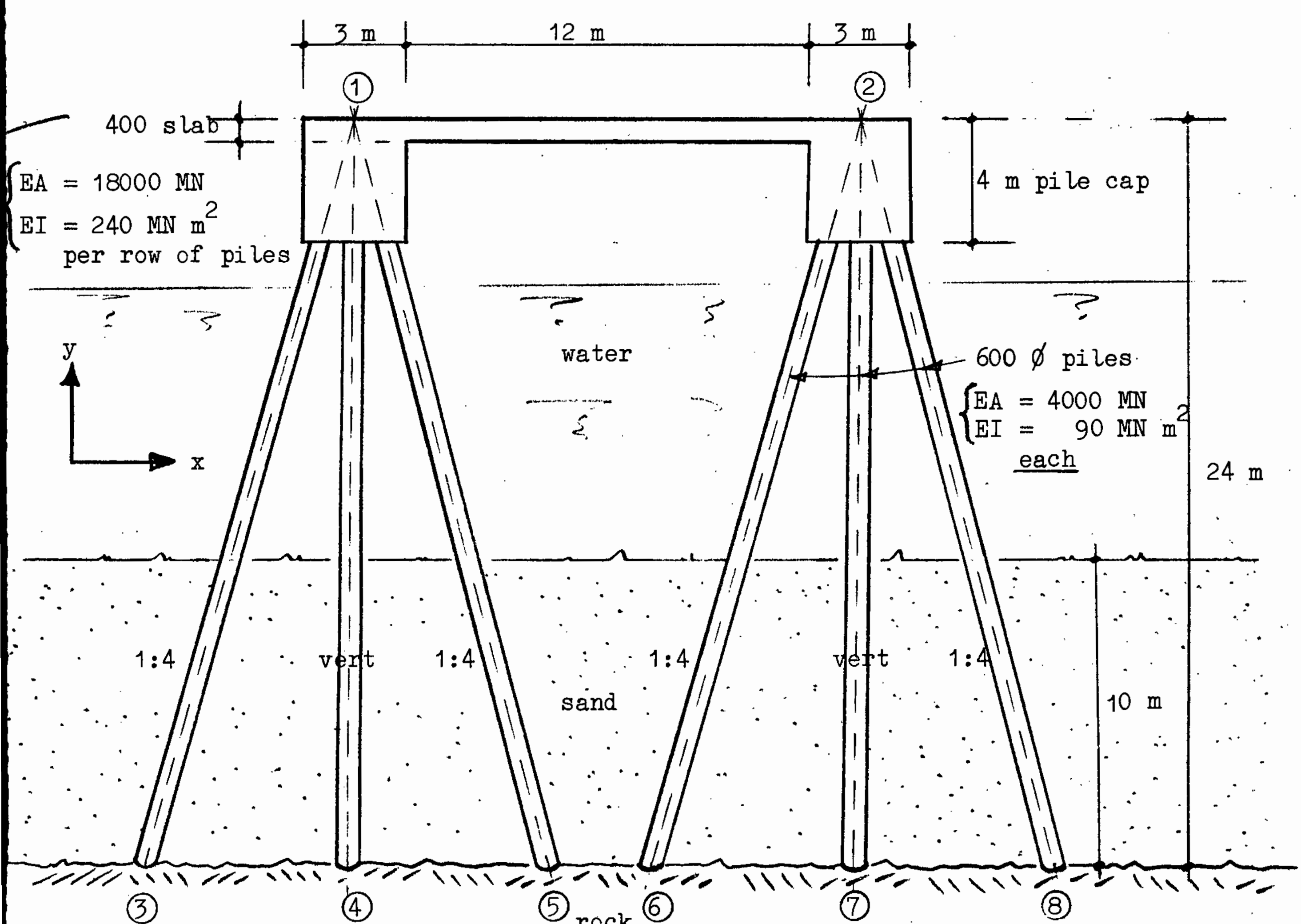

CROSS-SECTION

/2. ....

2. Bridge, monolithic concrete beam-slab deck and inclined columns, with vertical and horizontal loading applied to the deck.

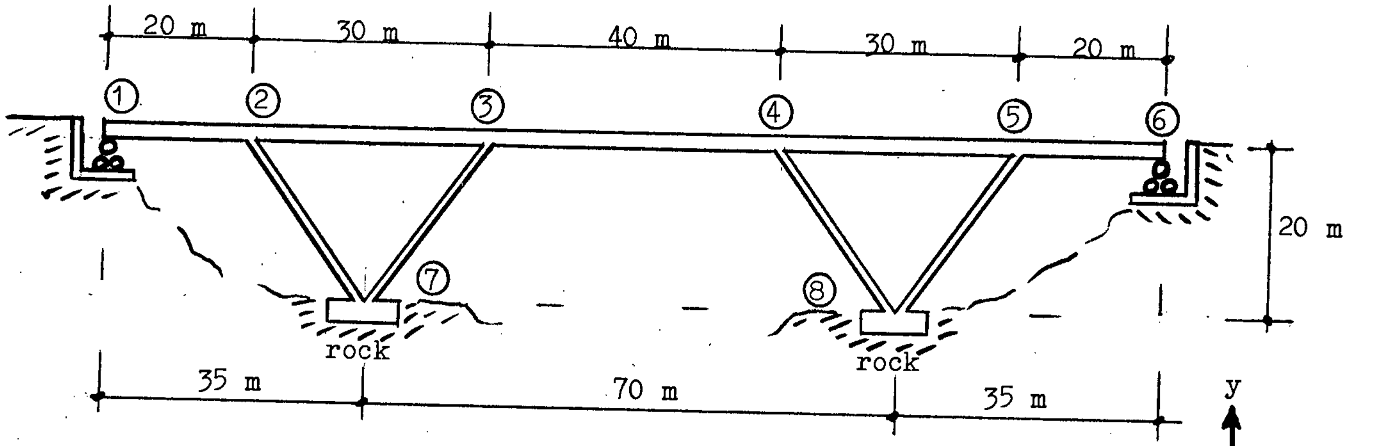

deck : EA = 140 000 MN; EI = 40 000 MN m^2

columns: EA = 36 000 MN; EI = 3 000 MN m^2

3. Tower, consisting of a single vertical tubular column fixed at the base and stayed at right angles on four levels with steel wire guy ropes, which are sufficiently pretensioned not to go slack. Loading is applied at the top only.

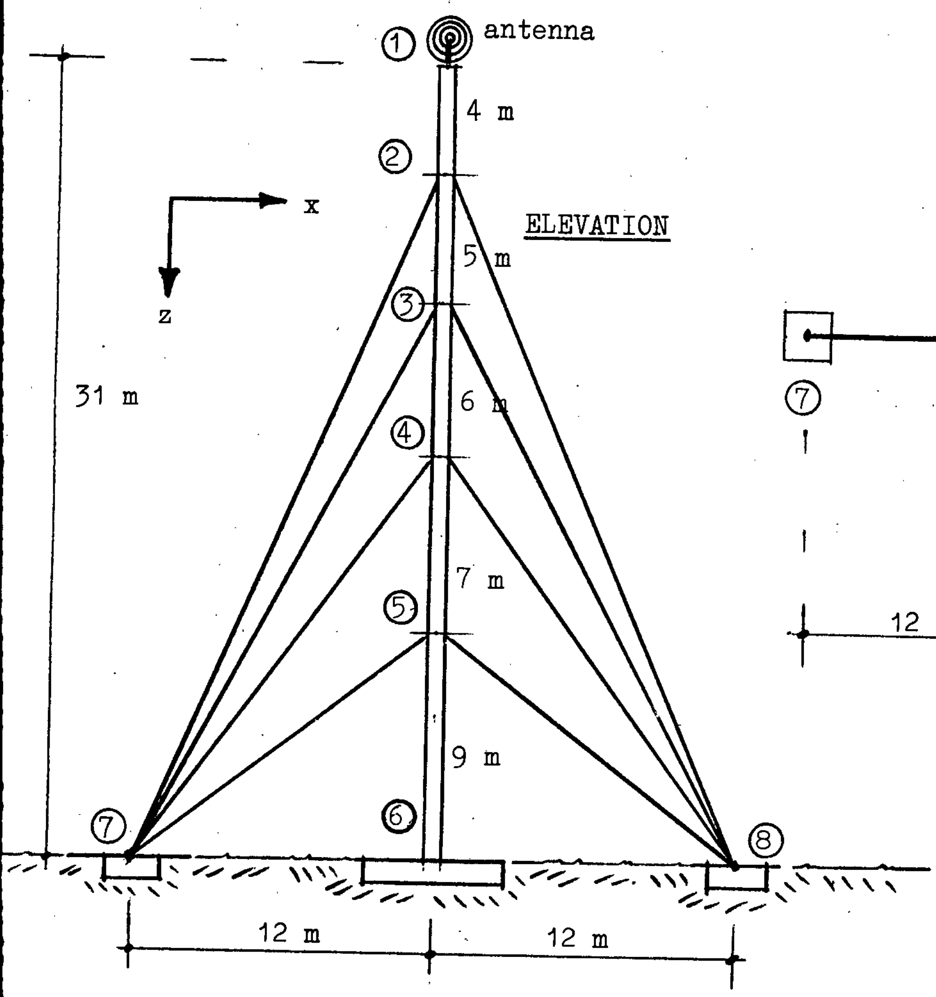

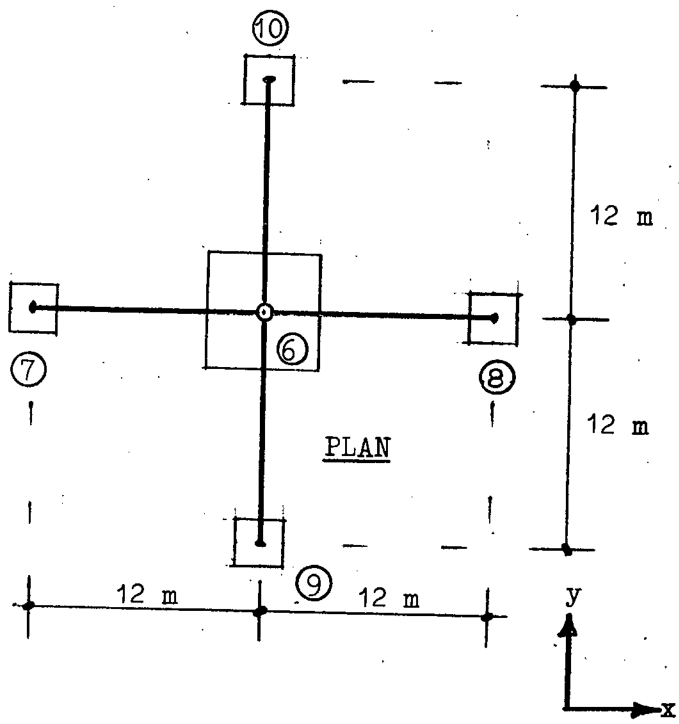

column : EA = 1300 MN; EI = 7 MN m^2(200 ∅)

wire rope: EA = 36 MN each: (15 mm ∅.)

4. Building, tied steel portal frame with two side bays. Wind, dead and imposed roof loading.

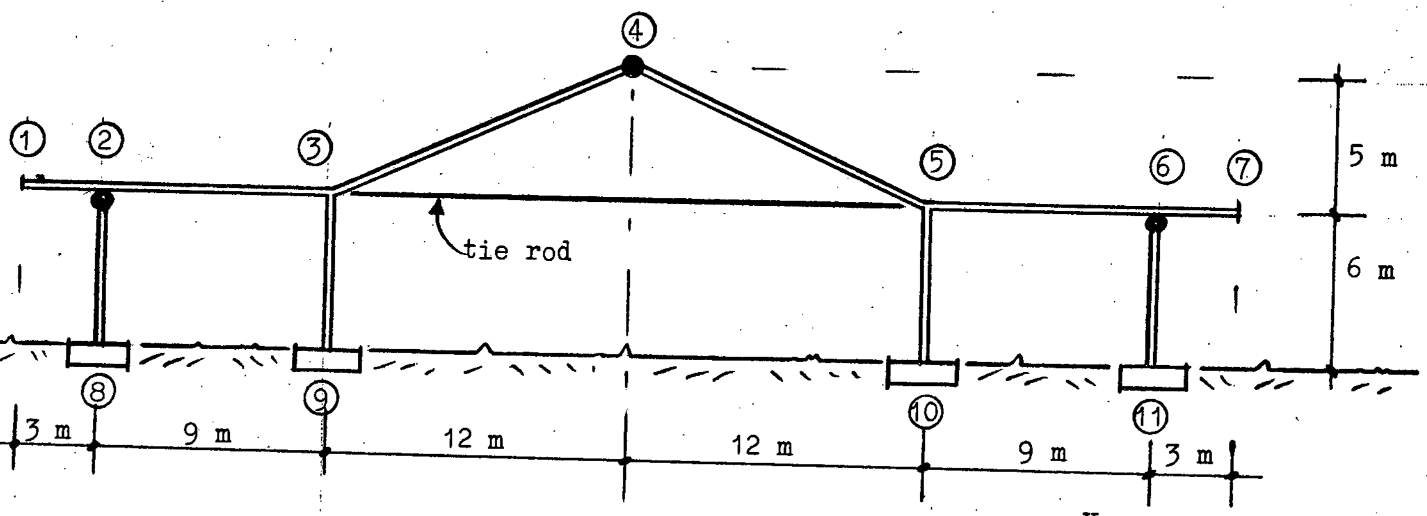

Rafters: EA = 1000 MN; EI = 20 MN m^2

Columns: EA = 1200 MN; EI = 9 MN m^2

Tie rod: EA = 60 MN (20 Ø).

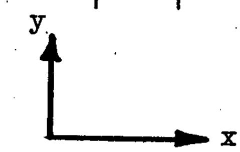

5. Roof, ball-jointed, double-layer, three-way grid on four columns fixed at their bases, all of tubular steel construction, with vertical and horizontal loading applied to the top joints.

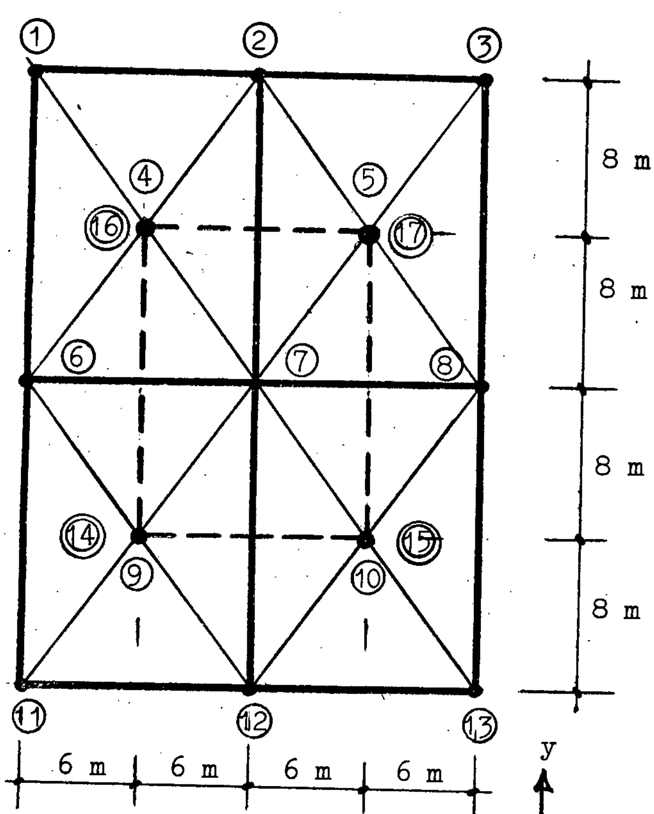

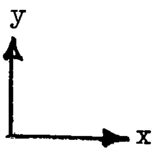

PLAN

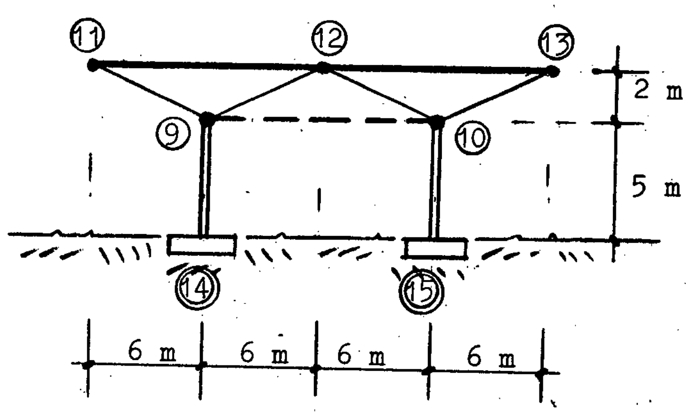

ELEVATION

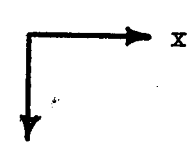

top layer	:	EA = 600 MN, (200 mm Ø)		
inclined	:	EA = 900 MN, (300 mm Ø)		
bottom layer	:	EA = 1200 MN, (400 mm Ø)		
columns	:	EA = 3000 MN, (500 mm Ø);	EI = 100 MN m^2	

- - - - - - - - - - -

UNIVERSITY OF CAPE TOWN

DEPARTMENT OF CIVIL ENGINEERING

UNIVERSITY EXAMINATION - JUNE, 1975

CE 513 - WASTEWATER TREATMENT

Q.1

(a) An activated sludge plant designed for nitrification and denitrification has been constructed. At the time in question only the reactors are complete. The volume of the main aeration reactor is 15 000 m^3. Eight mechanical aerators have been supplied with a guaranteed oxygen transfer rate of 2,4 kg O_2 $(kWh)^{-1}$ under standard conditions.

An unsteady state test was carried out to determine whether the manufacturers' guarantee figure is acceptable. On the day of the test the saturation concentration of oxygen in the clean tap water contained in the aeration basin was 9,2 mg ℓ^{-1}. Atmospheric pressure was 760 mm Hg. Average power drawn by each aerator was 198 kW. As a result of the test (which lasted about 4 minutes), the aerators were accepted. The actual oxygen transfer rate differed from the guarantee figure by a factor of 1,03.

Reconstitute the table showing the results likely to have been obtained during the test i.e. of dissolved oxygen concentration (mg ℓ^{-1}) with time (minutes).

(b) On completion of the reactors the designers are now faced with a problem: should they install a conventional secondary settler or a dissolved-air pressure flotation system.

(i) Given the following information, produce designs for the secondary settler(s) and as an alternative a flotation system. Sketch the two designs to scale on graph paper.

Design for solid-liquid separation based on Peak Wet Weather Flow = 3 * Mean Dry Weather Flow.

Mean Dry Weather Flow = 28 000 m^3 d^{-1}

Peak Dry Weather Flow = 2 * Mean Dry Weather Flow.

MLTSS concentration = 3 000 mg ℓ^{-1}.

(ii) For the flotation system, what features in design would you suggest, bearing in mind that it is to take the place of secondary settlers.

(iii) What concentrations (approximately) would you expect to achieve for the separated solids for both settling and flotation.

Q.1(iv)/page 2.

CE 513 - WASTEWATER TREATMENT

Q.1

(iv) If the sludge wasted per day from the plant is to be concentrated to say 60 000 mg ℓ^{-1} by flotation, discuss the advantages or disadvantages in withdrawing sludge from (1) the underflow from the secondary settler, or the float from the flotation unit and (2) the mixed liquor from the reactors.

(v) Discuss the factors you feel may influence the designer in his choice as to whether secondary settlers or a flotation system should be installed.

(c) The waste sludge from the activated sludge system is to be thickened to a concentration of 6%. Given that the sludge age of the plant is 15 days, design a dissolved-air (pressure) flotation system to achieve this concentration. Sketch your design, to scale, on graph paper.

Are there any design features in this application (i.e. thickening) which differ from those for the flotation system you designed to take the place of the secondary settler (i.e. clarification).

Q.2 An activated sludge plant is to be built for a town with a present population of 10 000 inhabitants in the Karoo. The population is projected to increase to 15 000 in 10 years. There is no significant wastewater contribution from industry. The water temperature ranges from 14°C in winter to 21°C in summer. Present water consumption figures are 140 ℓ/cap/day, but the figure is expected to increase to 160 ℓ/cap/day in 10 years. COD contribution is approximately 0,1 kg/cap/day.

It is required that the phospherous and nitrogen content of the waste flow be removed as much as possible by biological treatment methods requiring no addition of chemicals.

You wish to investigate the use of a completely mixed activated sludge system, designed for nitrogen and phospherous removal, to treat the raw sewage inflow. Furthermore, the climate is suitable for drying the sludge in drying beds, and you consider the sludge will be suitable for this purpose if the sludge age is maintained at 40 days.

Design and compare the biological processes of two proposed systems:-

(i) A system with a sludge age of 40 days.

(ii) A system with a sludge age between 10 and 20 days plus aerobic digestion of the wasted sludge. (You must justify the choice of your specific sludge age).

Q.2/page 3.

CE 513 - WASTEWATER TREATMENT

Q.2

The comparison must include the removal of phospherous. It is proposed that the waste sludge from the reactor will be thickened to 3% by flotation before any further treatment. You are not required to design the flotation system.

UNIVERSITY OF CAPE TOWN

UNIVERSITY EXAMINATION NOVEMBER 1974

APPLIED MATHEMATICS HONOURS

Mathematical Programming

Time : 3 hours

Not more than FIVE questions to be answered :

1. A LPP is given in the form:

$$Ax = q \ , \quad x \geq 0 \ , \quad \max z = cx$$

where $q \geq 0$ and A is an m by n matrix which contains an m by m identity submatrix.

Show how an initial Simplex tableau is set up from this data, state the Simplex Algorithm rules for proceeding to successive tableaux and prove that, in general, the algorithm terminates with an optimal solution to the LPP. Under what circumstances does the algorithm fail?

Consider the Simplex tableau

2	-1	-1	1	0	0	1
3	1	-2	0	1	0	2
-4	2	a	0	0	1	3
-2	2	b	0	0	0	6

in the two cases: (i) $a = 1\frac{1}{2}$, $b = -1\frac{1}{2}$, (ii) $a = -1\frac{1}{2}$, $b = 1\frac{1}{2}$. Prove that in one case the problem is unbounded. Find the optimal solution in the other case.

(22)

2. Discuss the Method of Penalties and the Two-Phase Method for solving the LPP

$$Ax = q \ , \quad x \geq 0 \ , \quad \max z = cx$$

when A does not contain an identity submatrix.

(20)

3. What is the main disadvantage of using the Simplex Algorithm to solve large linear programming problems on a computer? Discuss the use of the Revised Simplex Method to overcome this disadvantage.

(21)